Substituent Effects on the Photochemistry of 1,1-Diarylgermacyclobutanes and the Reactivity of Transient 1,1-Diarylgermenes

Substituent Effects on the Photochemistry of 1,1-Diarylgermacyclobutanes and the Reactivity of Transient 1,1-Diarylgermenes

By

GREGORY DAVID POTTER, B. Sc.

A Thesis
Submitted to the School of Graduate Studies
In Partial Fulfillment of the Requirements
For the Degree
Master of Science

McMaster University

MASTER OF SCIENCE (2003)	McMaster University
(Chemistry)	Hamilton, Ontario

TITLE:	Substituent Effects on the Photochemistry of 1,1-Diarylgermacyclobutanes and the Reactivity of Transient 1,1-Diarylgermenes
AUTHOR:	Gregory David Potter, B. Sc. (McMaster University)
SUPERVISOR:	Professor William J. Leigh
NUMBER OF PAGES:	xv, 159

ABSTRACT

1,1-Bis(4-(trifluoromethyl)phenyl)germacyclobutane and 1,1-bis(3,5-bis(trifluoromethyl)phenyl)germacyclobutane have been prepared, and their photochemistry studied by steady state and nanosecond laser flash photolysis (NLFP) techniques. Photolysis of the two compounds in the presence of methanol leads to the formation of products resulting from reaction of the alcohol with two germanium-containing reactive intermediates, the germenes and germylenes.

The reactivities of the two germenes with nucleophiles such as alcohols, carboxylic acids, and amines have been examined by NLFP techniques, and the results are compared to analogous data for 1,1-diphenylgermene and 1,1-diphenylsilene. Germene reactivity is shown to increase with increasing electron-withdrawing power of the substituents, consistent with a mechanism initiated by nucleophilic attack at germanium. The increased electrophilicity of the substituted 1,1-diarylgermenes results in kinetic behavior indistinguishable from that of 1,1-diphenylsilene, indicating that germenes and silenes form a mechanistic continuum in their reactions with nucleophiles.

ACKNOWLEDGEMENTS

Three years ago I met Dr. Willie Leigh during my search for a fourth year thesis project, and his excitement and enthusiasm of chemistry were exactly the traits I was looking for in a supervisor. I have always admired his professionalism and integrity for scientific excellence. I will always remember the chats in his office or over a few beers at the Phoenix and the fantastic dinners at his home.

The Leigh lab has been an extremely rewarding and enjoyable place to work over the past few years. I would like to thank former group members Drs. Tracy Morkin, Ed Lathioor, Dino Mangion and Xiaojing Li for helping me start here on the right foot. I would also like to acknowledge the support and assistance of the current Leigh lab members Tom Owens, Cameron Harrington, Ileana Dumbrava and Farah Lollmahomed. I would especially like to thank Cameron Harrington who greatly contributed to this work and took me under his wing when I first started here.

I wish to thank Don Hughes and Brian Sayer for their instrumental help with NMR experiments. I also want to thank Jim Britten for his patience and guidance with X-ray crystallography. I would also like to extend my gratitude to

Mike Malott for his assistance and support with all types of computer problems. I'd also like to acknowledge the administrative staff of the chemistry department: Josie, Barb, Tammy and especially Carol.

I want to thank some of the friends that I have made during my years at McMaster: Gina Dimopoulos, Amanda Donovan, Erica Robinson, Kevin Moonoosawmy, Matt Moran, Pippa Lock, and especially Mark Marynowicz. Thanks for all the nights at the Phoenix, the board game nights, and long chats. Mark, you've been my best friend here at Mac, thanks so much for sticking by me during this long journey and I look forward to celebrating the end with you.

To Chrissy, Heather, Bry and Mahsa: You've been such terrific, supportive friends and I am grateful for all the times we've spent together. I would sincerely like to thank my dearest friend Katie Elmslie. It has been a long road that we've shared and I would not be who I am today without you. Thanks for believing in me.

To my Mom, Dad and Jenny who were always supportive of my endeavours and encouraging me to pursue my aspirations no matter how far or difficult they were. I am so grateful for every Sunday night, the roller blading trips around Pier 4, and for the long phone calls across the sea. You guys have such big hearts and I couldn't ask for a better family.

Finally, I want to express my sincerest gratitude to Jennifer. Jen, you have been such a loving, caring support in my life. You will never know how much your strength, encouragement and selflessness have made me a better person. I look forward to our future together.

TABLE OF CONTENTS

LIST OF TABLES

LIST OF FIGURES

CHAPTER 1: INTRODUCTION

1.1 Properties of Silenes and Germenes

Alkenes are one of the fundamental building blocks in organic chemistry. In general, alkenes are stable enough that they can be bought in a bottle and their chemistry is well understood. If one of the carbons is replaced with a heavier group 14 atom such as silicon or germanium, the properties of the "metallaenes" are drastically different from those of alkenes. Compounds containing a silicon-carbon or germanium-carbon double bond, known as silenes and germenes respectively, are species with intrinsically low kinetic stabilities and are usually reactive intermediates. In fact, up until the 1960s silenes were considered too unstable to exist![1]

The first indication that silenes do exist was reported by Gusel'nikov and Flowers in 1967.[2] The gas-phase thermolysis of 1,1-dimethylsilacyclobutane (**1**) was found to yield 1,1,3,3-tetramethyl-1,3-disilacyclobutane (**3**, eq 1.1). The stoichiometry of the reaction as well as the formation of ethylene led them to suggest that the product was formed by the head-to-tail [2 + 2] dimerization of the intermediate 1,1-dimethylsilene (**2**).

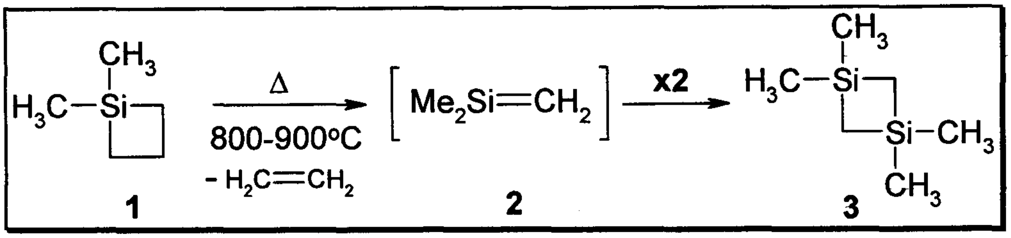

1.1

It was not until 1973 that the first germene was discovered by Barton and coworkers.[3] Complete pyrolysis of the bicycle **4** in a nitrogen flow system led to the formation of 1,1,3,3-tetraethyl-1,3-digermacyclobutane (**7**, eq 1.2). The stoichiometry of the reaction and the production of the substituted benzene **5** allowed them to suggest that 1,1-diethylgermene (**6**) is formed from the pyrolysis of **4**.

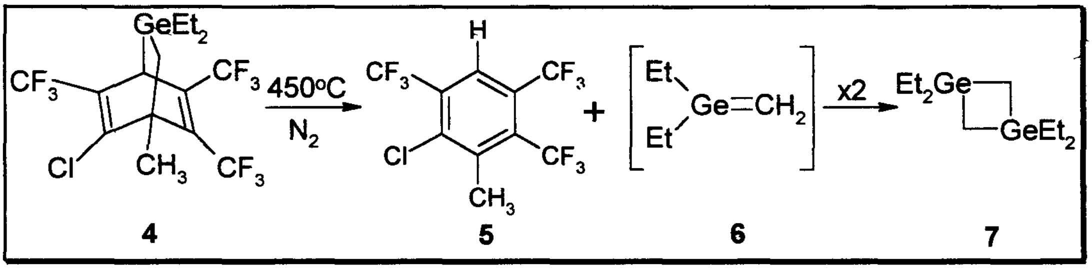

1.2

Since these discoveries, a large number of metallaenes have been studied. Silenes have been studied more extensively than their germanium counterparts, however both silene and germene chemistry have been frequently reviewed.[4-11] The majority of silenes and germenes reported have been reactive intermediates and exhibit physical properties that cause them to be reactive.

Some of the theoretically-predicted physical properties of silene (**4b**) and germene (**4c**) as well as ethene (**4a**) are outlined in Table 1.1.

Table 1.1 A comparison of the physical properties of ethene **4a**, silene **4b** and germene **4c**, as predicted by theoretical calculations.

	$H_2C{=}CH_2$ (**4a**)[12]	$H_2Si{=}CH_2$ (**4b**) [13-17]	$H_2Ge{=}CH_2$ (**4c**) [13, 17-19]
Bond length / Å	1.33	1.70	1.77
E_π / kcal mol^{-1}	65	38	31
Dipole Moment	0	0.81	0.89

The strength of the π bond between the metal and carbon has been calculated for silene (**4b**) as 38 kcal/mol[14, 16, 17] and for germene (**4c**) as 31[17], 33[17, 18] kcal/mol, which can be compared with the experimental π bond energy of 65 kcal/mol for ethene (**4a**).[12]

The energy of the π bond represents the activation barrier for *cis-trans* isomerization. Silenes and germenes have considerably weaker π bonds because of the poor overlap between the 2p orbital on carbon and the 3p and 4p orbitals on silicon and germanium, respectively (Figure 1.1.1).[12, 16, 18]

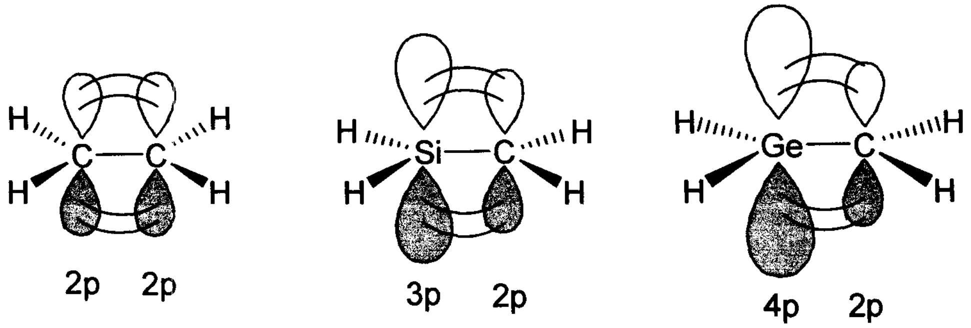

Figure 1.1.1 A schematic of the overlap of p orbitals in ethene **4a**, silene **4b** and germene **4c**.

The M=C bond length in silene and germene have been calculated to be 1.70 Å and 1.77 Å, respectively.[13, 15, 17, 18] These bonds are much longer than the C=C bond length of ethene (1.33 Å).[12]

Another important property exhibited by metallaene bonds is their polarity. Polarity can be qualitatively described by comparing the difference in electronegativities of the atoms that are bonded. The larger the difference in electronegativities of the two atoms, the greater the bond dipole. A comparison of the electronegativities of carbon (2.55)[20] with silicon (1.90)[20] and germanium (2.01)[20] indicates that in silenes and germenes there will be a partial positive charge present on the silicon and germanium, respectively, whereas carbon will bear a partial negative charge. The calculated dipole moments for silene (**4b**) and germene (**4c**) are 0.81 D[15] and 0.89 D,[13, 18] respectively. Thus, the calculated dipole moments indicate that the Si=C and Ge=C bonds are polar with partial positive charges present on the metal. This particular property is important with regards to silene and germene reactivity as the polar nature of the bond dictates the products produced by the many reactions that these species undergo.

1.2 Examples of Stable Silenes and Germenes

Although silenes and germenes are typically reactive intermediates, there have been many 'stable' examples of these species prepared. In these cases the term 'stable' refers to the compound's propensity towards dimerization. Although these silenes and germenes do not undergo dimerization they are typically quite reactive towards nucleophiles. The first stable silene (**5**) was prepared by A.G. Brook and coworkers[21] and is shown in Figure 1.2.1. The silene was characterized by x-ray crystallography and the Si=C bond distance was determined to be 1.764 Å[21] which is in good agreement with the calculated Si=C bond length in silene **4b** (Table 1.1). On the basis of theoretical calculations, Apeloig and coworkers[22] have attributed the stability of the silene to the resonance π-donor substituents (Me_3SiO-) at carbon and the π-acceptor (Me_3Si-) at silicon as well as steric effects from the other two substituents.

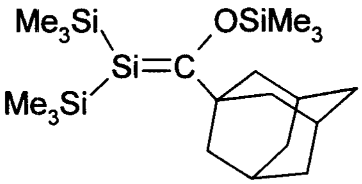

5

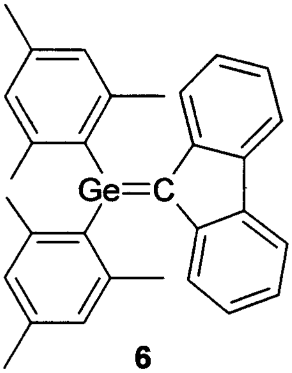

6

Figure 1.2.1 The first reported stable silene (**5**) prepared by A. G. Brook and coworkers[21] in 1982 and stable germene (**6**) prepared by J. Satgé and coworkers[23] in 1987.

The first stable germene (**6**) to be reported was synthesized by J. Satgé and coworkers[23] in 1987 and is illustrated in Figure 1.2.1. Subsequent characterization of the molecule by x-ray crystallography showed the Ge=C bond length to be 1.803 Å[24], which is in good agreement with the calculated Ge=C bond length in **4c** (Table 1.1). The stabilization of germene **6** has been attributed primarily to the steric hindrance caused by the bulky mesityl and fluorenyl substituents.[25]

1.3 Generation of Silenes and Germenes

There are a wide variety of established methods for the generation of silenes and germenes from stable precursors. Generally it has been found that methods that are successful in synthesizing silenes[7] also work for the germanium analogues.[10] For the purpose of this thesis only the most important synthetic routes for preparing germenes will be discussed. The most commonly reported methods are: a) thermal salt eliminations, b) photolysis or pyrolysis of (trimethylgermyl)-diazomethanes, and c) thermally- or photochemically-induced [2 + 4] or [2 + 2] cycloreversions.[10]

a) Thermal salt eliminations

Germenes formed using this method generally require the precursor (**7**) to have a suitable leaving group (X) on germanium and lithium bound to the adjacent carbon. A typical example is that of N. Wiberg and coworkers,[26] illustrated in eq 1.3. In this case, germene **8** was obtained by thermal elimination of LiX (between –110 and +100°C, depending on X) from **7**. In the absence of trapping reagents the dimer **9** was obtained.[26]

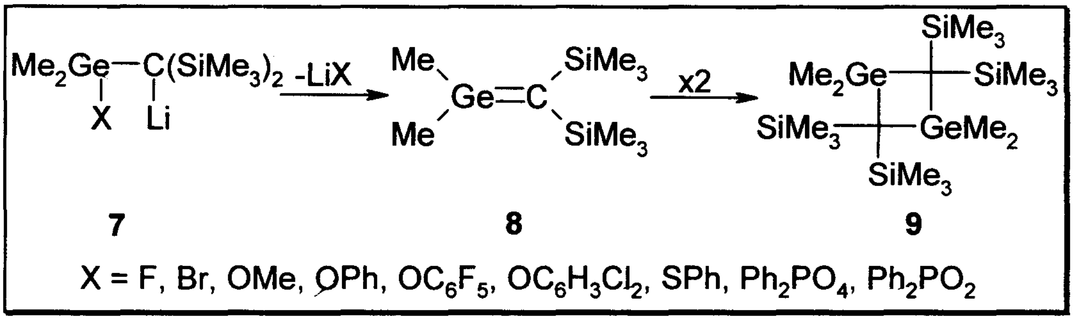

X = F, Br, OMe, OPh, OC_6F_5, $OC_6H_3Cl_2$, SPh, Ph_2PO_4, Ph_2PO_2

1.3

b) Photolysis or pyrolysis of (trimethylgermyl)-diazomethanes

α-Silyldiazomethanes have been established as excellent precursors for the generation of silenes either thermally or photochemically[27, 28] however, there are only a couple of reports where germenes were prepared in the same manner.[27, 29] Barton and coworkers reported that the thermolysis or photolysis of the diazomethane **10** yields germene **12** (Figure 1.4).[27, 29] In the absence of suitable trapping reagents, germene **12** dimerizes in a head-to-head fashion to produce **13**. It has been proposed that germene **12** forms via [1,2]-methyl migration in the carbene intermediate **11**.[27, 29]

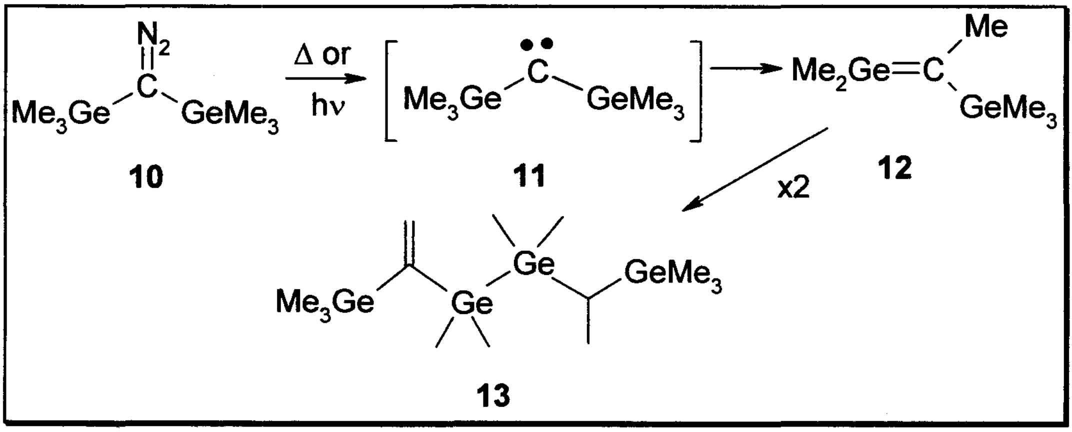

1.4

c) [2 + 4] or [2 + 2] cycloreversions

The thermal decomposition of various bicyclic compounds has been shown to be successful in generating both silenes[30] and germenes[3, 31] through a [2 + 4] retro-Diels-Alder reaction. An example of this reaction was already shown in eq 1.2 where germene **6** was formed from the thermolysis of bicycle **4**.

A wide variety of metallaenes have been formed in the gas phase[32-34] as well as in the condensed phase[35-37] from the thermolysis or photolysis of silacyclobutanes and germacyclobutanes. Ring opening is understood to proceed by cleavage of the M-C bond to form a 1,4-biradical,[38] which then collapses to form the metallaene and ethene. An example of a gas-phase thermal decomposition of germacyclobutane **14** by R. T. Conlin and coworkers[32] is shown in eq 1.5. Vacuum pyrolysis of 1,1-dimethylgermacyclobutane (**14**) yielded ethene, propene, cyclopropane, 1,1,3,3-tetramethyl-1,3-digermacyclobutane (**17**) and 1,1,2,2-tetramethyl-1,2-digermacyclopentane (**18**). Compound **17** is understood to be the dimerization product of 1,1-dimethylgermene (**15**), whereas the formation of **18** suggests the insertion of dimethylgermylene (**16**) into the strained germanium-carbon bond of **14**.

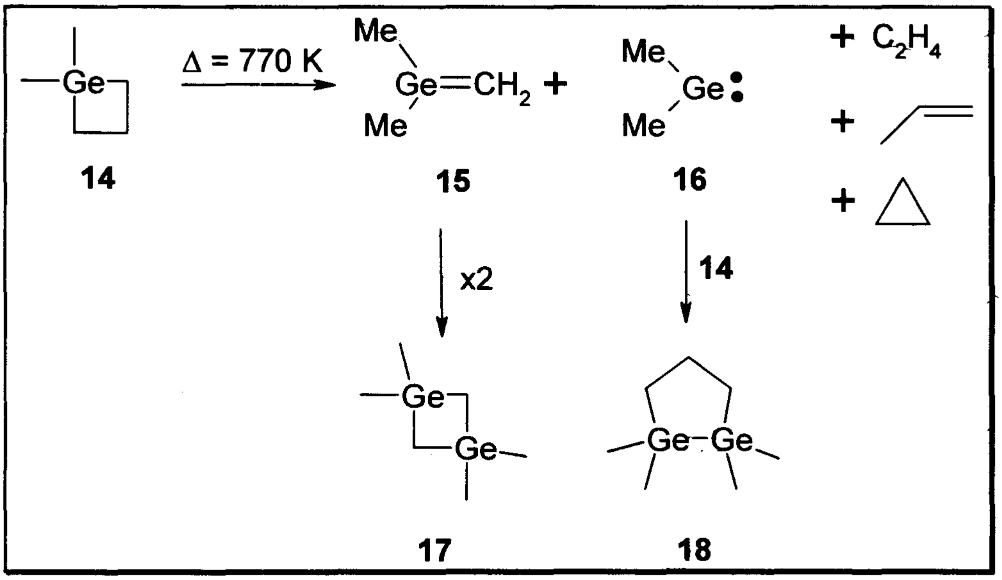

1.5

This reaction has also been demonstrated to proceed in the solution phase photolysis of 1,1-diphenylgermacyclobutane **19a** (eq 1.6).[36, 39] The intermediacy of 1,1-diphenylgermene **20a** in the photolysis of **19a** is suggested by the formation of its head-to-tail dimer **21a**, and adducts with various trapping reagents as discussed in the following section. These particular cycloreversion reactions ([2 + 4] and [2 + 2]) provide an excellent method for the generation of both silenes and germenes.

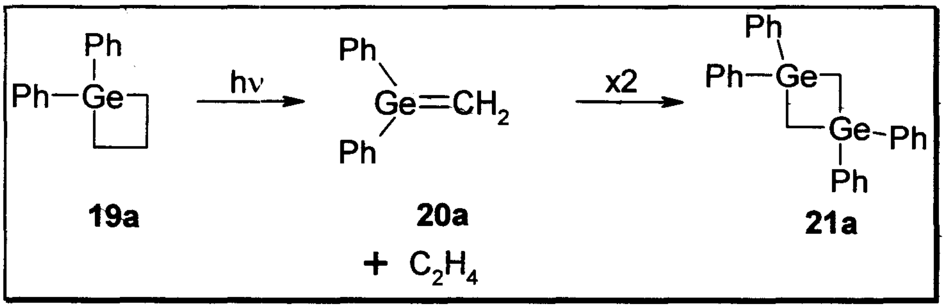

1.6

1.4 Reactivity of Silenes and Germenes

1.4.1 Trapping Reactions of Group 14 Metallaenes

Since the majority of group 14 metallaenes are transient species their presence can be inferred by the products that form upon reaction with various nucleophiles. Commonly employed traps used with metallaenes are amines, alcohols and dienes, which give the products **23**, **24** and **25**, respectively (eq 1.7).[6, 7, 10, 40]

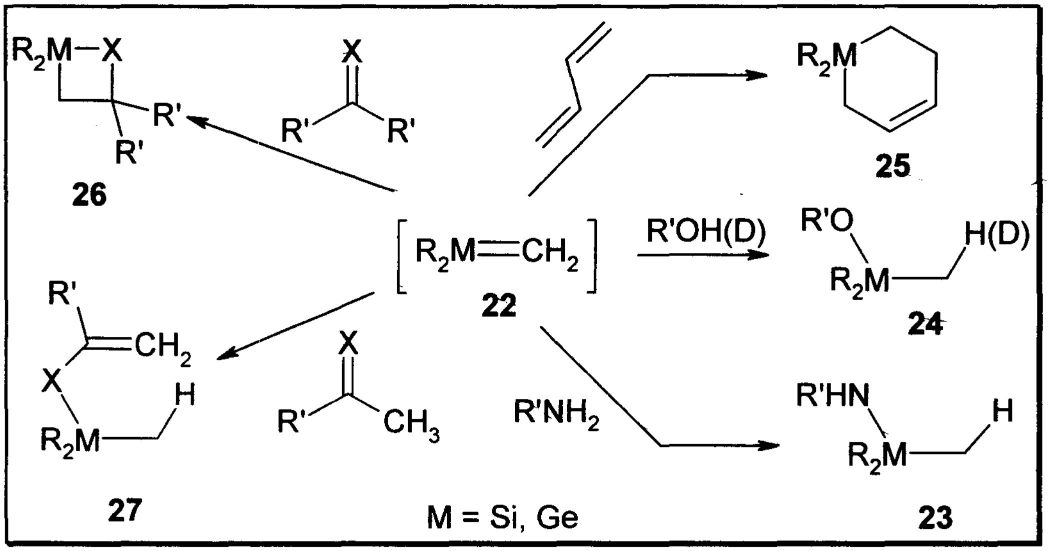

1.7

Metallaenes have also been reported to react with alkenes and ketones in a [2 + 2] cycloaddition to yield products **26** or via ene-reaction to yield **27**.[6, 7, 10, 40] Aliphatic alcohols are the most commonly used trapping reagents for silenes and germenes. The mechanism of alcohol addition to metallaenes has been of great interest over the past twenty years[11, 36, 41-43] and will be discussed in the following section.

1.4.2 Mechanism of Alcohol Addition to Silenes

N. Wiberg[11] was the first to study silene reactivity with aliphatic alcohols in the condensed phase. Thermolysis of **28** led to the formation of 1,1-dimethyl-2,2-bis(trimethylsilyl)-silene (**8**) through a [2 + 2] cycloreversion. Generation of **8** in the presence of a variety of alcohols allowed for the determination of relative rate constants for the reaction of **8** with alcohols (eq 1.8).

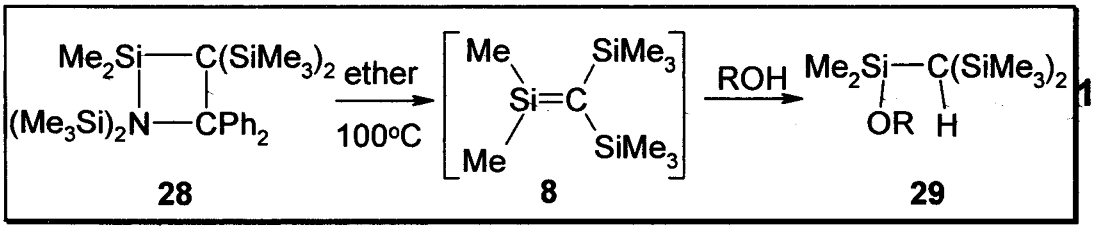

1.8

Wiberg[11] reported that the relative rates of reaction of **8** with alcohols was dependent on the steric bulk and nucleophilicity of the alcohol. The relative rates of alcohol addition to **8** in ether at 100 °C are: methanol > ethanol > isopropanol > *tert*-butanol > 1-pentanol > cyclohexanol > phenol. The fact that the most acidic alcohol (phenol) reacts the slowest with silene **8** suggests that the first step of the reaction is nucleophilic attack at silicon.[11]

This work exemplifies the difference in reactivity between alkenes and metallaenes. Typically, alkenes react with alcohols through electrophilic additions, commonly called Markovnikov additions. This involves initial protonation of the alkene with a strong acid to yield a carbocation which is subsequently attacked by an alcohol to form the corresponding ether (eq 1.9).[44] Nucleophilic attack of alkenes by alcohols are only observed when one of the carbons in the double bond is made electrophilic through resonance or inductive effects (eq 1.9). Under these special conditions the nucleophilic addition of the alcohol is called a Michael reaction.[44]

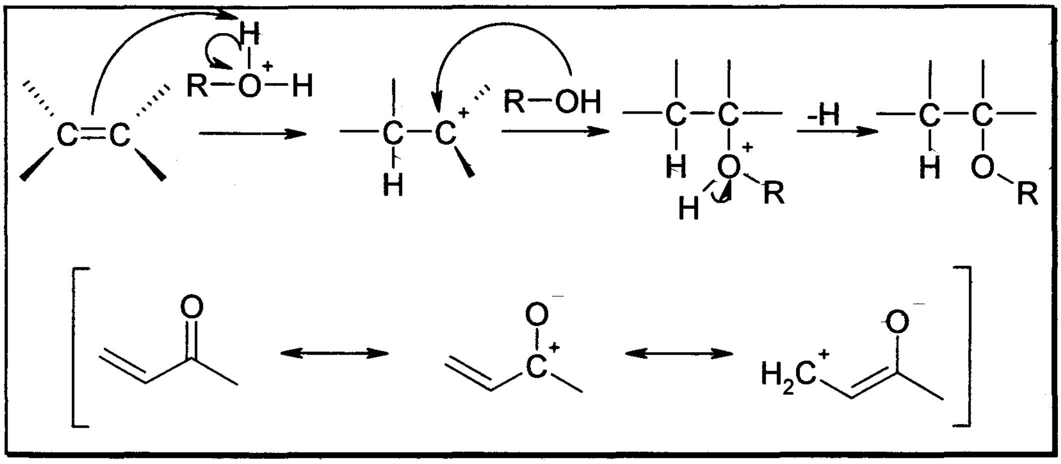

1.9

On the other hand, results from the reaction of **8** with alcohols show that silenes are initially attacked by the oxygen atom of the alcohol. Considering the polarity of the Si=C bond and the products formed, the nucleophilic attack must take place at the silicon atom to yield a zwitterionic intermediate. This intermediate then collapses via a proton-transfer to form the corresponding silyl ether **29** (eq 1.10).[11] This mechanism is analogous to the Michael addition mentioned above.

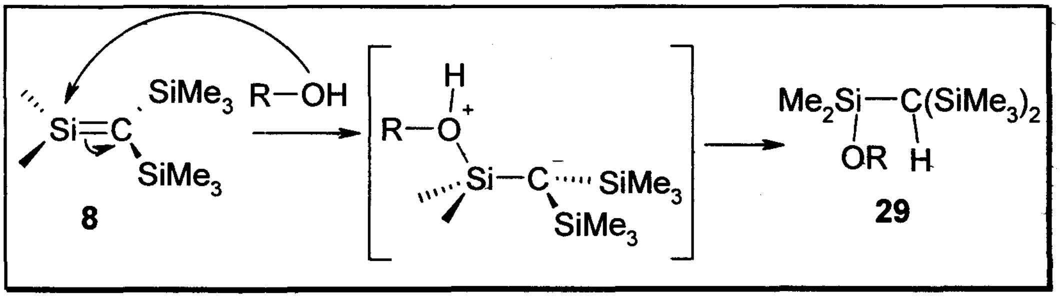

1.10

Further work involving silene **31** by Kira and coworkers[43] provided further mechanistic details about alcohol addition to silenes, specifically concerning the nature of the proton transfer step. Steady-state photolysis of the cyclic disilane **30** led to the formation of silene **31** which was trapped with alcohols to produce the silyl ethers **32** and **33** (eq 1.11). Silyl ether **32** is the result of *syn*-addition of alcohol to **31**, whereas **33** is the product of *anti*-addition.[43] In the case of methanol trapping, the product distribution of silyl ethers **32** and **33** are shown to be dependent on the concentration of the alcohol, with the *anti*-isomer (**33**) predominating at high concentrations of alcohol, and the *syn*-isomer (**32**) predominating at low concentrations.[43]

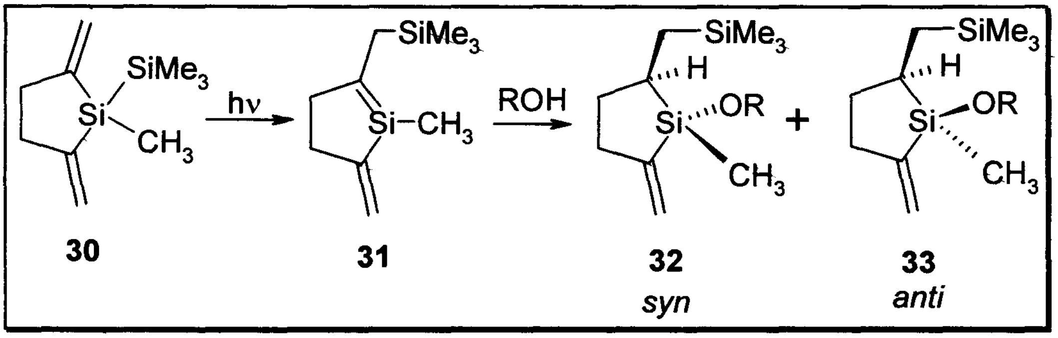

1.11

These results shed more light on the mechanism of addition of alcohol to silenes. The initial step involves nucleophilic attack of the alcohol to the silene to yield the zwitterionic intermediate described in eq 1.10. The intermediate then collapses to product by two competing pathways. One pathway consists of an *intra*molecular proton transfer to **32** and is favoured at low alcohol concentrations. At higher concentrations an *inter*molecular proton transfer occurs involving a second molecule of alcohol to facilitate the formation of **32**.

A study of the kinetics of addition of alcohols to the transient conjugated silene **35** provided support for the mechanism proposed by Wiberg and Kira. Photolysis of **34** leads to a [1,3]-sigmatropic shift of a silyl group to the phenyl ring to yield 1,3,5-silahexatriene **35**. Addition of methanol produces a delocalised zwitterion which collapsed by proton transfer to yield a mixture of alkoxysilanes (eq 1.12).[45-48] It was observed that the product distribution from the photolysis of **34** was also dependent on the concentration of methanol. At low concentrations of methanol, the [1,2]-addition product **36** was found to predominate, whereas at higher concentrations of methanol, the major products were the [1,4]- and [1,6]-addition products, **37** and **38**, respectively.

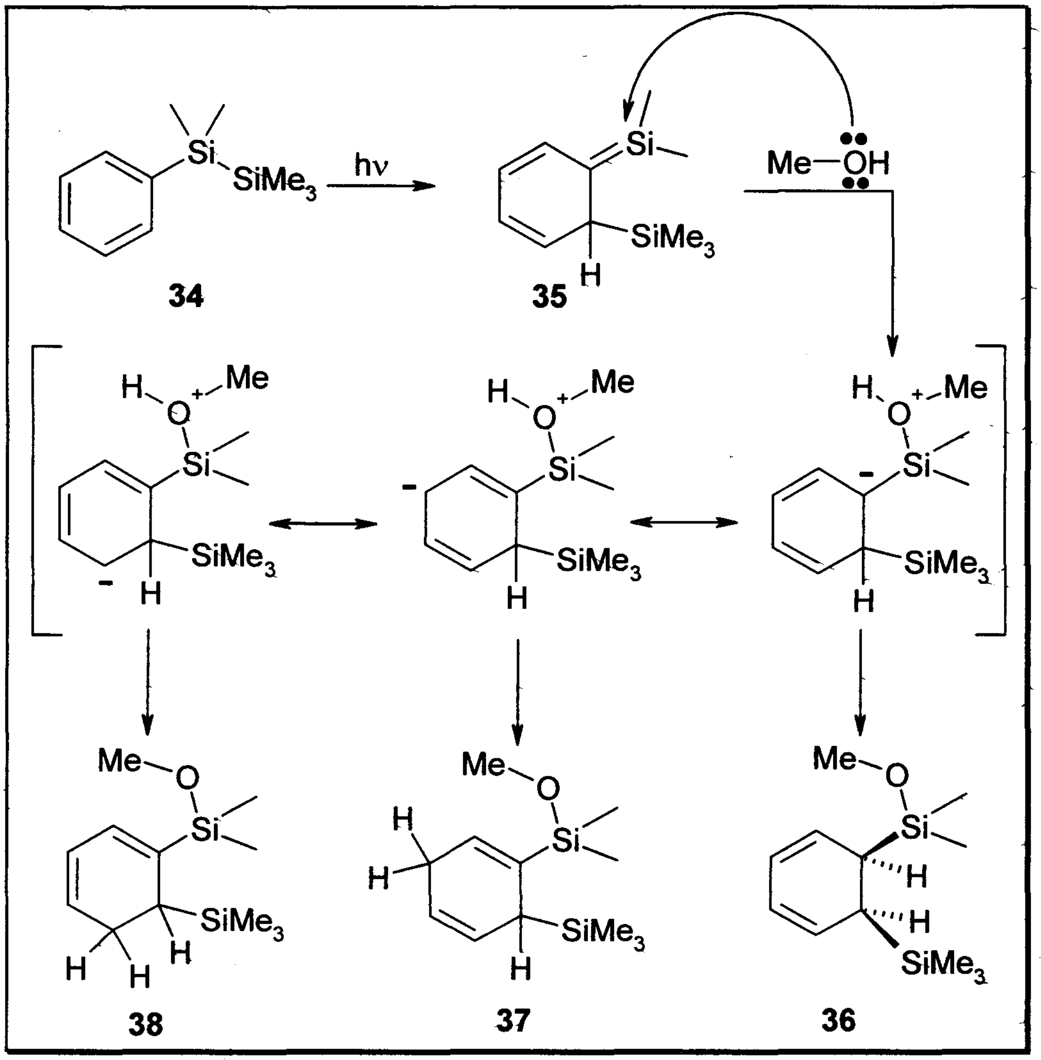

1.12

The mechanism of alcohol addition to silene **35** was also studied directly using time-resolved methods. Nanosecond laser flash photolysis of **35** led to the formation of a transient that had λ_{max} = 425 nm in acetonitrile[45] and was identified as silahexatriene **36**. Upon addition of methanol, the lifetime of **36** is shortened and it decays with pseudo-first order kinetics, allowing determination of absolute rate constants by monitoring the lifetime as a function of concentration. Plots of methanol concentration versus the observed rate of decay (k_{decay}) led to curved plots that were fitted to the expression of eq 1.13, where k_o represents the rate constant for decay of the silene in absence of quencher, k_q is the second order rate constant for the reaction of silene with methanol, and k_{2q} is the third order rate constant for the reaction of silene with two molecules of methanol.

$$k_{decay} = k_o + k_q[\mathrm{MeOH}] + k_{2q}[\mathrm{MeOH}]^2 \qquad \mathbf{1.13}$$

The rate constants for addition of methanol to **35** in acetonitrile at 21 °C[42] were reported as $k_q = (2.3 \pm 0.7) \times 10^8\ \mathrm{M^{-1}s^{-1}}$ and $k_{2q} = (49 \pm 10) \times 10^8\ \mathrm{M^{-2}s^{-1}}$. The quadratic relationship between methanol concentration and the observed rate constant provides further validity to the mechanism proposed by Kira and Wiberg. The mechanism of methanol addition to silene involves initial nucleophilic attack (k_1) of methanol to form a zwitterionic intermediate. The initial step is reversible meaning that the intermediate may convert back to free silene (k_{-1}) or undergo two competing proton transfers. The proton transfers can be *intra*molecular (k_2) or *inter*molecular (k_3) to form the alkoxysilane (eq 1.15). When the steady-state approximation is used for the intermediate, the observed rate of decay (k_{decay}) can be expressed as:

$$k_{decay} = k_Q + \frac{k_1[\mathrm{MeOH}]}{(k_{-1} + k_2 + k_3[\mathrm{MeOH}])}\{k_2 + k_3[\mathrm{MeOH}]\} \qquad \mathbf{1.14}$$

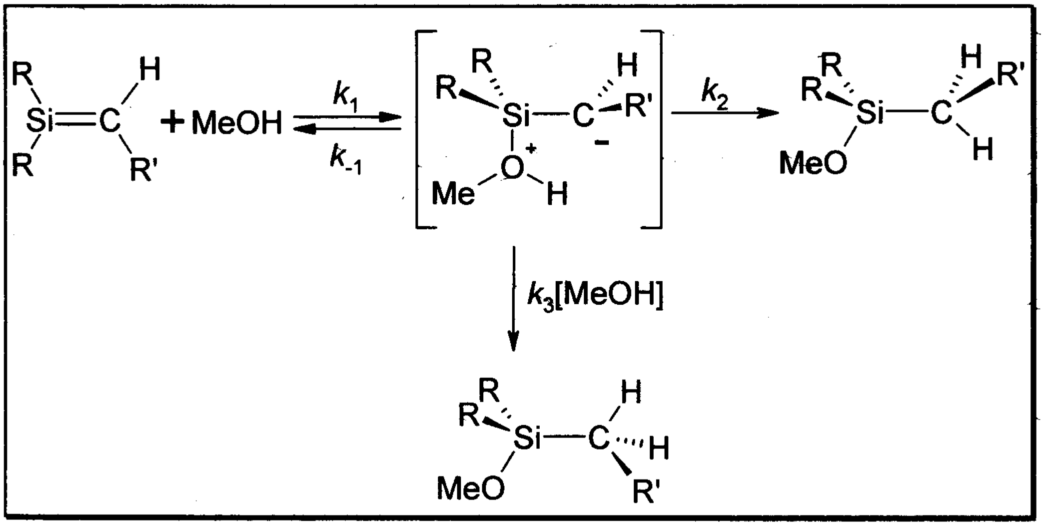

1.15

1.4.3 Reactivity of Group 14 1,1-diphenylmetallaenes

The photolysis of 1,1-diphenylsilacyclobutane (**39**) produces a transient that absorbs at λ_{max} = 320 nm in acetonitrile[41] which has been assigned to 1,1-diphenylsilene (**40**) (eq 1.16). 1,1-Diphenylsilene (**40**) reacts with methanol to form methoxydiphenylsilane **41** (eq 1.19). Silene **40** is considerably

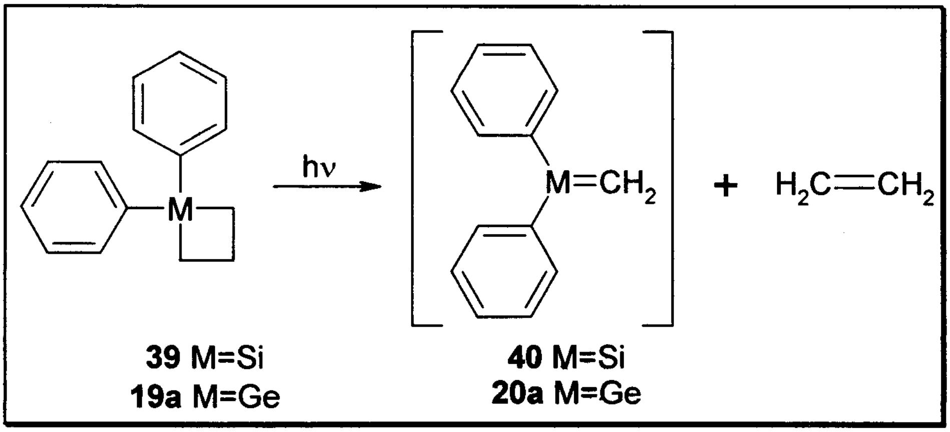

1.16

more reactive than **35** and its k_{decay} shows a linear dependence on alcohol concentration.[41] This result indicates that the zwitterionic complex collapses exclusively by the *intra*molecular proton transfer (k_2) over the concentration ranges studied.[41] With the assumption that k_3[MeOH] << k_2, the expression in eq 1.14 can be reduced to:

$$k_{decay} = k_o + \frac{k_1}{(k_{-1} + k_2)} k_2[\mathrm{MeOH}] \qquad \mathbf{1.17}$$

In this case the rate constant for addition of methanol to silene is dependent on the initial rate of complexation (k_1) and a partitioning ratio for reaction of the complex $k_2/(k_{-1} + k_2)$. The revised mechanism for the reaction of silene **40** with nucleophiles is shown in eq 1.19. The rate of decay of **40** versus the concentration of methanol in acetonitrile can be fit to the expression shown in eq 1.18.[41, 49] In addition, a primary isotope effect is observed ($k_H/k_D = 1.5$) for the addition of deuterated methanol to **40**, indicating that the rate-determining step in the mechanism is the *intra*molecular proton transfer from the zwitterionic intermediate (Table 1.2).[41]

$$k_{decay} = k_o + k_q[\mathrm{MeOH}] \qquad \mathbf{1.18}$$

Reaction of 1,1-diphenylsilene with acetic acid affords a rate constant faster than that of methanol (Table 1.2).[41] The measured kinetic isotope effect for this reaction is near unity, indicating that the proton transfer is not the rate-determining step. Acetic acid is a substantially more acidic trapping reagent than methanol causing $k_2 >> k_{-1}$ and making the initial formation of the complex (k_1) the rate-determining step for reaction (eq 1.19).[41, 50] However, this is not the only mechanistic possibility that is consistent with the isotope effect data and linear dependence on acetic acid concentration. The data is also consistent with a step-wise pathway initiated by protonation at carbon or a concerted mechanism.

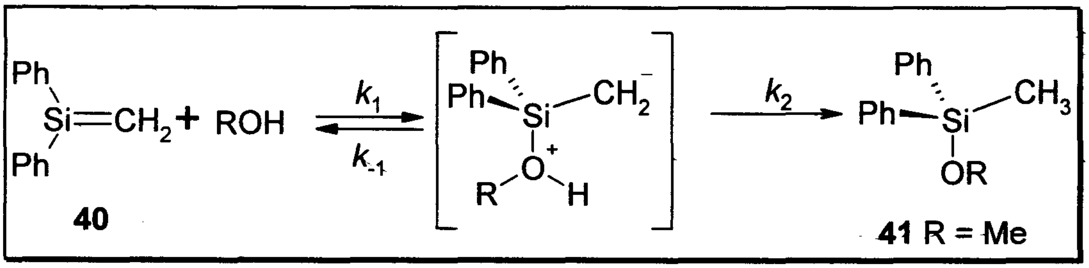

1.19

Acetone addition to 1,1-diphenylsilene is an order of magnitude slower than both methanol and acetic acid additions.[51] The rate constant for reaction is lowered by α-deuteration of acetone leading to a measured kinetic isotope effect of $k_H/k_D = 2.2 \pm 0.2$. This indicates that the α-hydrogen transfer is the rate-determining step of the reaction. This is consistent with the mechanism in eq 1.20 which is similar to that of methanol and acetic acid. Acetone is a weak acid ($pK_a = 20$[44]) causing the proton transfer to be slower which affords a larger kinetic isotope effect.[51] The rate constants for addition of methanol, *tert*-butanol, acetic acid, acetone and *n*-butylamine to silene **40** are shown in Table 1.2.[41]

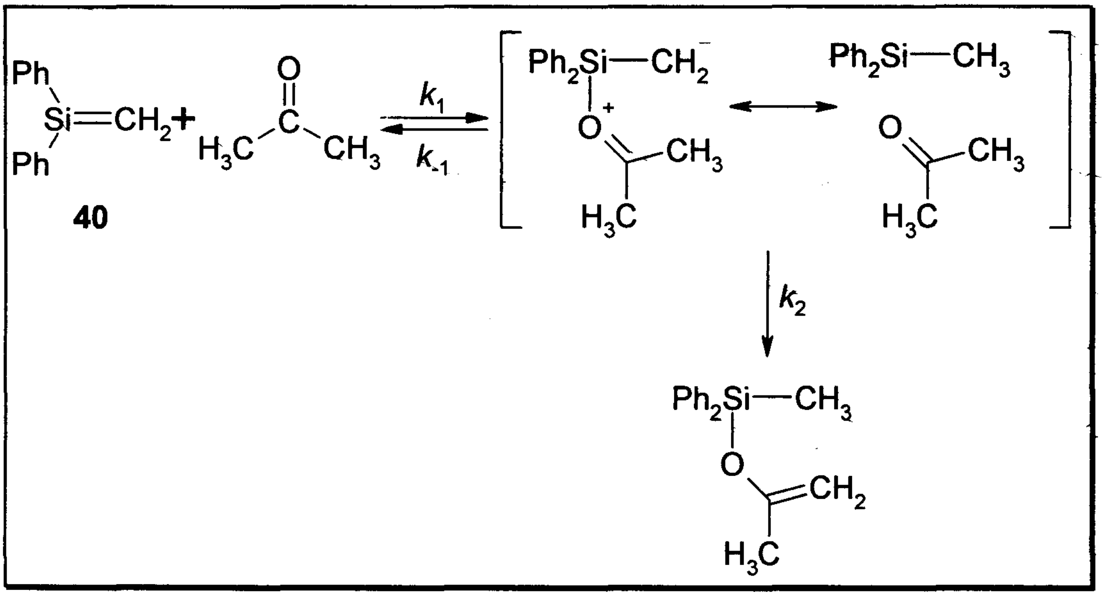

1.20

The germanium analogue, 1,1-diphenylgermacyclobutane (**19a**), has also been shown to produce a transient upon photolysis that has a λ_{max} = 320 nm in hexane (eq 1.16).[36] This transient has been assigned to 1,1-diphenylgermene (**20a**) and shows reduced reactivity toward nucleophiles in comparison to 1,1-diphenylsilene (**40**). In fact, the decay rate of **20a** in acetonitrile has been shown to have a squared dependence on methanol concentration[36] over the concentration ranges studied. This indicates that the *intra*molecular proton transfer (k_2) is very slow and that the complex collapses exclusively by the *inter*molecular proton transfer (k_3). This type of behaviour most likely proceeds via a protonation–deprotonation sequence involving a second molecule of methanol (eq 1.22).[43, 52] Application of the equilibrium assumption for the germene-alcohol complex leads to the expression shown in eq 1.21 for the pseudo-first order rate constant for decay of **20a** in the presence of alcohol.

$$k_{\mathrm{decay}} = k_0 + \frac{k_1}{k_{-1}} k_3[\mathrm{MeOH}]^2 \qquad \mathbf{1.21}$$

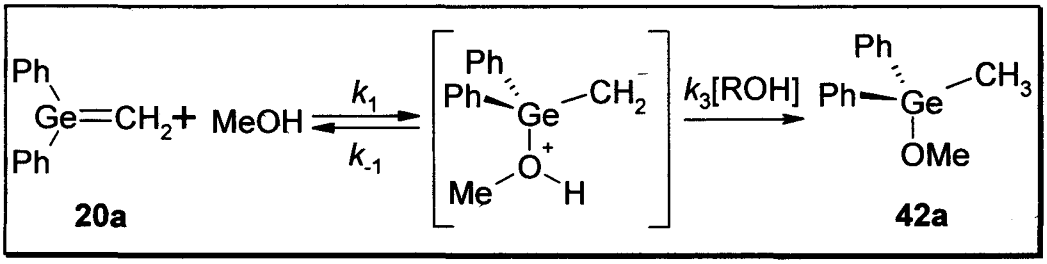

1.22

A primary isotope effect is also observed for the addition of alcohols to germene **20a** in hexane, indicating the proton transfer is rate determining. 1,1-Diphenylgermene **20a** shows the same general trend in reactivity toward nucleophiles as 1,1-diphenylsilene, but with reduced rate constants. In fact, no evidence for a reaction between 1,1-diphenylgermene **20a** and acetone could be obtained by either steady state or fast time-resolved spectroscopic methods. The bi- and termolecular rate constants for addition of methanol, *tert*-butanol, acetic acid, acetone and *n*-butylamine with 1,1-diphenylgermene (**20a**) and the

Table 1.2 Rate constants for the addition of nucleophiles to 1,1-diphenylsilene (**40**) and 1,1-diphenylgermene (**20a**) in air-saturated hexane at 23-25 °C[a] unless otherwise stated.

	$Ph_2Si{=}CH_2$ (**40**)[41, 51, 53]		$Ph_2Ge{=}CH_2$ (**20a**)[36, 37]		
Quencher	k_q / 10^9 $M^{-1}s^{-1}$	k_H/k_D	k_q / 10^7 $M^{-1}s^{-1}$	k_{2q} / 10^7 $M^{-2}s^{-1}$	k_H/k_D
MeOH[b]	1.2 ± 0.1	1.5 ± 0.2	<0.03 ± 0.2	2.2 ± 0.2	c
t-BuOH[b]	0.22 ± 0.02	1.6 ± 0.1	<0.04 ± 0.3	0.14 ± 0.02	c
AcOH	3.1 ± 0.3	1.1 ± 0.1	16 ± 2	–	0.9 ± 0.1
Acetone	0.18 ± 0.01[d]	2.2 ± 0.2[d]	< 0.04 ± 0.01	–	c
n-$BuNH_2$	6.5 ± 0.1	c	5 ± 1	–	c

a. Errors reported as ± 2σ from linear least squares analysis of k_{decay} – concentration data according to eq 1.18 or 1.21.
b. Rate constants reported in air-saturated acetonitrile.
c. Not measured.
d. Rate constants reported in air-saturated isooctane.

silicon analogue **40** are collected in Table 1.2,[36] to illustrate the differences between the two metallaenes.

The much lower reactivity of 1,1-diphenylgermene **20a** compared to 1,1-diphenylsilene **40** toward nucleophiles has been attributed primarily to the higher electronegativity of germanium compared to silicon.[36, 37] This leads to a reduction in the electrophilicity of the M=C bond, which in turn reduces the rate of the initial complexation step of these reactions. The resulting zwitterionic complex is weaker causing the rate of proton transfer to be less than the rate of reverting back to the germene.

In a similar study,[54] the germacyclobutanes **19b,c** were studied using nanosecond laser flash photolysis in hexane solution. It was found that upon 248 nm photolysis, the precursors produced transients that had absorption maxima at 325 nm. On the basis of the observed transient absorption maxima and steady-state photolysis studies with methanol, the transients were assigned to the corresponding 1,1-diarylgermenes (**20b**,**c**) as illustrated in eq 1.23.[54] Steady-state photolysis of **19b,c** in the presence of methanol also provided evidence for the formation of a second transient, the diarylgermylenes **59b,c**.[54] Quenching of germene **20b** with methanol in air-saturated hexane solutions were found to be quadratic in concentration with bi- and termolecular rate constants of (5 ± 4) x 10^7 $M^{-1}s^{-1}$ and (1.1 ± 0.2) x 10^{10} $M^{-2}s^{-1}$, respectively. On the other hand, it was found that the lifetime of germene **20c** was found to decrease linearly with methanol concentration over the concentration range studied to yield the bimolecular rate constant of (22 ± 2) x 10^7 $M^{-1}s^{-1}$.[54]

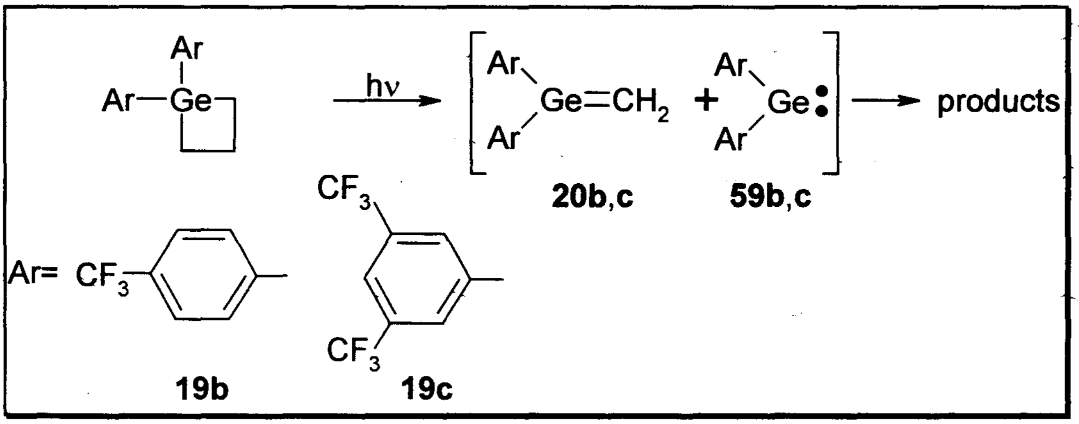

1.23

Another category of precursors that have been shown to produce 1,1-diphenylmetallaenes upon photolysis are shown in eq 1.24. The photolysis of 1,1,1-trimethyl-2,2,2-triphenyldisilane (**43a**) in non-polar solvents has been shown to cleanly extrude the transient 1,1-diphenyl-(1-sila)hexatriene **44a** in high yield[40, 42, 45, 55] via [1,3]-$SiMe_3$ migration into the phenyl ring. In polar solvents the photolysis of **43a** leads to high yields of the corresponding silyl free radicals, with silene **44a** being formed in low amounts. The higher yield of silyl free radicals formed in polar compared to non-polar solvents is attributed to the enhancement of intersystem crossing to the triplet state of the aryldisilanes.[55]

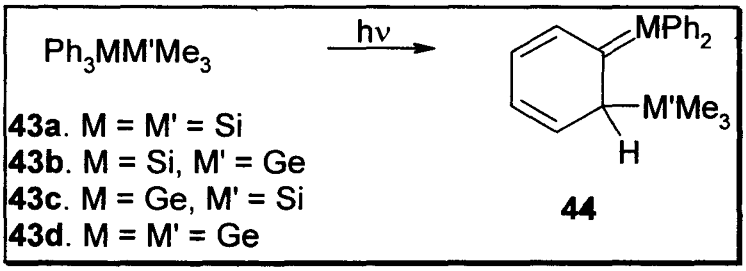

1.24

Recently this group studied the photochemistry of the trimethyltriphenylgermasilane derivatives **43b,c** and of 1,1,1-trimethyl-2,2,2-triphenyldigermane **43d** using steady-state and laser flash photolysis techniques.[56] The purpose of this work was to study the effects on the photochemistry of **43a** by systematically replacing one and then both silicon atoms with germanium. Upon photolysis, these precursors yielded the corresponding (1-metalla)hexatrienes **44b-d** and their reactivity towards various trapping reagents was studied by flash photolysis techniques.

Steady-state photolysis of a deoxygenated cyclohexane solution containing **43a** and DMB yielded the silatriene-DMB adduct **45a** in ~70% yield.[45] However, photolysis of **43b-d** under similar conditions in each case afforded complex mixtures containing more than a dozen products.[56] With each photolysis the metallahexatriene-DMB adducts (**45b-d**) were identified in the product mixtures, indicating that the desired metallahexatrienes **44b-d** are indeed produced from the photolysis of the precursors **43b-d** (eq 1.25-27). The yields of these adducts are significantly lower than that of silene **44a**. In addition, germacyclopentenes (**46** and **48a**) are observed, resulting from the [1+4] chelotropic addition of either dimethyl- or diphenylgermylene with 2,3-

dimethylbutadiene (eq 1.25-1.27), as well as silyl- and germyl-radical derived products.

These results indicate that the lowest excited singlet states of the three precursors react via two competing pathways to form reactive intermediates that are subsequently trapped by DMB. The first pathway involves a [1,3]-$SiMe_3$ or [1,3]-$GeMe_3$ migration to yield the corresponding (1-metalla)hexatrienes (**44b-d**) which is subsequently trapped by DMB to form **45b-d**. The other pathway involves the extrusion of dimethyl- or diphenylgermylene along with the co-product Ph_3MMe (**47_M**) or $Me_3M'Ph$ (**49_M**). Germylene extrusion is the major reaction pathway of the excited singlet states in each case. In contrast, this process does not occur in significant amounts upon photolysis of the disilane anologue **43a**.[45, 55]

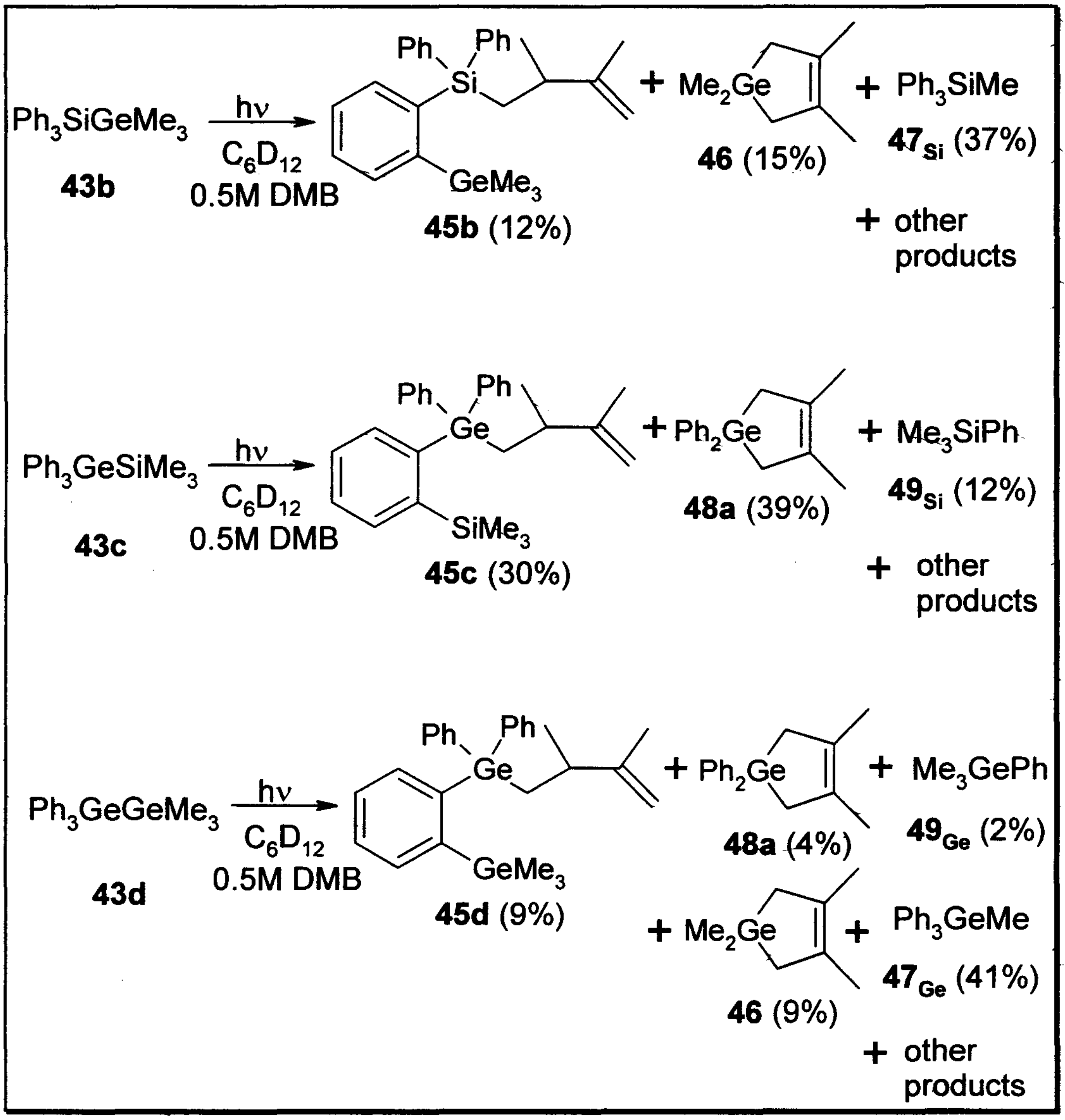

1.25

1.26

1.27

The photolysis of **43b-d** in deoxygenated cyclohexane-d_{12} solutions containing 0.07M chloroform afforded the trimethylchlorometallaenes **50_M** (30-40% yield), the triphenylchlorometallanes **51_M**, dichloromethane **52**, 1,1,2,2-tetrachloroethane **53**.[56] The formation of **50_M** and **51_M** are attributed to the reaction of Ph_3M• and Me_3M'• radicals with chloroform. The resulting dichloromethyl radicals then abstract hydrogen to form dichloromethane **52** or dimerize to yield **53** (eq 1.28). The formation of the radicals has been attributed to occur via the triplet states of **43b-d**.[56]

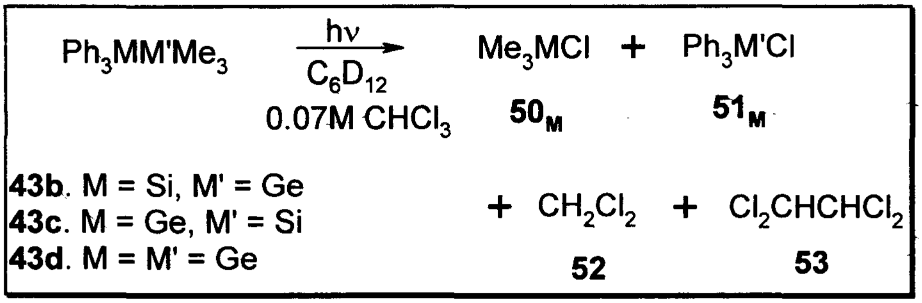

$$\mathrm{Ph_3MM'Me_3} \xrightarrow[\substack{\mathrm{C_6D_{12}}\\ \mathrm{0.07M\ CHCl_3}}]{h\nu} \underset{\mathbf{50_M}}{\mathrm{Me_3MCl}} + \underset{\mathbf{51_M}}{\mathrm{Ph_3M'Cl}} + \underset{\mathbf{52}}{\mathrm{CH_2Cl_2}} + \underset{\mathbf{53}}{\mathrm{Cl_2CHCHCl_2}}$$

43b. M = Si, M' = Ge
43c. M = Ge, M' = Si
43d. M = M' = Ge

1.28

Laser flash photolysis studies of **43b-d** showed similar transient absorption spectra. In each case two strong absorption were observed centering at short (300-320 nm) and long (480-490 nm) wavelengths. The observed absorptions were assigned to two transient species: triphenylsilyl or triphenylgermyl radicals and the (1-metalla)hexatrienes **44b-d**. The radical species exhibit a strong absorption at shorter wavelengths (300-320 nm) and were identified by comparison with previously published spectra.[57, 58] Moreover, these transient are quenched by chloroform with rate constants on the order of $k_q \approx 1.7 \times 10^8\ M^{-1}s^{-1}$, which is also in excellent agreement with published results.[57]

The transients at λ_{max} = 480-490 nm were identified based on a comparison with the reported transient absorption spectra of **44a**,[55] and the fact that the lifetimes of the transients are reduced by typical silene and germene trapping reagents such as acetic acid, acetone, DMB and methanol. Plots of k_{decay} versus concentration of methanol for **44b** were curved, but fit acceptably to the second-order polynomial expression of eq 1.13. Similar plots for the other trapping reagents were linear and could be analyzed using eq 1.18. The bi- and termolecular rate constants for reaction of **44b** with methanol, acetic acid, acetone and DMB are shown in Table 1.3. The listed rate constants for reaction of **44b** are very similar to that of the (1-sila)hexatriene **44a**.

The (1-germa)hexatriene **44c** is one to three orders of magnitude less reactive than the silicon analogues **44a** and **44b**. In fact, the lifetime of germene **44c** was not affected by additions of methanol up to a total methanol concentration of 1.7 M. Plots of k_{decay} versus concentration for the other trapping agents were linear and were fit to eq 1.18. Finally, the rate constant of reaction of germenes **44c** and **44d** with various trapping reagents were measured and are listed in Table 1.3.

Table 1.3 Rate constants (in units of $10^8\ M^{-1}s^{-1}$) for quenching of transient 1-Metallahexatrienes (**44a** – **44d**)[56] with Methanol, Acetic Acid, Acetone and 2,3-Dimethyl-1,3,butadiene (DMB) in Hexane Solution at 23°C[a].

Quencher	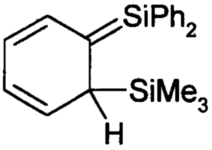 **44a**	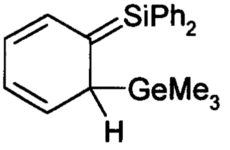 **44b**	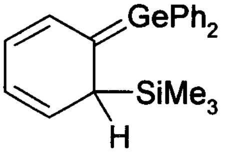 **44c**	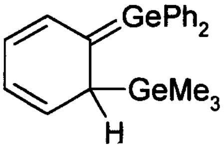 **44d**
MeOH	(1.1 ± 0.4)+ (64±12)[MeOH]	(1.5 ± 0.6)+ (58±13)[MeOH]	<0.001[c]	b
AcOH	3.69 ± 0.48	2.21 ± 0.20	0.0039 ± 0.0005	b
Acetone	5.42 ± 0.05	5.68 ± 0.03	0.0021 ± 0.0005	b
DMB	0.30 ± 0.01	0.34 ± 0.03	0.030 ± 0.003	0.027 ± 0.002

a. From least-squares fitting of k_{decay} vs [Q] data according to eq 1.13 or 1.18. Errors are quoted as ±2σ.
b. Not determined.
c. Addition of up to 1.7 M MeOH had no effect on the lifetime in deoxygenated solution.

1.5 Objectives of this work

The goal of this work is to study the photochemical behaviour of two novel potential germene precursors, 1,1-bis(4-trifluoromethylphenyl)germacyclobutane **19b** and 1,1-bis(3,5-bis(trifluoromethyl)phenyl)germacyclobutane **19c** (Figure 1.6.1). The photolysis of these compounds is expected to afford the corresponding 1,1-diarylgermenes **20b** and **20c** in sufficiently high yields to allow direct detection by time-resolved UV absorption spectroscopy, so that various aspects of their reactivity might be studied.

The mechanisms of addition of methanol to 1,1-diphenylsilene **40** and 1,1-diphenylgermene **20a** were shown to be quite different (section 1.4.3). Germene **20a** is considerably less reactive than the silicon analogue and its lifetime exhibits a second order dependence on methanol concentration,whereas **40** exhibits a first order dependence on methanol concentration over a similar concentration range. This reduction in reactivity has been attributed to the low electrophilicity of the Ge=C bond in **20a**.

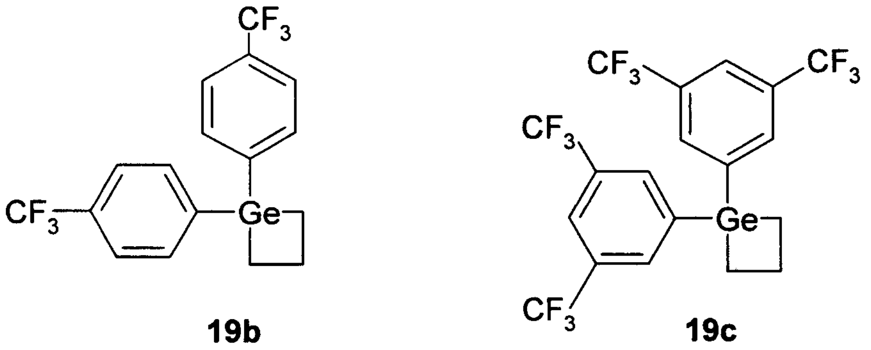

19b **19c**

Figure 1.6.1 1,1-bis(4-(trifluoromethyl)phenyl)germacyclobutane **19b** and 1,1-bis(3,5-bis(trifluoromethyl)phenyl)germacyclobutane **19c**.

The idea behind the present project is to determine whether the intramolecular proton transfer pathway can be activated by increasing the electrophilicity of the Ge=C bond in 1,1-diarylgermenes. Trifluoromethyl groups are good electron withdrawing groups and are an ideal substituent to increase the electrophilicity of the Ge=C bond. These two novel germenes (**20b**, **20c**) may be able to bridge the mechanistic difference between 1,1-diphenylgermene (**20a**) and 1,1-diphenylsilene (**40**) (Figure 1.6.2).

Other goals of this project include steady-state photolysis studies of **19b** and **19c** with methanol, 2,3-dimethyl-1,3-butadiene (DMB), and acetone, as well as in the absence of trapping reagents. In addition, absolute rate constants for addition of germenes **20b** and **20c** with various nucleophiles will be measured using nanosecond laser flash photolysis techniques. These rate constants will be directly compared with the equivalent rate constants reported for 1,1-diphenylgermene **20a** and 1,1-diphenylsilene **40**.

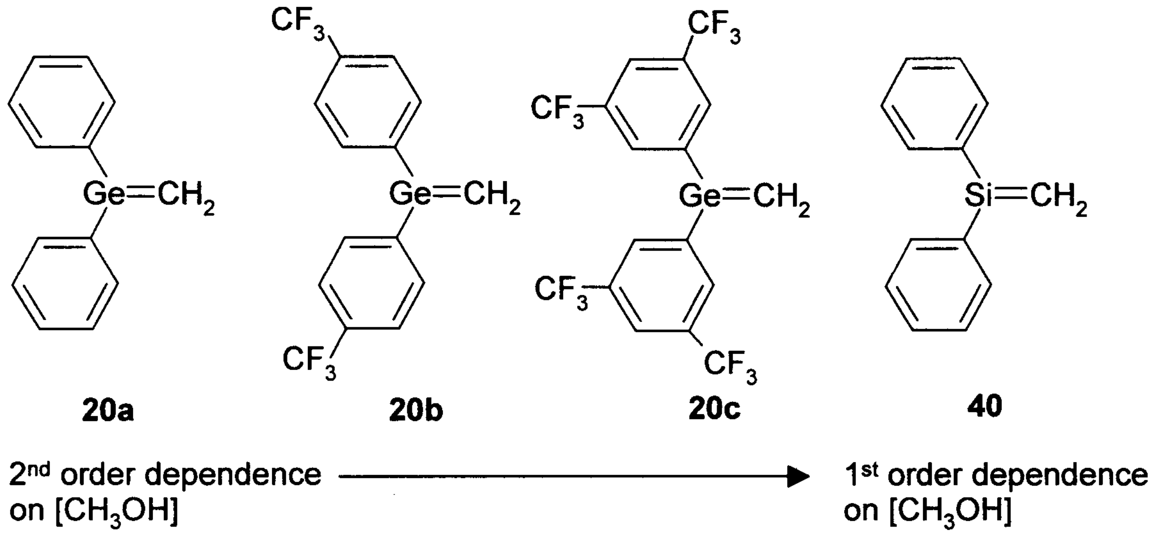

Figure 1.6.2 A possible mechanistic continuum between 1,1-diphenylgermene and 1,1-diphenylsilene using **20b** and **20c**.

CHAPTER 2: RESULTS

2.1 Synthesis

The syntheses of 1,1-bis(4-(trifluoromethyl)phenyl)germacyclobutane (**19b**) and 1,1-bis(3,5-bis(trifluoromethyl)phenyl)germacyclobutane (**19c**) were accomplished according to eq 2.1 and 2.2. The appropriate arylmagnesium bromide (either 4-trifluoromethylphenylmagnesium bromide **54b** or 3,5-bis(trifluoromethyl) phenylmagnesium bromide **54c**) was added to germanium tetrachloride at –78°C, resulting in mixtures of mono-, di-, and triarylated products as shown in eq 2.1. Identification of the products was carried out using GC/MS; all three compounds show prominent molecular ions in their mass spectra. GC analysis gave a product ratio of 1:4:1 for **55b**: **56b**: **57b** and 1:6:1 for **55c**: **56c**: **57c**, respectively.

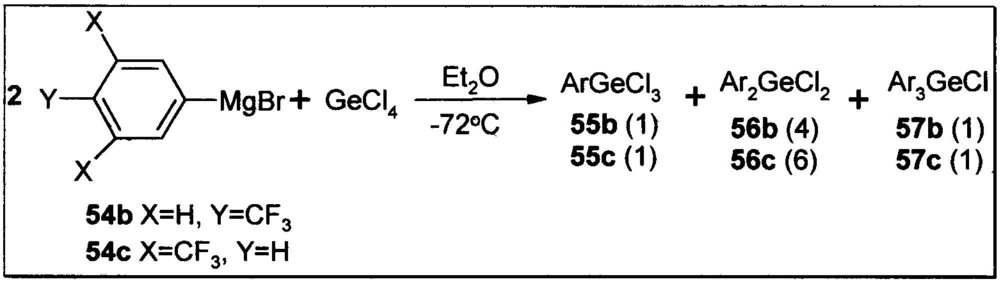

2.1

The second step in the syntheses of **19b** and **19c** employed the crude reaction mixtures of mono-, di-, and triarylgermanium chlorides, and was carried out by a modification of the procedure of Bickelhaupt and coworkers.[59] The modification in the preparation was that freshly ground magnesium turnings were used instead of sublimed magnesium in order to produce the 1,3-diGrignard reagent. As a result, reaction of a ~10 molar excess of ground magnesium with 1,3-dibromopropane followed by addition of ca. 0.1 molar equivalents of the aryl germanium chloride mixtures afforded the corresponding 1,1-diarylgermacyclobutanes (**19b** and **19c**) along with several other products (eq 2.2).

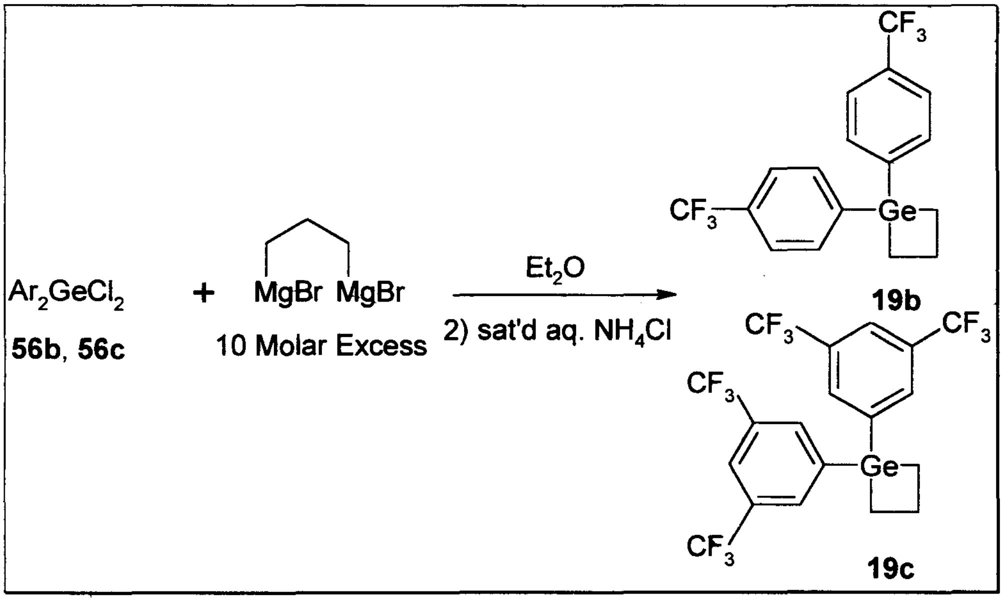

2.2

The desired germacyclobutanes were isolated by column chromatography, and then purified further by repeated column chromatography, followed by several recrystallizations from methanol. The purities of the two germacyclobutanes were >99.9% by GC. The overall yields of **19b**, **19c** starting from $GeCl_4$ were 31.3% and 20.7% respectively.

Both compounds were identified on the basis of ^1H, ^{13}C and ^{19}F NMR spectroscopy, mass spectrometry, combustion analysis and single crystal x-ray diffraction. (see Experimental Section 5.3 and Appendix 1). The crystal structures and the ^1H NMR spectra of **19b** and **19c** are shown in Figures 2.1.1 and 2.1.2, respectively. Both ^1H NMR spectra show the expected germacyclobutane splitting patterns of a triplet and a quintet; **19b** at δ = 2.06 ppm and δ = 2.45 ppm, and **19c** at δ = 2.18 ppm and δ = 2.50 ppm, respectively. In comparison, the ^1H NMR spectrum of 1,1-diphenylgermacyclobutane exhibits a triplet at δ = 1.96 ppm and a quintet at δ = 2.40 ppm.[36] The presence of the trifluoromethyl groups in **19b** and **19c** would be expected to cause a downfield shift of the signals from the parent compound, which is consistent with what is observed.[60] In the aromatic region compound **19b** shows two doublets at δ =

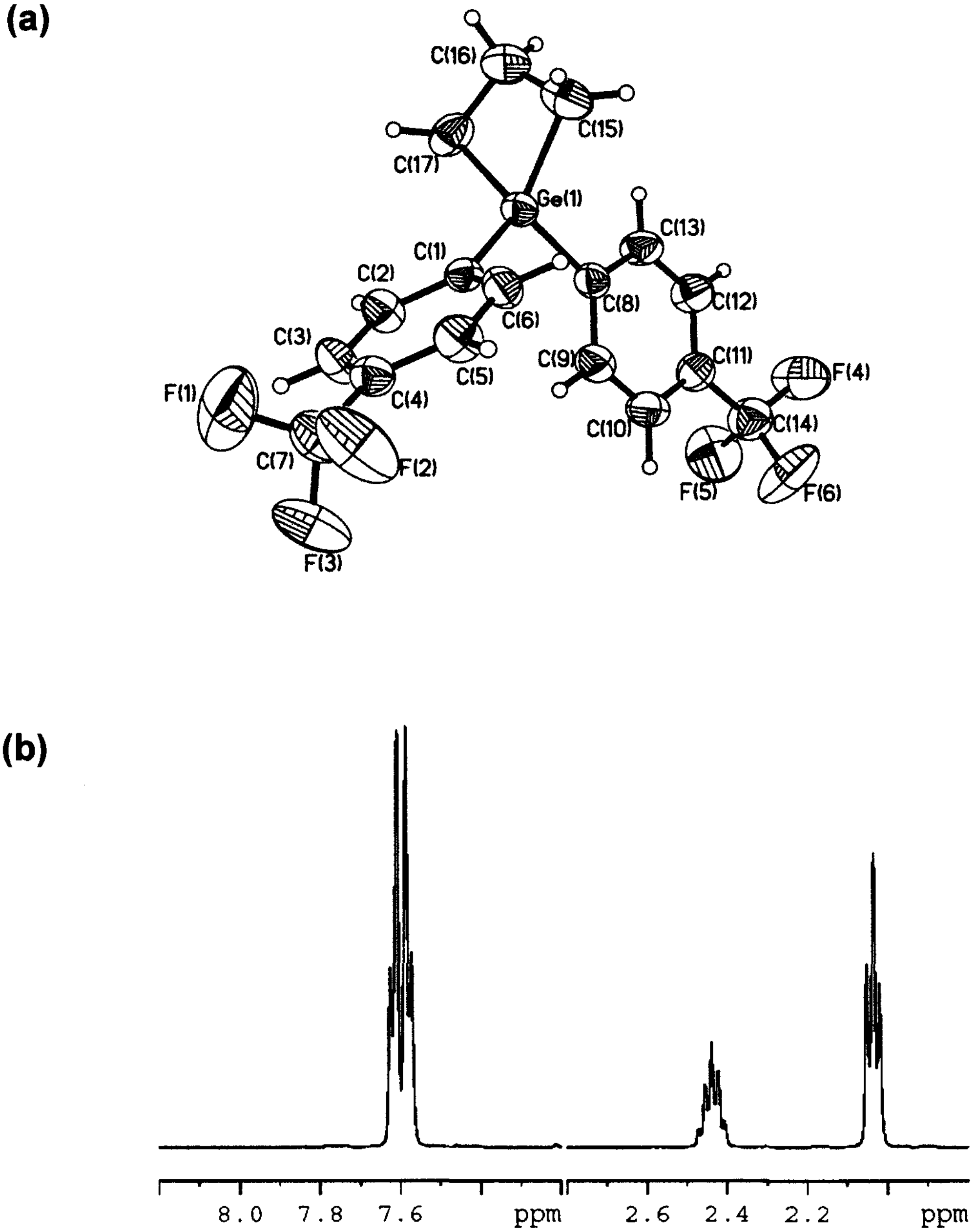

Figure 2.1.1 (a) The crystal structure of **19b**; ellipsoids are shown at the 50% probability level.
(b) The ^{1}H NMR (500 MHz) spectrum of purified 1,1-bis(4-(trifluoromethyl)phenyl)germacyclobutane **19b** recorded in $CDCl_3$.

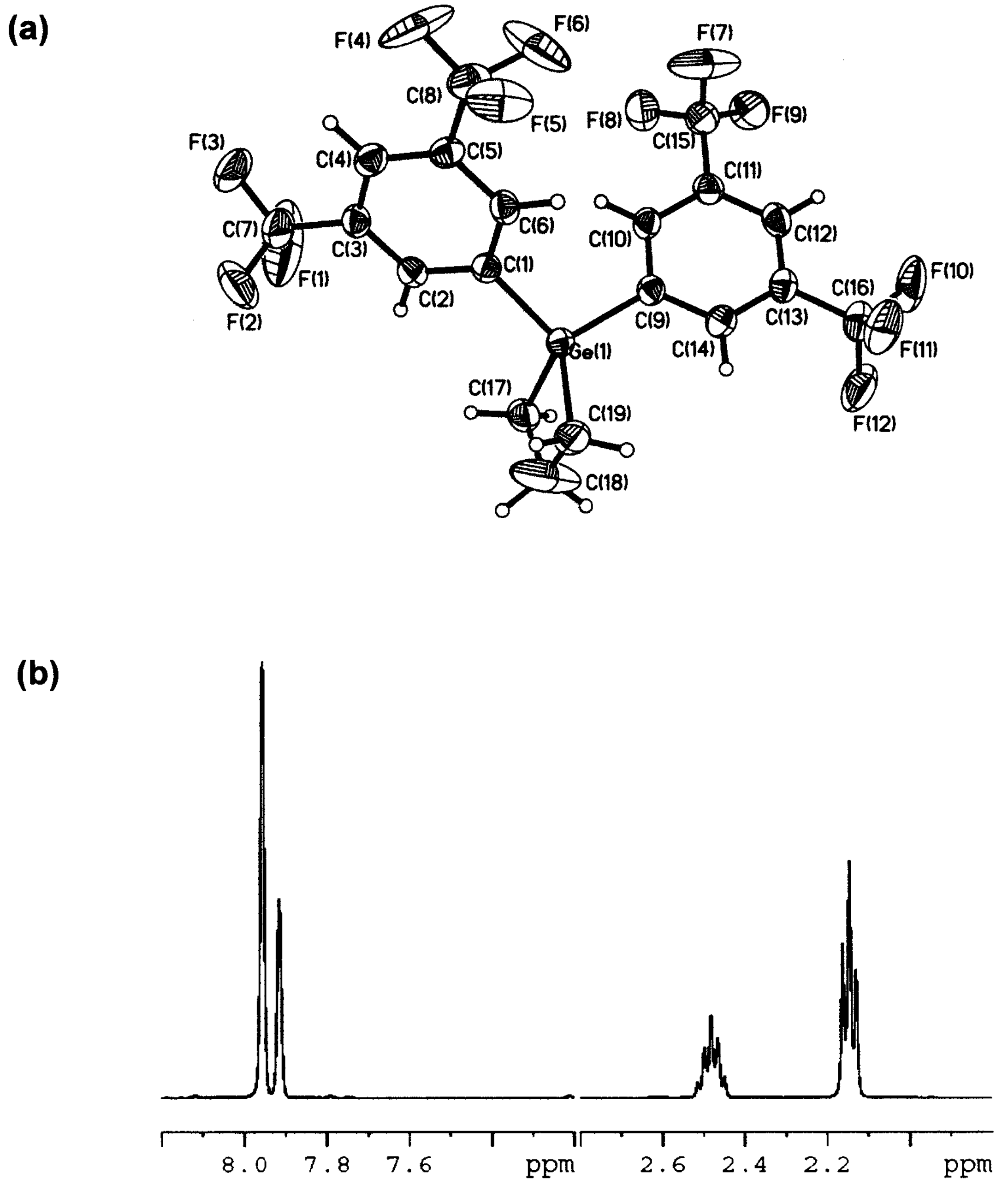

Figure 2.1.4 (a) The crystal structure of **19c**; ellipsoids are shown at the 50% probability level.
(b) The ^{1}H NMR (500 MHz) spectrum of purified 1,1-bis(3,5-bis(trifluoromethyl)phenyl)germacyclobutane **19c** recorded in $CDCl_3$.

7.67 ppm and δ = 7.70 ppm, whereas compound **19c** shows two singlets at δ = 7.96 ppm and δ = 7.98 ppm.

2.2 Ultraviolet Absorption Spectra of 19b and 19c

The UV absorption spectra of **19b** and **19c** in hexane solution at room temperature are shown in Figures 2.2.1 and 2.2.2, respectively, as plots of molar extinction coefficient (ε) versus wavelength (λ). The spectra of **19b** and **19c** show absorption maxima at 265 nm and 264 nm, respectively, corresponding to a benzenoid π,π^* absorption.[60] The extinction coefficients at 248 nm (ε_{248}) were found to be 1880 and 1423 $M^{-1}cm^{-1}$ for **19b** and **19c**, respectively.

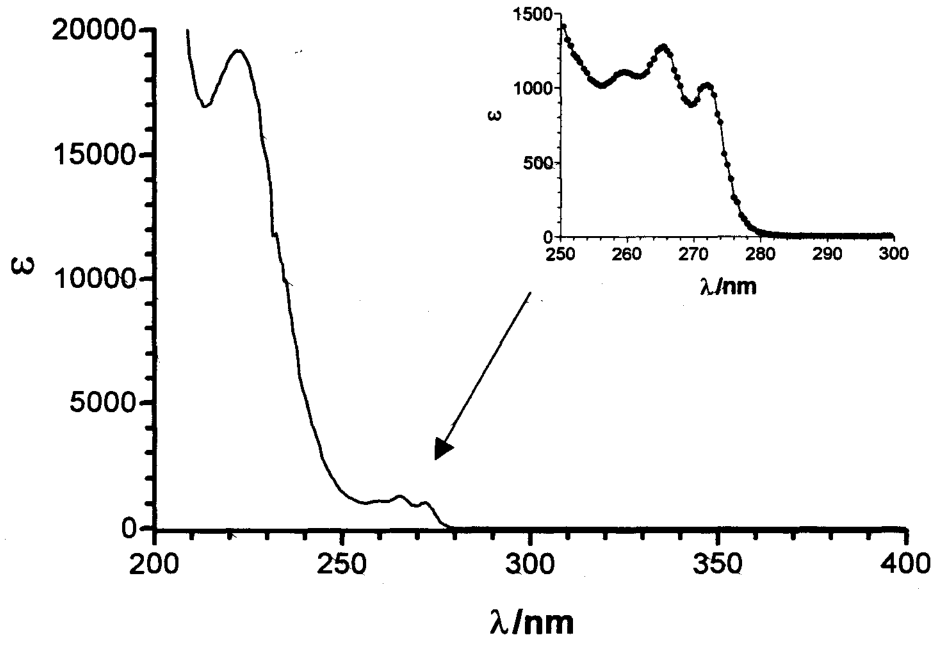

Figure 2.2.1 Ultraviolet absorption spectrum of **19b** in hexane at room temperature (ε_{248} = 1889 ± 10 $M^{-1}cm^{-1}$).
The inset shows the fine vibrational structure associated with the long wavelength absorption.

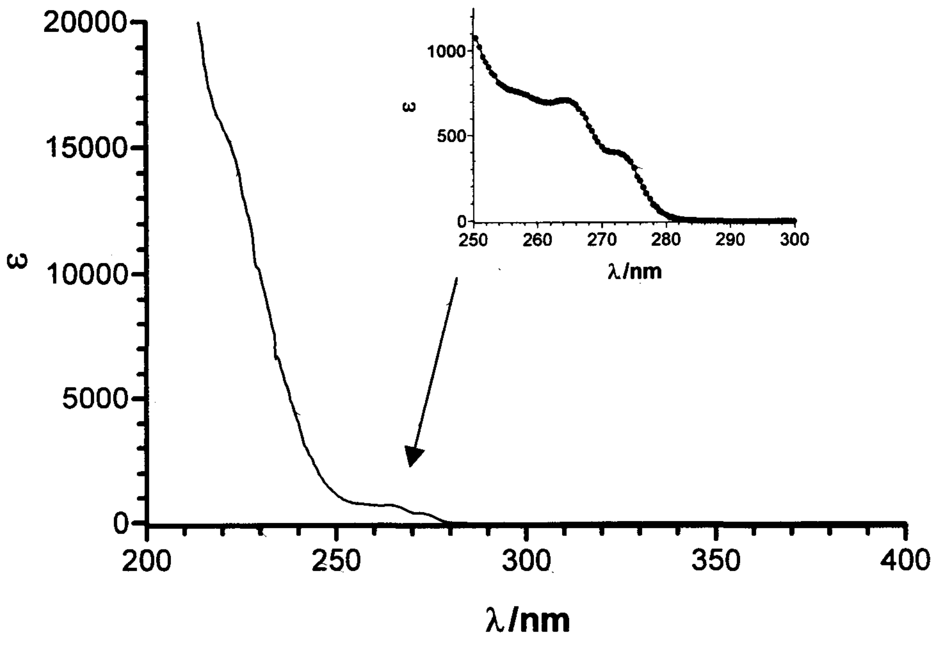

Figure 2.2.2 Ultraviolet absorption spectrum of **19c** in hexane at room temperature (ε_{248} = 1423 ± 9 $M^{-1}cm^{-1}$).
The inset shows the fine vibrational structure associated with the long wavelength absorption.

2.3 Steady-state photolysis studies

2.3.1 Photolysis of 19b and 19c in the presence of methanol

Photolysis at 254 nm (6 lamps) of a deoxygenated cyclohexane-d_{12} solution containing **19b** (0.0189 M) and methanol (0.300 M) led to the formation of ethylene and three other products, as shown by ^{1}H NMR and GC/MS analysis. The products were identified as cyclopropane, bis(4-trifluoromethylphenyl)methoxymethylgermane **42b** and bis(4-trifluoromethylphenyl)methoxygermane **58b** (eq 2.3) on the basis of ^{1}H NMR and

GC/MS analysis of the crude reaction mixtures. The progress of the reactions were followed by ^{1}H NMR spectroscopy, as illustrated in Figure 2.3.1.

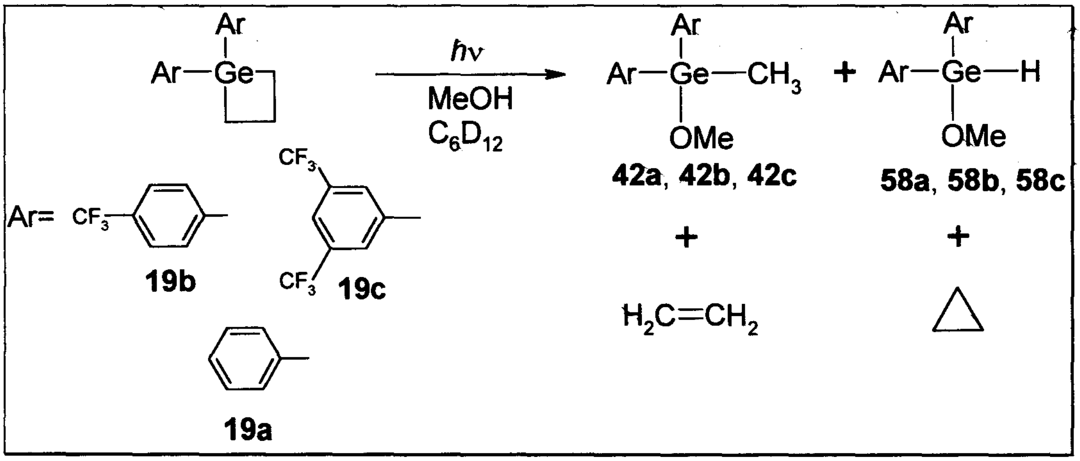

2.3

Cyclopropane exhibits a singlet at δ = 0.20 ppm (^{1}H NMR) in the reaction mixture and was identified by co-injection of an authentic sample. The synthesis of cyclopropane is outlined in the Experimental Section 5.4. Diarylmethoxymethylgermane **42b** shows ^{1}H NMR signals at δ = 3.49 ppm (singlet, OCH_3) and δ = 0.81 ppm (singlet, CH_3) with an integral ratio of 1:1. GC/MS analysis of the product showed a set of molecular ions at 406/408/410, consistent with the molecular formula $C_{16}H_{14}OF_6Ge$. Compound **42b** exhibited the following fragmentation pattern; only m/z of the heaviest isotope is listed for simplicity: (m/z, (%)) = 410 (5, $M^{+\cdot}$), 395 (100, M - $CH_3^{\cdot}$), 365 (78, M - $CH_2OMe^{\cdot}$), 235 (36, M - $ArOCH_2^{\cdot}$), 219 (52, $ArGe^{+}$).

These results can be compared with previously published results for the photolysis of 1,1-diphenylgermacyclobutane **19a** in the presence of methanol, which results in the formation of methoxymethyldiphenylgermane **42a**.[36] Compound **42a** exhibits ^{1}H NMR signals at δ = 3.44 ppm (singlet, OCH_3) and δ = 0.71 ppm (singlet, CH_3) as well the expected aromatic proton resonances. The mass spectrum of **42a** shows the following fragmentation pattern: (m/z, (%)) = 274 (6, $M^{+\cdot}$), 259 (100, M - $CH_3^\cdot$), 229 (60, M - $CH_2OMe^\cdot$), 167(20, M - $PhOCH_2^\cdot$), 151(50, $PhGe^+$).[36] The similarity of the ^{1}H NMR spectra and MS fragmentation patterns between **42b** and **42a** validates the structural assignment of 1,1-diarylmethoxymethylgermane **42b**.

Diarylmethoxygermane **58b** exhibits ^{1}H NMR signals at δ = 6.18 ppm (singlet, Ge-H) and at δ = 3.58 ppm (singlet, OCH_3) in an intensity ratio of 1:4.3. The ratio of integration between the two signals was not the expected 1:3, but it was roughly constant over the 7-50% conversion range. GC/MS analysis of **58b** displayed a set of molecular ions at 392/394/396, which is consistent with the molecular formula $C_{15}H_{12}OF_6Ge$. The mass spectrum of **58b** shows a similar fragmentation pattern to those of **42a** and **42b**: (m/z, (%)) = 396 (2, $M^{+\cdot}$), 395 (12, M - $H^\cdot$), 365 (33, M - $OMe^\cdot$), 219 (38, $ArGe^+$).

Diarylmethoxygermane **58b** has been shown to be the exclusive germanium-containing product from the photolysis of the germacyclopentene **48b** in the presence of methanol (eq 2.4).[61] A sample of the photolysis mixture containing **58b** was used to identify **58b** in the germacyclobutane photolysis mixture by GC co-injection.[61]

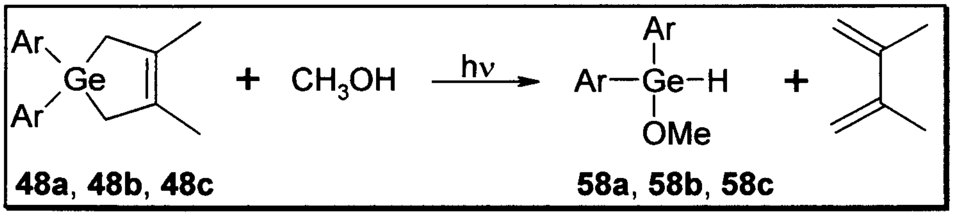

48a, 48b, 48c **58a, 58b, 58c**

2.4

Figure 2.3.2 (a) shows a plot of product concentration versus percent conversion for the photolysis of **19b**. The concentrations of the various products were calculated as follows. Initially the signals were standardized using the $C_6D_{11}H$ signal at 1.38 ppm. All integrations were then corrected for the number of protons that they represent. Subsequently, the ^1H integral of **19b** at time = 0 seconds was set equal to the initial concentration of **19b**, 0.0189 M. Using this ratio, the rest of the product integrations were converted to absolute concentrations. Concentrations of **19b**, **42b**, and **58b** were calculated using the signals at δ = 2.04, 0.81, and 3.58 ppm, respectively. The percent conversion was calculated by dividing the integration of **19b** at different times by the initial integration of **19b**.

From Figure 2.3.2 (a) the chemical yields of diarylmethoxymethylgermane and diarylmethoxygermane at 17% conversion of starting material were found to be 38 and 34%, respectively, based on the relative areas of the MeO peaks. This corresponds to a product ratio of 1.1 : 1 of **42b** to **58b** from the photolysis of **19b**. The chemical yield of cyclopropane at 17% conversion was found to be 25%. The mass balance of the reaction was 72%. At longer photolysis times the absolute concentrations of **42b** and **58b** begin to diminish with the appearance of new ^{1}H NMR signals suggesting that the products are absorbing light and undergoing photodecomposition.

An experiment was conducted in which hexane solutions of **19b** and methanol were photolysed simultaneously with a similar solution of 1,1-diphenylgermacyclobutane **19a** (Φ for the formation of **42a** = 0.21 ± 0.03[36]). Plots of product formation versus time yielded straight lines at < 30% conversion of starting material. The slope of the plot of [**42b**] versus time was divided by that of [**42a**] versus time to yield 0.52 ± 0.06 (Figure 2.3.2(b)). This number multiplied

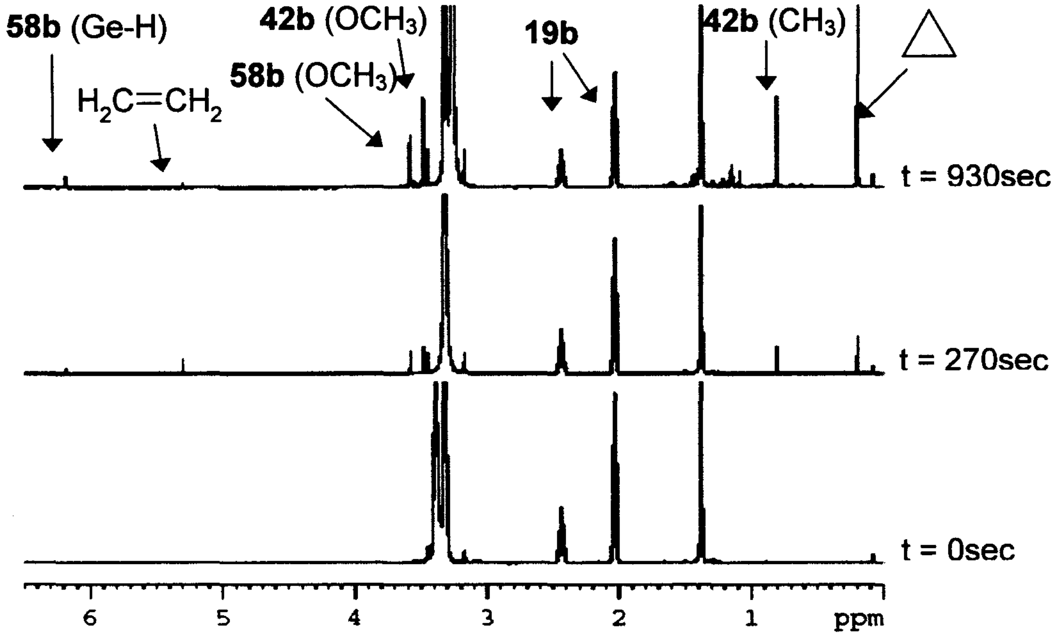

Figure 2.3.1 Steady State Photolysis of [**19b**] = 0.0189 M and [Methanol] = 0.30 M in deoxygenated C_6D_{12} with 6 x 254 nm lamps, monitored by 500 MHz ^1H NMR spectroscopy.

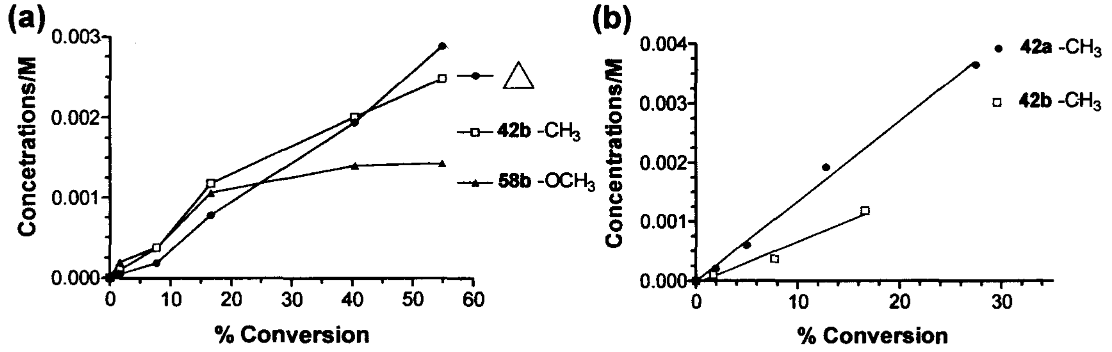

Figure 2.3.2 (a) Product concentration versus % Conversion of the starting materials for the photolysis of **19b** in deoxygenated C_6D_{12} containing MeOH (0.3 M).

(b) Product concentration versus % Conversion for the photolysis of **19a** and **19b** in deoxygenated C_6D_{12} containing MeOH (0.3 M). Integrals were converted to concentrations by using ratios where the initial integral of germacyclobutane equals 0.0189 M. All integrations were corrected for the number of protons.

by the quantum yield of formation of **42a** yields the quantum yield of formation of **42b**. The quantum yield for formation of diarylmethoxymethylgermane **42b** was thus found to be 0.11 ± 0.01.

A solution containing **19c** (0.0204 M) and methanol (0.30 M) in deoxygenated cyclohexane-d_{12} was photolysed with 6 lamps (254 nm) and led to the formation of ethylene, cyclopropane (identified by co-injection of authentic cyclopropane) and two other germanium-containing products detectable by ^{1}H NMR and GC/MS. The germanium containing products were identified as diarylmethoxymethylgermane **42c** and diarylmethoxygermane **58c** (eq 2.3) on the basis of ^{1}H NMR and GC/MS analysis of the crude photolysis mixtures. The progress of the reaction can be seen in the ^{1}H NMR spectra of the crude reaction mixtures at different times of photolysis, as illustrated in Figure 2.3.3.

Diarylmethoxymethylgermane **42c** exhibits ^{1}H NMR signals at δ = 3.53 ppm (singlet, OCH_3) and δ = 0.92 ppm (singlet, CH_3) with an integral ratio of 1:1. GC/MS analysis of **42c** showed a molecular ion of 542/544/546, consistent with the molecular formula $C_{18}H_{12}OF_{12}Ge$. The following fragmentation pattern was observed in the mass spectrum of **42c**: (m/z, (%)) = 546 (6, $M^{+\cdot}$), 531 (100, M - $CH_3^{\cdot}$), 501 (60, M - $CH_2OMe^{\cdot}$), 303 (20, M - $ArOCH_2^{\cdot}$), 287(50, $ArGe^{+}$). Both the ^{1}H NMR spectrum and MS fragmentation pattern of **42c** are analogous to the corresponding data for **42b** and methoxymethyldiphenylgermane **42a**,[36] validating the identity of the product.

The second germanium-containing product (**58c**) exhibits ^{1}H NMR signals at δ = 6.31 ppm (singlet, Ge-H) and at δ = 3.63 ppm (singlet, OCH_3), with a proton integration ratio of 1:3.5. The integration ratio was independent of photolysis time. The mass spectrum of **58c** exhibits a set of molecular ions at m/z = 528/532/534, which is consistent with the molecular formula $C_{17}H_{16}OF_{12}Ge$. In addition the following fragmentation pattern was observed: (m/z, (%)) = 534 (5, M+•), 533 (8, M - H•), 501 (30, M - OMe•), 287 (45, ArGe+). This species was also identified by GC co-injection of a photolysis mixture[61] containing **58c** from the photolysis of the germacyclopentene **48c** in the presence of methanol (Eq 2.4).

Figure 2.3.4 (a) shows a plot of product concentration versus percent conversion for the photolysis of **19c**. The concentrations of the various products were calculated following the method described previously for Figure 2.3.3 using the signals at δ 2.15, 0.92, and 3.63 ppm representing **19c**, **42c**, and **58c**, respectively.

As calculated from Figure 2.3.4 (a), the chemical yields of diarylmethoxymethylgermane **42c** and diarylmethoxygermane **58c** at 13% conversion of starting material are 30 and 52% respectively, based on the relative areas of the MeO peaks. This corresponds to a product ratio of **58c**:**42c** equal to 1:1.67. The chemical yield of cyclopropane at 13% conversion is 51%, in good correspondence with the yield of **58c**. The material balance of the reaction is 82%. In addition, as found for the photolysis of **19b** with methanol, the absolute concentrations of the germanium containing products level off at high conversions with the appearance of new peaks in the ^{1}H NMR spectra, suggesting that secondary photolysis of the products is occurring.

The quantum yield of formation of diarylmethoxymethylgermane was determined as described for **19b** and using the plot in Figure 2.3.4 (b). The value found is 0.08 ± 0.01.

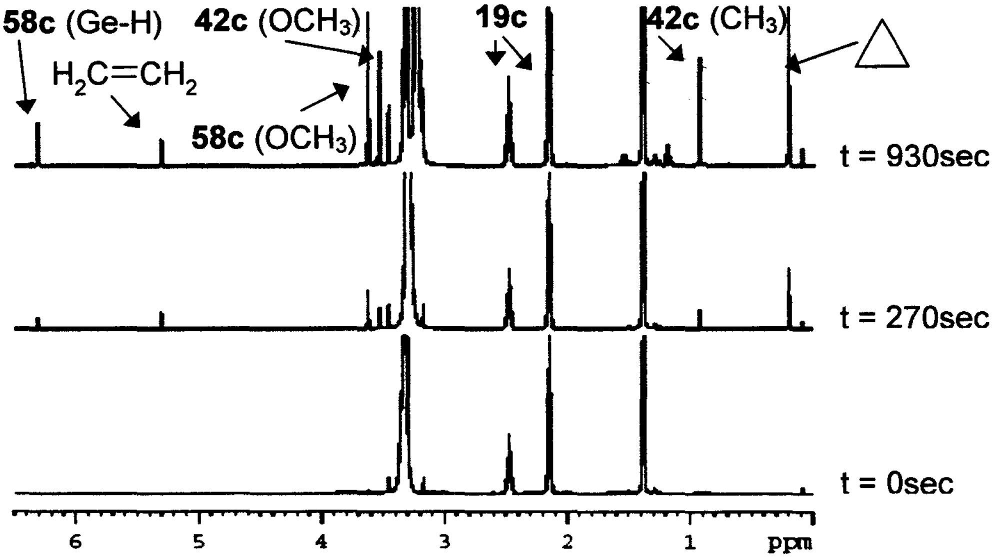

Figure 2.3.3 Steady State Photolysis of [**19c**] = 0.0204 M with [Methanol] = 0.30 M in deoxygenated C_6D_{12} with 6 x 254 nm lamps, monitored by 500 MHz ^{1}H NMR spectroscopy.

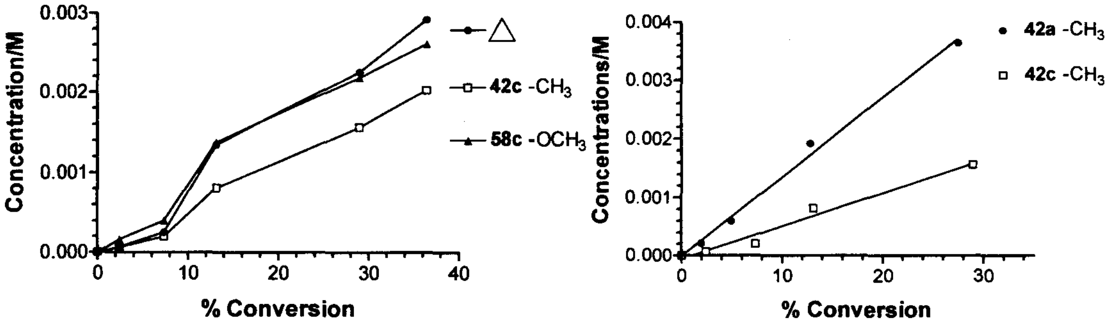

Figure 2.3.4 (a) Product concentration versus % Conversion of the starting materials for the photolysis of **19c** in deoxygenated C_6D_{12} containing MeOH (0.3 M).

(b) Product concentration versus % Conversion for the photolysis of **19a** and **19c** in deoxygenated C_6D_{12} containing MeOH (0.3 M). Integrals were converted to concentrations by using ratios where the initial integral of germacyclobutane equals 0.0204 M. All integrations were corrected for the number of protons.

The results of the methanol-trapping studies are consistent with the formation of two transient products from the photolysis of **19b** and **19c**: 1,1-diarylgermene **20b**, **20c** and 1,1-diarylgermylene **59b**, **59c**.

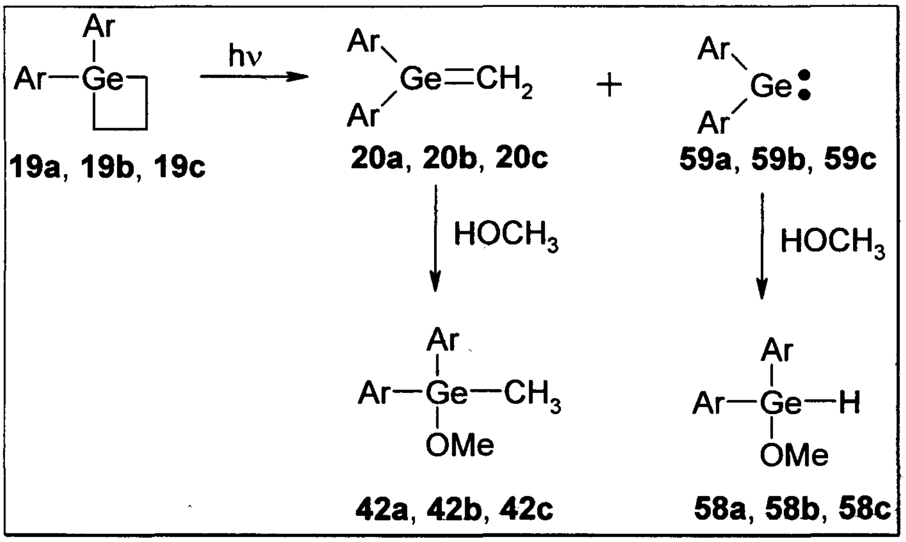

2.5

Both species are known to react with methanol[36, 62] to yield products analogous to those observed in the reaction mixtures (eq 2.5).

These results prompted a re-examination of the photolysis of 1,1-diphenylgermacyclobutane (**19a**) with methanol, in order to determine whether 1,1-diphenylgermylene is produced from **19a**. A deoxygenated hexane solution containing 0.200 M of **19a** and 0.30 M methanol was photolysed with 6 lamps (254 nm). This led to the formation of ethylene, cyclopropane (identified by co-injection of authentic cyclopropane) and two other germanium containing products detectable by ^{1}H NMR and GC/MS. The products were identified as methoxymethyldiphenylgermane **42a** and methoxydiphenylgermane **58a**, on the basis of ^{1}H NMR and MS of the crude reaction mixtures. The progress of the reaction can be seen in the ^{1}H NMR spectra of the crude reaction mixtures at different times of photolysis, as illustrated in Figure 2.3.5.

Methoxymethyldiphenylgermane **42a** was identified by comparison of ^{1}H NMR and MS spectra with previously published results[36]. Methoxydiphenylgermane **58a** exhibits ^{1}H NMR signals at δ = 6.10 ppm (singlet, Ge-H) and δ = 3.56 ppm (singlet, OCH_3) with an integral ratio of ~1:3.5, which does not vary with photolysis time. These values match previous results reported for the ^{1}H NMR spectrum of methoxydiphenylgermane.[61] **58a** was not detected by GC/MS analysis. This may be due to the products **42a** and **58a** eluting together.

Figure 2.3.6 shows a plot of product concentration versus percent conversion for the photolysis of **19a**. The concentrations of the various products were calculated following the method described previously for Figure 2.3.3 using the signals at δ 1.95, 0.74, and 3.56 ppm representing **19a**, **42a**, and **58a**, respectively.

As calculated from Figure 2.3.6, the chemical yields of methoxymethyldiphenylgermane **42a** and methoxydiphenylgermane **58a** at 38% conversion of starting material are 65 and 17% respectively. This corresponds to a product ratio of **42a**:**58a** equal to 3.8:1. The chemical yield of cyclopropane at

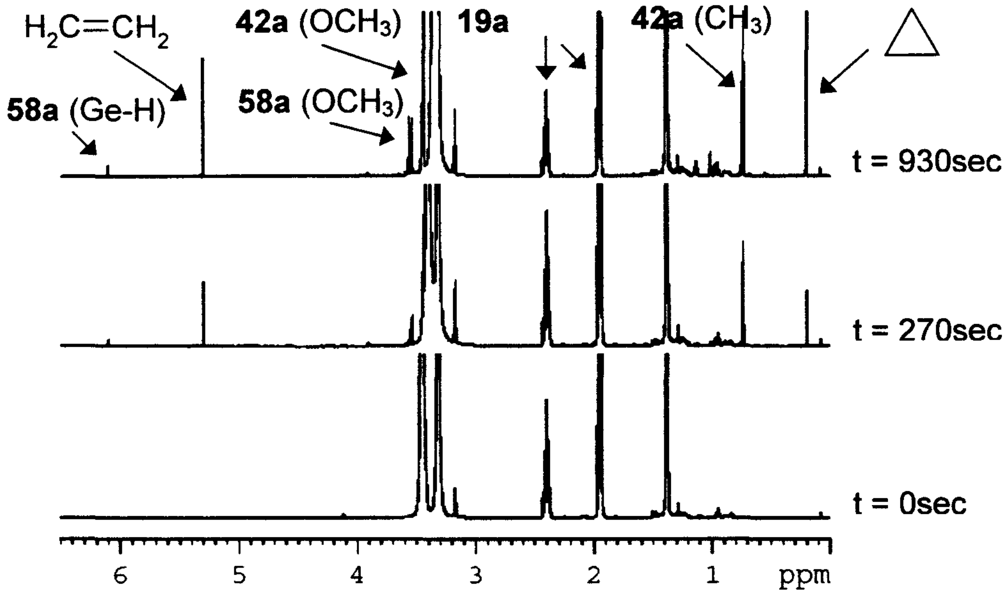

Figure 2.3.5 Steady State Photolysis of [**19a**] = 0.0200 M with [Methanol] = 0.30 M in deoxygenated C_6D_{12} with 6 x 254 nm lamps, monitored by 500 MHz ^{1}H NMR spectroscopy.

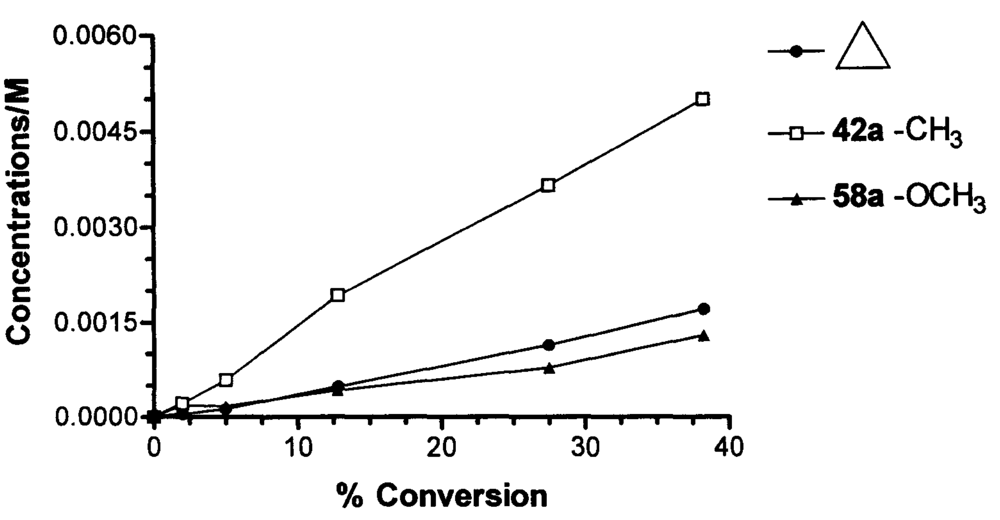

Figure 2.3.6 Product concentration versus % Conversion of the starting materials for the photolysis of **19a** in deoxygenated C_6D_{12} containing MeOH (0.3 M).
Integrals were converted to concentrations by using ratios where the initial integral of germacyclobutane equals 0.0200 M. All integrations were corrected for the number of protons.

38% conversion is 22%, in good correspondence with the calculated yield of **58a**. The material balance of the reaction is 82%. Unlike the previous photolyses of **19b** and **19c**, the concentration of products formed from the photolysis of **19a** did not diminish at longer photolysis times (up to 40% conversion).

Several attempts were made to prepare authentic samples of the diarylmethoxymethylgermanes **42b**, **42c**, following the procedure shown in eq 2.6. The diaryl germanium dichlorides were prepared as mixtures with $ArGeCl_3$ and Ar_3GeCl by the procedure outlined in section 2.1. Afterwards, the crude dichlorides were slowly added to a suspension of lithium aluminum hydride in THF at –78°C and reduced to the corresponding hydridogermanes **60b**, **60c**.

The isolation of **60b** was accomplished by vacuum distillation, which afforded the compound as a clear, colourless oil in 22.4% yield, and a purity of 97.6% as estimated by GC. The full spectroscopic characterization of **60b** is given in the Experimental Section 5.5.3. Isolation of **60c** was accomplished by vacuum sublimation, which afforded white fine needles in a yield of 24.3%. The identity of **60c** was confirmed by comparing its ^{1}H NMR spectrum with previously published data.[63]

Additional steps involved in the preparation of **42b** and **42c** were attempted, following a previously published literature procedure.[61, 64] After further complications involving difficult isolations the final products **42b** and **42c** were not obtained.

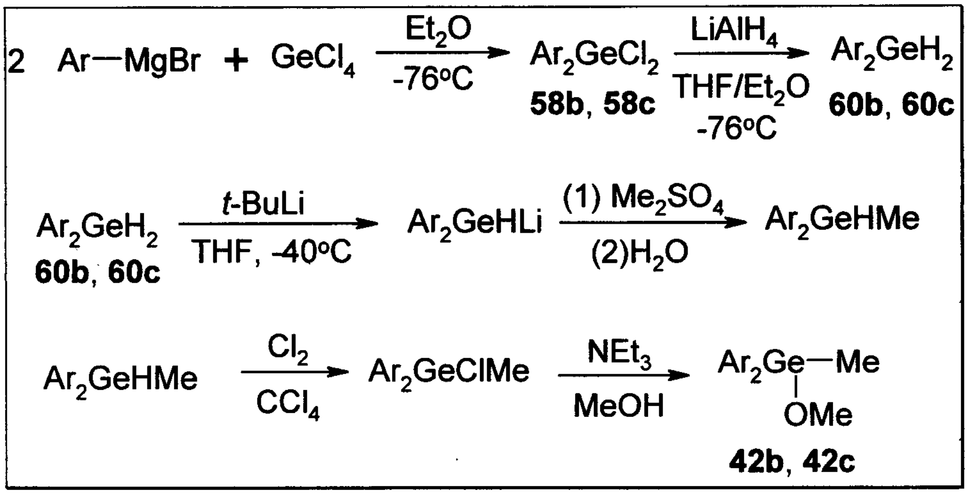

2.6

2.3.2 Photolysis of 19b and 19c in cyclohexane solution

Steady-state photolysis (254 nm) of a 0.047 M solution of **19b** in deoxygenated cyclohexane-d_{12} in a quartz NMR tube led to the disappearance of the starting material and the formation of several new signals in the ^{1}H NMR spectrum of the crude reaction mixture: a singlet at $\delta = 0.20$ ppm assignable to cyclopropane, a second singlet at $\delta = 5.3$ ppm assignable to ethylene, a third singlet at $\delta = 1.71$ ppm, and a broad underlying absorption in the aromatic region. GC analysis of the reaction mixture showed only the starting material as the major volatile species present in the reaction mixture. At longer photolysis times the reaction mixture began to turn yellow with the formation of a white precipitate.

The signal at $\delta = 1.71$ ppm was compared with 1,1,3,3-tetraphenyl-1,3-digermacyclobutane[36, 39] which has a ^{1}H NMR signal at $\delta = 1.62$ ppm (representing the protons at position * in eq 2.5). As with **19b** and **19c** the presence of the CF_3 groups at the para position on the phenyl rings in **21b** is expected to cause this signal to shift downfield relative to that of the parent 1,1,3,3-tetraphenyl-1,3-digermacyclobutane **21a**.[60] This allows the tentative assignment of the signal at $\delta = 1.71$ ppm as **21b** (eq 2.7).

It was found that at conversions of 20% or greater, the absolute concentration of this product began to diminish, indicating that it is undergoing secondary photolysis. The chemical yield of the product at 59% conversion was determined to be 7.1% by NMR. The chemical yield was determined by dividing the concentration of dimer at 59% conversion by the concentration of **19b** used. The underlying broad band in the aromatic region is tentatively attributed to polymeric material, possibly initiated by the reaction of germylene **54b** with germene **20b**.

Preparative steady-state photolysis of **19b** was performed in order to attempt isolation of the dimer for characterization. A solution of **19b** (0.050 M) in deoxygenated hexane was put in a photoreactor equipped with a Vycor filter and a low pressure mercury lamp. The sample was photolysed for two hours, causing the solution to turn dark yellow and the formation of a significant amount of white precipitate. ^{1}H NMR analysis revealed a broad band in the aromatic region along with three intense singlets in the aliphatic region. Radial chromatography afforded the starting material **19b**, but none of the expected digermacyclobutane **21b**, based on ^{1}H NMR analysis of the various fractions eluted.

A solution containing [**19c**] = 0.049 M in deoxygenated cyclohexane-d_{12} in a quartz NMR tube was photolysed (254 nm), leading to the disappearance of the starting material and the formation of several new signals in the ^{1}H NMR spectrum of the crude reaction mixture: a singlet at $\delta = 0.20$ ppm assignable to cyclopropane, a second singlet at $\delta = 5.3$ ppm assignable to ethylene, a third singlet at $\delta = 1.87$ ppm, and several new peaks as well as an underlying broad band in the aromatic region. GC analysis of the reaction mixture displayed only the starting material along with several low intensity signals. As in the photolysis of **19b**, the solution began to turn yellow and a white precipitate formed in the NMR tube at longer photolysis times.

The signal at $\delta = 1.87$ ppm is tentatively assigned to the CH_2 protons in the 1,3-digermacyclobutane **21c**, based on the spectrum of 1,1,3,3-tetraphenyl-1,3-digermacyclobutane **21a**.[36] As in the photolysis of **19b** under similar conditions the concentration of the dimer decreases at conversions of 20% and higher, suggesting secondary photolysis of **21c**. The chemical yield of the dimer at 36% conversion was found to be 3.4% by NMR. The yield of the dimer was determined by dividing the concentration of dimer at 36% conversion by the concentration of **19c** used. The formation of polymeric material is considered responsible for the broad band in the aromatic region of the ^{1}H NMR spectra.

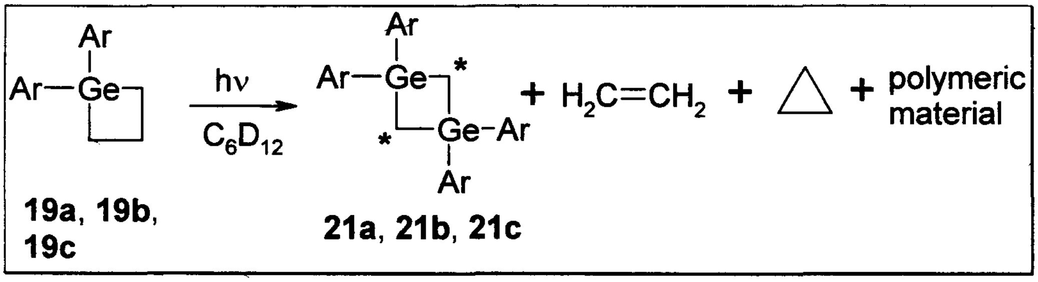

2.7

2.3.3 Photolysis of 19b and 19c in the presence of 2,3-dimethyl-1,3-butadiene

A solution containing **19b** (0.0557 M) and 2,3-dimethyl-1,3-butadiene (DMB, 0.0407 M) in deoxygenated cyclohexane-d_{12} was photolysed (2 lamps 254 nm) and monitored by ^{1}H NMR spectroscopy, GC and GC/MS. Continued irradiation resulted in the disappearance of the starting materials and the formation of ethylene, cyclopropane and two other products, which were identified as the germene dimer **21b** and 1,1-bis(4-trifluoromethylphenyl)-3,4-

dimethylcyclopent-3-ene **48b** (eq 2.8) in a ratio of 1:5. Another product was observed by GC/MS analysis as discussed below.

Compound **48b** exhibits singlets in the aliphatic region of the ^{1}H NMR spectrum at δ = 1.80 ppm (CH_3) and δ = 2.04 ppm (CH_2), and was rigorously identified by GC co-injection with an independently synthesized authentic sample.

GC/MS analysis of the remaining product showed the typical germanium isotopic pattern indicating that it contains germanium with a molecular ion of 456/458/460, which is consistent with the molecular formula $C_{21}H_{20}F_6Ge$. The product exhibited the following fragmentation pattern: m/z (%) = 460 (90, $M^{+\cdot}$), 391 (25), 365 (50), 271 (100), 262 (100), 219 (80), 201 (20), 140 (20), 126 (25), 107 (45). The mass spectrum is consistent with an adduct between **20b** and DMB among other things. However, the ^{1}H NMR spectra of the reaction mixtures showed many signals in the aliphatic region and no discernible features to help elucidate its structure.

The photolysis was performed until the percent conversion of the starting material (**19b**) was 29%. The chemical yields of **21b** and **48b** at 29% conversion were 6% and 31%, respectively. These yields were calculated by dividing the concentrations of the products at 29% conversion by the concentration of **19b** consumed. The estimated chemical yield of the unidentified compound (calculated from GC analysis) is 13%. In addition the chemical yield of cyclopropane from this photolysis was 16%. The mass balance of the reaction, including the unidentified product, is 50%. The concentrations of the various products were calculated as follows. The initial integration of the GC signal for the germacyclobutane **19b** was set equal to its initial concentration (0.0557 M). Using this ratio the rest of the product GC signal integrations were converted to absolute concentrations. The GC yields for the germacyclopentene **48b** corresponded well with the ^{1}H NMR yields.

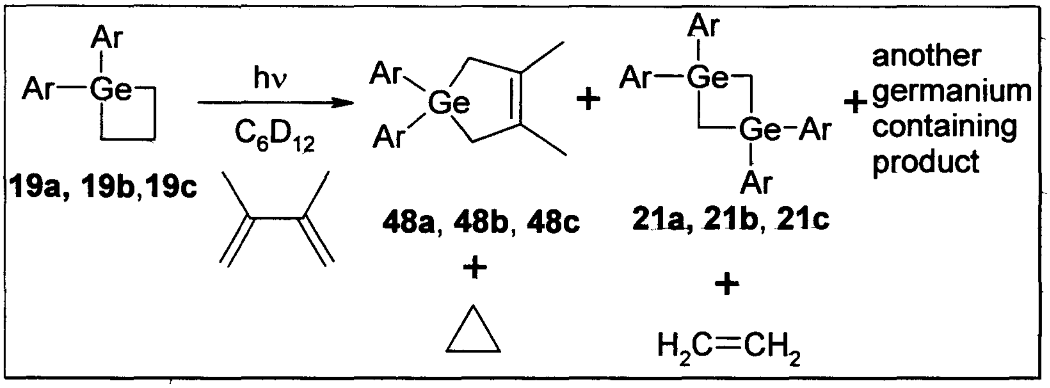

2.8

In a similar manner a deoxygenated cyclohexane-*d*$_{12}$ solution containing **19c** (0.0525 M) and DMB (0.0407 M) was photolysed (2 lamps 254 nm) and monitored by ^{1}H NMR, GC and GC/MS. The photolysis led to the disappearance of starting material over time and the formation of ethylene, cyclopropane and a single identifiable product (eq 2.7). In this case **21c** was not detected, perhaps because its ^{1}H NMR signal overlaps with the starting material DMB at δ = 1.88 ppm. The other product was identified as 1,1-diaryl-3,4-dimethylgermacyclopentene **48c** (eq 2.8). A third germanium-containing product was detected in the reaction mixture by GC/MS, but it could not be identified.

Compound **48c** shows singlets in the aliphatic region of the ^{1}H NMR spectrum at δ = 1.822 ppm (CH_3) and δ = 2.127 ppm (CH_2), and was identified by GC co-injection of an independently synthesized authentic sample. The remaining unknown product was found to display the typical germanium isotopic pattern in its mass spectrum, with a molecular ion of 592/594/596. This mass is consistent with the molecular formula $C_{23}H_{18}F_{12}Ge$. The fragmentation pattern found gave the following ions (m/z (%)): 596 (5), 527 (5), 388 (25), 287 (35), 263 (15), 208 (35), 194 (80), 175 (65), 155 (35), 95 (100). As in the previous case the ^{1}H NMR spectrum did not help elucidate the structure, but the mass spectrum is consistent with an adduct between **21c** and DMB.

The photolysis was continued until 27% of the starting material (**19c**) was converted into products, at which point the chemical yields of **48c** and cyclopropane were determined to be 58 and 28%, respectively. The estimated chemical yield of the unidentifiable product is 16% as determined by GC analysis. The mass balance of this reaction, including the unidentifiable product, is 74%. The results of this study confirm the formation of 1,1-diarylgermylene **48b** and **48c** from the photolysis of the corresponding germacyclobutanes (eq 2.9).

An additional experiment was performed with 1,1-diphenylgermacyclobutane **19a** under analogous conditions to provide further evidence that 1,1-diphenylgermylene is formed from the corresponding germacyclobutane. A deoxygenated cyclohexane-d_{12} solution containing **19a** (0.0494 M) and DMB (0.0407 M) was photolysed with 2 lamps (254 nm) and the reaction was monitored by ^{1}H NMR spectroscopy, GC and GC/MS. The photolysis led to the disappearance of starting material over time and the formation of ethylene, cyclopropane and two identifiable products (eq 2.8). The products were identified as 3,4-dimethyl-1,1-diphenylcyclopent-3-ene **48a** and 1,1,3,3-tetraphenyl-1,3-digermacyclobutane **21a** (eq 2.8).

Compound **48a** shows ^{1}H NMR signals at δ = 1.78 (CH_3) and 1.97 (CH_2) ppm and was identified by GC co-injection with authentic **48a**. The dimer **21a** was identified by comparison of ^{1}H NMR data with previously published data[36].

At 25% conversion of starting material **19a** the chemical yields of **21a**, **48a**, and cyclopropane are 18, 21 and 12%, respectively. The chemical yields were calculated by dividing the concentration of the product at 25% conversion by the concentration of **19a** used. The mass balance of the reaction is 39%.

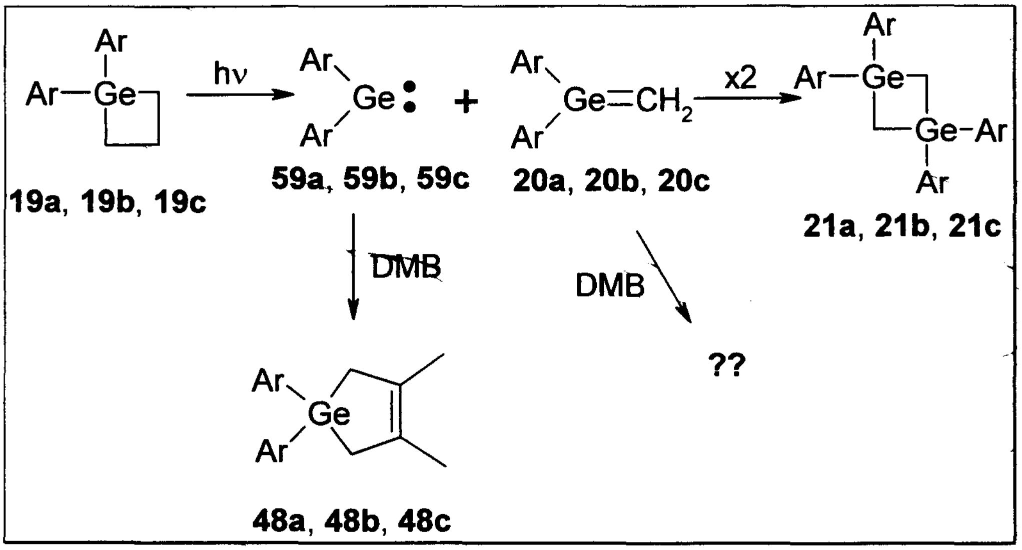

2.9

2.3.4 Photolysis of 19b and 19c in the presence of acetone

Separate solutions were prepared containing **19b** (0.0461 M) and **19c** (0.0539 M) in cyclohexane-d_{12} containing acetone (0.2 M), deoxygenated and photolysed (4 lamps, 254 nm). The reaction was monitored at regular time intervals using ^{1}H NMR and GC analysis. The reactions were carried to 39.6% and 51.7% conversion of starting materials for **19b** and **19c**, respectively. The ^{1}H NMR spectra showed peaks characteristic of ethylene, cyclopropane, a broad band in the aromatic region, and a multitude of peaks in the aliphatic region (eq

2.10). The ^{1}H NMR spectra of the crude reaction mixtures at 0 and 42 minutes of photolysis for **19b** and **19c** are illustrated in Figure 2.3.7 and 2.3.8, respectively.

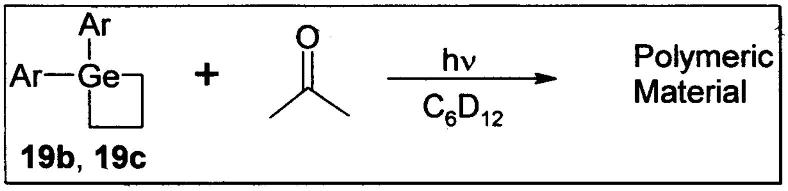

2.10

The new signals in the aromatic and aliphatic region are attributed to the formation of polymeric material. No products other than **19b** or **19c** could be detected in significant amounts by GC. These results are similar to previously published results for the photolysis of 1,1-diphenylgermacyclobutane under similar conditions.[36]

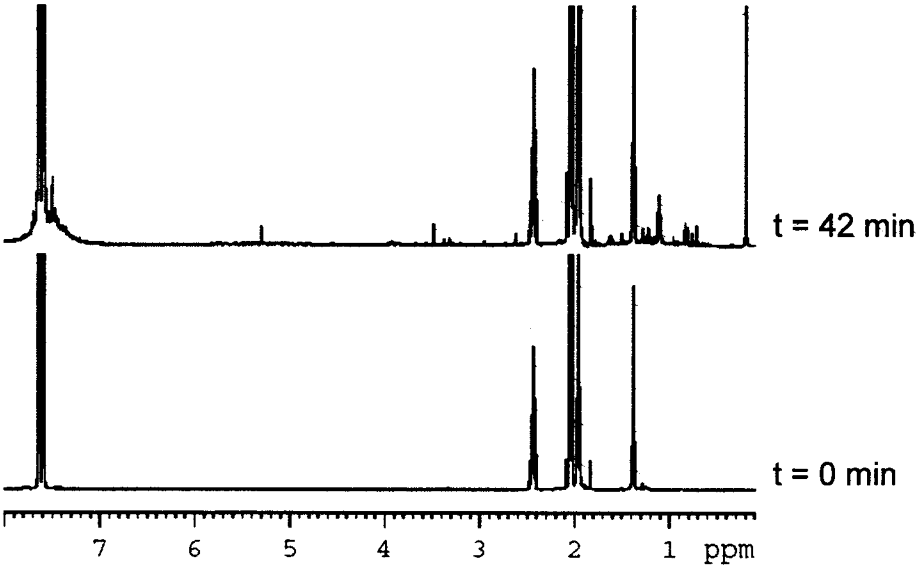

Figure 2.3.7 Steady State Photolysis of [**19b**] = 0.0461 M with [Acetone] = 0.20 M in deoxygenated C_6D_{12} with 4 x 254 nm lamps, monitored by 500 MHz ^{1}H NMR spectroscopy.

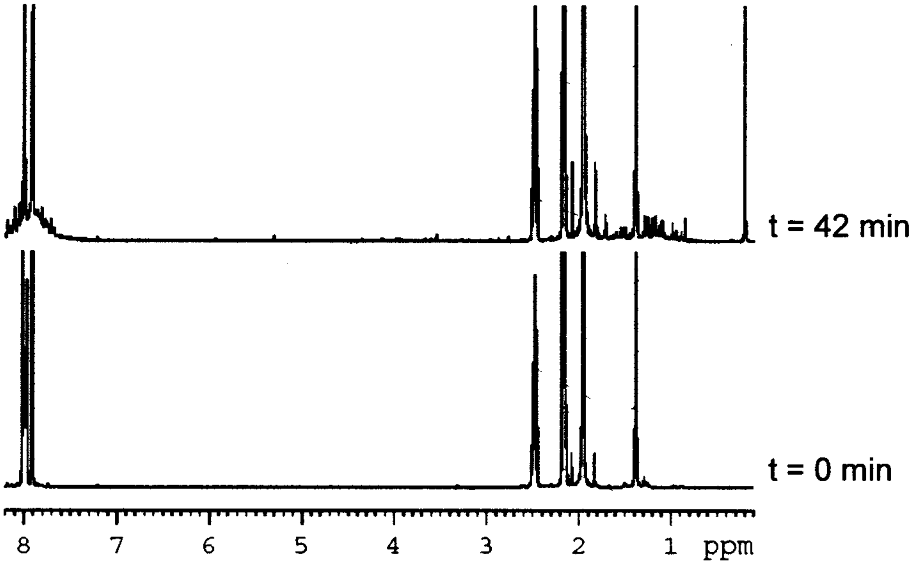

Figure 2.3.8 Steady State Photolysis of [**19c**] = 0.0539 M with [Acetone] = 0.20 M in deoxygenated C_6D_{12} with 4 x 254 nm lamps, monitored by 500 MHz ^{1}H NMR spectroscopy.

2.4 Nanosecond Laser Flash Photolysis

2.4.1 Transient Absorption Spectra

Nanosecond laser flash photolysis (*NLFP*)[65-67] experiments were carried out using a system that allows continuous flow of solutions containing **19b** or **19c** in dry deoxygenated solvents. The flow system is necessary in experiments such as these, where irreversible photolysis of the substrate occurs; it ensures that fresh solution of the substrate is present in the cell for each laser pulse, and avoids the buildup of products that will compete with the substrate for light absorption and perhaps undergo photochemistry of their own. Solutions containing **19b** and **19c** at concentrations of 5.3×10^{-4} M and 7.0×10^{-4} M, respectively, in dry, deoxygenated hexane were photolysed with the pulses from a KrF excimer laser (~20 ns, 80-120 mJ, 248 nm), resulting in readily detectable transient absorptions in the spectral range from 280 – 480 nm. Transient decay traces were recorded at a fixed wavelength where the transient of interest absorbs; the traces are plots of transient absorbance (Δ-OD) versus time. Time-resolved UV absorption spectra of the transients at various time intervals after the laser pulse were acquired in point-by-point fashion, by recording decay traces at a series of monitoring wavelengths throughout the 300 – 600 nm range.

Initial work involved identifying the transient species responsible for the complicated transient absorption spectra generated from the photolysis of **19b** and **19c**. At 325 nm (the expected value of λ_{max} for germenes **19b** and **19c**[36]), photolysis of both compounds gives rise to transients that decay with complex kinetics; the decays fit acceptably to the sum of two first-order exponentials (Figure 2.4.1 (a) and Figure 2.4.4 (a)). In addition, both compounds exhibit an additional weak transient absorption at λ_{max}=440 nm that initially grows and then decays over several tens of microseconds (Figure 2.4.1 (b) and Figure 2.4.5 (a)).

Time-resolved UV absorption spectra of a solution containing **19b** (4.2 x 10^{-4} M) in deoxygenated hexane were recorded over the 0.6-2.1 μs, 4.0-6.4 μs, and 62-88 μs time intervals after the laser pulse, and are shown in Figure 2.4.2 (a), Figure 2.4.2 (b), and Figure 2.4.2 (c), respectively. The first time window (0.6-2.1 μs, Figure 2.4.2 (a)) was recorded in an attempt to obtain an absorption spectrum free of the 450 nm transient species. This spectrum contains a broad absorption band with a maximum at λ_{max} = 325 nm and a shoulder at 300 nm; there is also present a very weak absorption centred at 450 nm. The second time window (4.0-6.4 μs, Figure 2.4.2 (b)) clearly shows that the absorption of the 450 nm species has intensified with time, while the species at 325 nm has decreased in intensity. Finally, in the long time window (62-88 μs, Figure 2.4.2(c)) the shorter lived transients are no longer present, revealing a broad absorption band with a maximum at 310 nm. A transient decay trace recorded at 280 nm shows predominantly a very long lived transient (Figure 2.4.1 (c)).

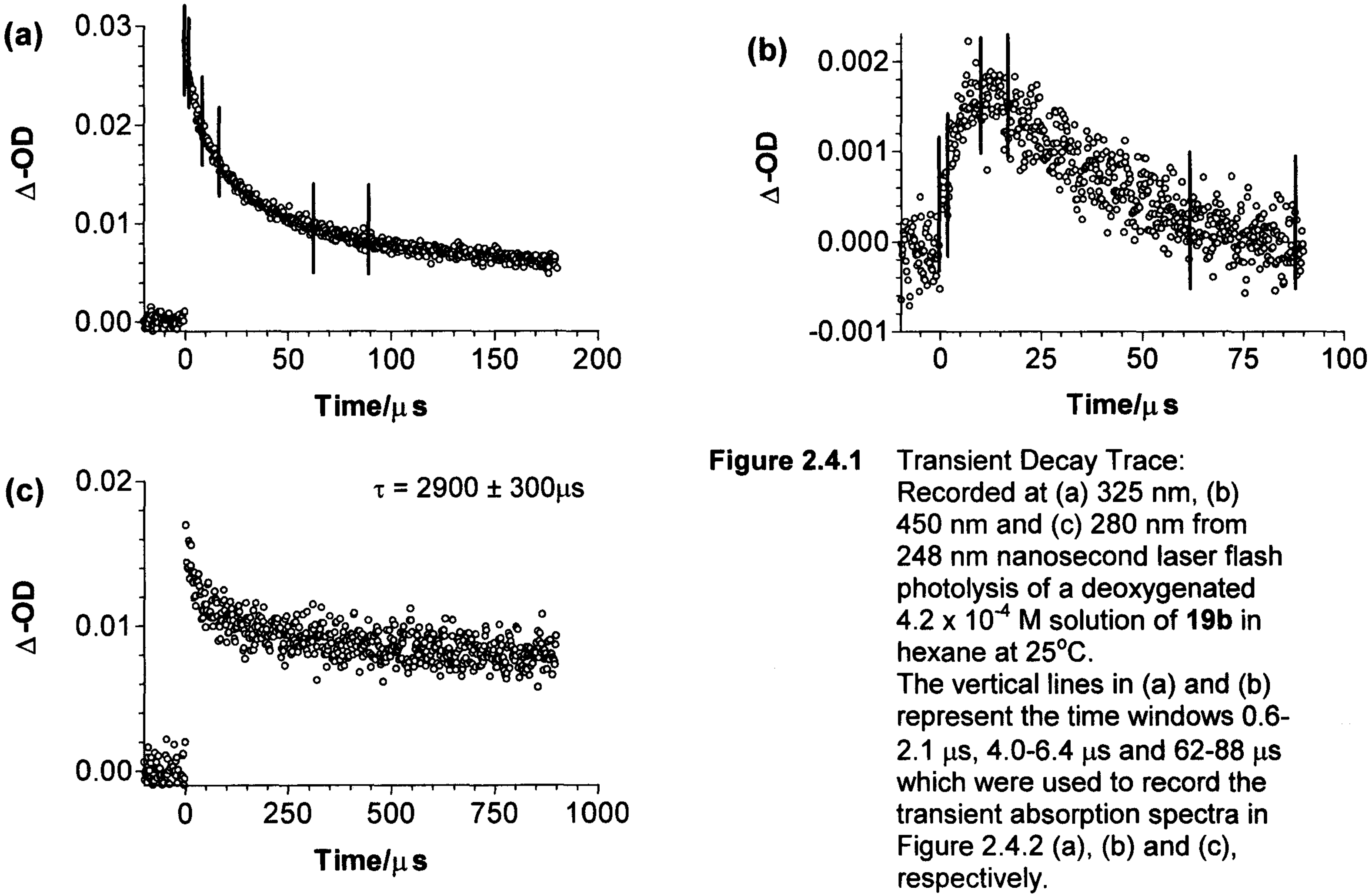

Figure 2.4.1 Transient Decay Trace: Recorded at (a) 325 nm, (b) 450 nm and (c) 280 nm from 248 nm nanosecond laser flash photolysis of a deoxygenated 4.2 x 10^{-4} M solution of **19b** in hexane at 25°C.
The vertical lines in (a) and (b) represent the time windows 0.6-2.1 μs, 4.0-6.4 μs and 62-88 μs which were used to record the transient absorption spectra in Figure 2.4.2 (a), (b) and (c), respectively.

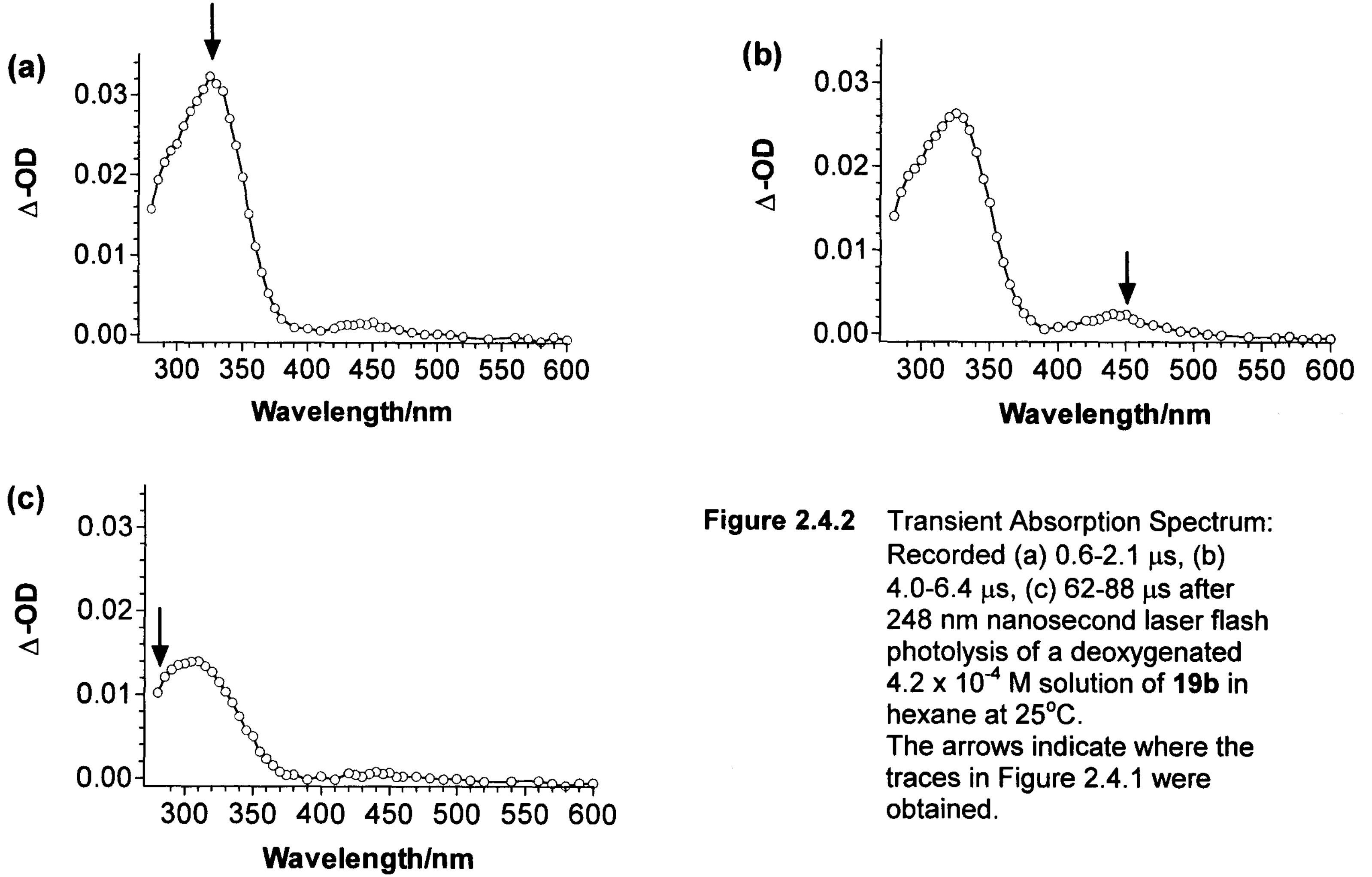

Figure 2.4.2 Transient Absorption Spectrum: Recorded (a) 0.6-2.1 μs, (b) 4.0-6.4 μs, (c) 62-88 μs after 248 nm nanosecond laser flash photolysis of a deoxygenated 4.2 x 10^{-4} M solution of **19b** in hexane at 25°C.
The arrows indicate where the traces in Figure 2.4.1 were obtained.

The fact that the transient absorption spectrum changes (i.e. shifts to shorter wavelengths) with time indicates that photolysis of **19b** produces more than one transient species, which decay with different rate constants. Isolation of the spectra of those species present immediately after the laser pulse, and which decay the fastest, is possible by subtracting Figure 2.4.2 (c) from Figure 2.4.2 (a); the results of this manipulation are shown in Figure 2.4.3(a).

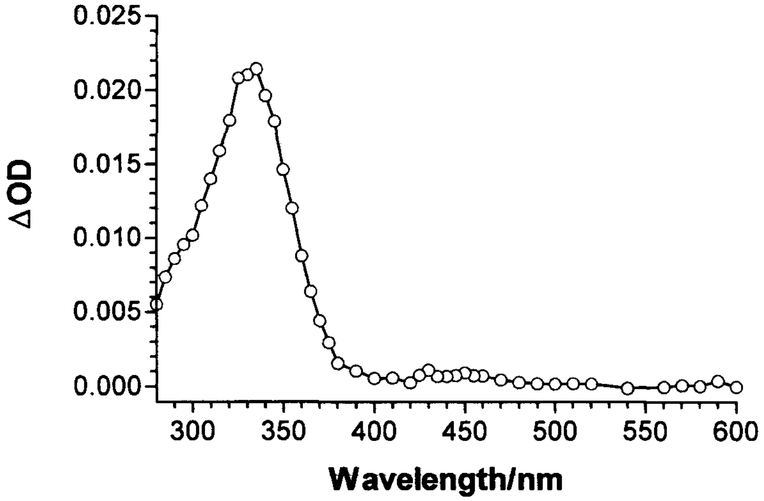

Figure 2.4.3 Transient Absorption Spectrum of **20b**: The subtraction of the long lived transient (Figure 2.4.2(c)) from the spectrum recorded immediately after the laser pulse (Figure 2.4.2(a)); laser flash photolysis of a deoxygenated 4.2 x 10^{-4} M solution of **19b** in hexane at 25°C.

Comparison of Figure 2.4.2 (a) with Figure 2.4.2 (c) indicates that the transient in Figure 2.4.3 comprises ca. 60% of the initial transient absorption produced upon laser excitation. From the two-component analysis of the decay trace of Figure

2.4.1 (a), its lifetime is estimated to be 16 ± 1μs in deoxygenated hexane solution at 25°C. The lifetime of the 310 nm transient is estimated to be 2900 ± 300μs (errors reported are ±2σ from least squares regression analysis). The error associated with the lifetime of the long lived transient is derived from the least squares analysis of the concentration-time data of Figure 2.4.1(c) and is underestimated considering the decay is monitored over much less than one half-life. A more reasonable estimate of the error would be ca. 50%.

The lifetime of the transient in Figure 2.4.3 is insensitive to the presence of oxygen (indicating that it is not a radical or triplet species), but is shortened upon addition of aliphatic alcohols or acetic acid to the solution (vide infra). Moreover, the λ_{max} of the transient is 330 nm which is very close to the reported λ_{max} of 1,1-diphenylgermene **20a** (325nm)[36]. On the basis of these observations, the transient is assigned to 1,1-bis(4-(trifluoromethyl)phenyl)germene **20b**.

The kinetic character of the transient absorbing at λ_{max} = 440 nm can only be commented on in a qualitative manner because of its very low signal intensity. The species grows in over ca. 10 μs and then decays over ca. 100 μs (Figure 2.4.1 (b)). It disappears completely when small amounts of oxygen, aliphatic alcohols or acetic acid are added to the solution. On the basis of this behaviour, this species is identified as tetrakis ((4-trifluoromethyl)phenyl)digermene **61b**, formed by dimerization of bis ((4-trifluoromethyl)phenyl)germylene **59b**. The same transient has been previously observed upon laser flash photolysis of the germylene precursor **48b** as mentioned in section 1.5 (eq 2.11).[61]

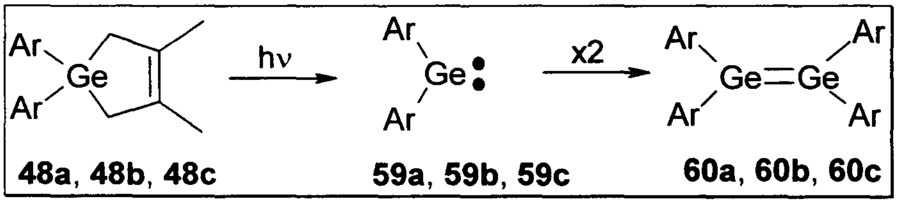

2.11

The long lived transient with λ_{max} = 310 nm has a lifetime of 2900 μs and its lifetime is sensitive to oxygen. Because the absorption band of this transient substantially overlaps with the absorption band of **20b**, it is impossible to obtain a clean decay trace and determine whether the transient is formed immediately after the laser pulse or grows in (Figure 2.4.1(c)). Assignment of this transient can only be speculated, however it may be due to germylene **59b** inserting into germene **20b** to form a digermirane (eq 2.12). 1,1,2,2-tetrakis(2,6-diethylphenyl)digermirane has been previously prepared by Ando and coworkers[68, 69] and shown to have a λ_{max}=300 nm which is consistent with the absorption maximum of the long lived transient.

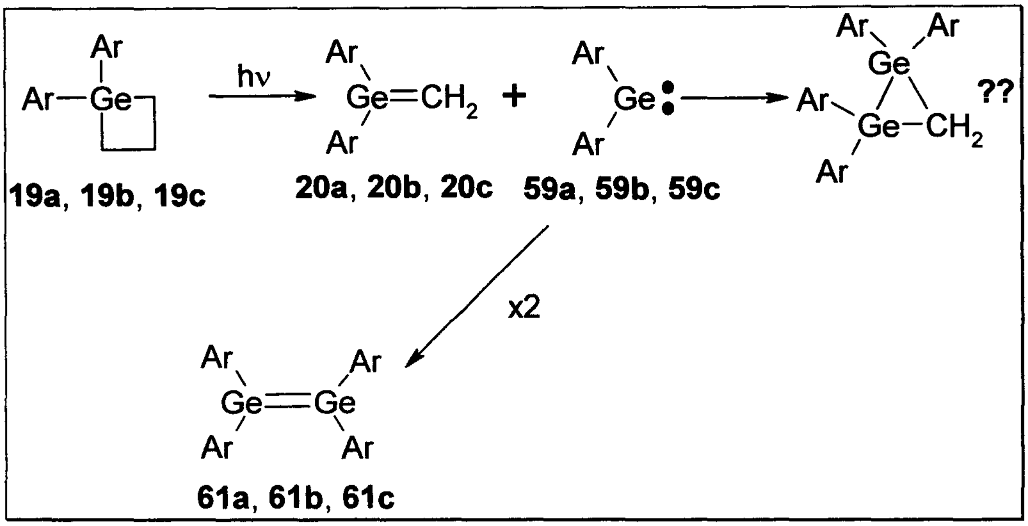

2.12

Time-resolved UV absorption spectra of a solution containing **19b** (3.1 x 10^{-4} M) in air saturated acetonitrile was recorded over the time intervals 60-300 ns and 20-35 μs after the laser pulse (Figure 2.4.4(b)). A transient decay trace at 325 nm exhibits complex kinetics, as shown in Figure 2.4.4(a). The transient absorption spectrum in the first time window (60-300 ns, Figure 2.4.4 (b)) only displays a broad band centred at 325 nm. The lack of an absorption at 450 nm confirms the absence of digermene in solution. The second time window (20-35 μs, Figure 2.4.4 (b)) shows an absorption centered at 310 nm. The fact that the transient absorption spectrum changes (shifts to shorter wavelengths) with time indicates that photolysis of **19b** produces more than one transient species, which decay with different rate constants. Germylenes have been shown to complex with aprotic polar solvents such as acetonitrile to form a complex.[61, 62] These

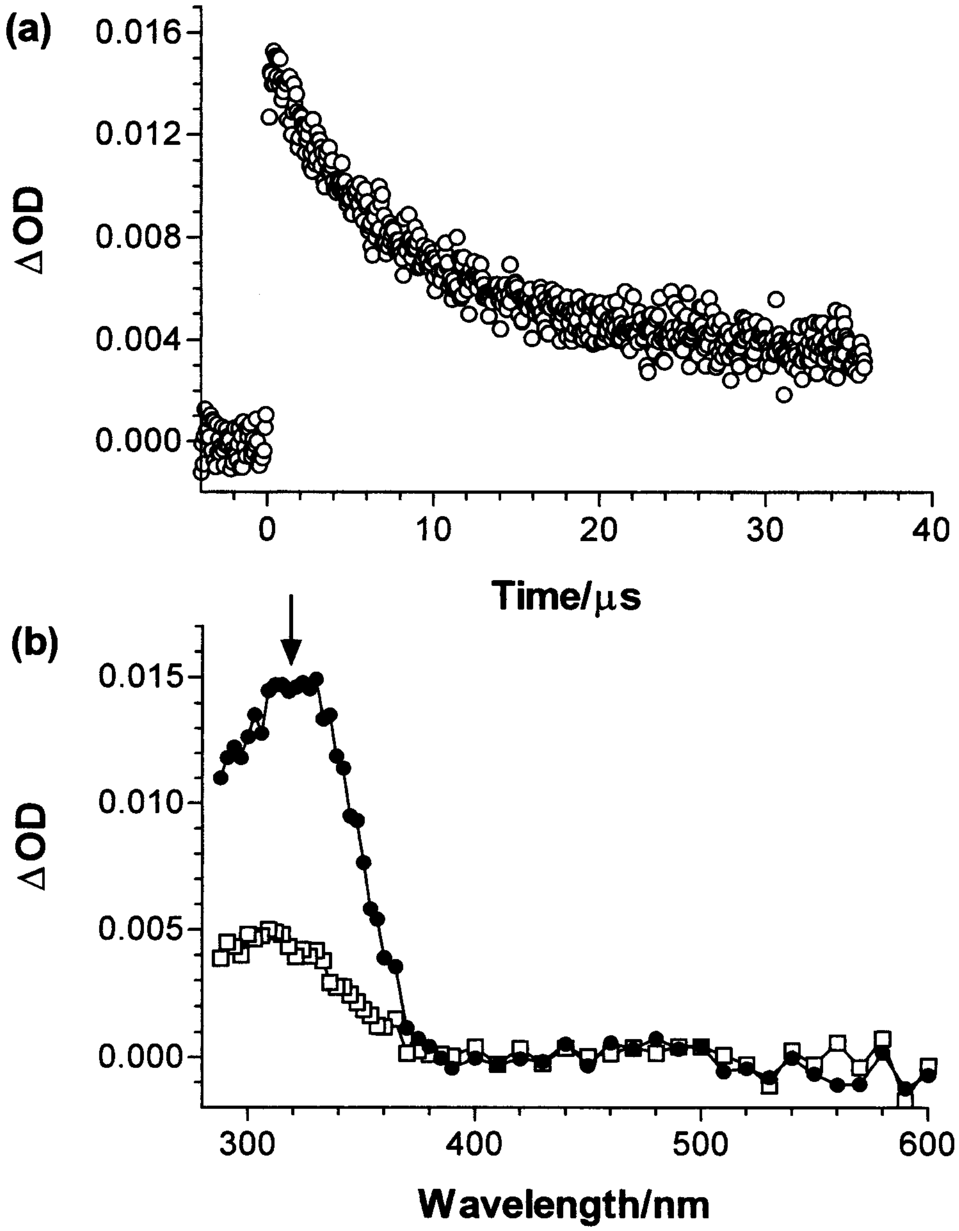

Figure 2.4.4 (a) Transient Decay Trace: Recorded at 325 nm from 248 nm nanosecond laser flash photolysis of a deoxygenated 3.1 x 10^{-4} M solution of **19b** in acetonitrile at 25 °C
(b) Transient Absorption Spectra: Recorded 0.06-0.3 μs (●) and 20-35 μs (□) after 248 nm nanosecond laser flash photolysis of an air saturated 3.1 x 10^{-4} M solution of **19b** in acetonitrile at 25 °C.

complexes have been shown to have a λ_{max}≈320 nm which directly overlaps with the absorption of germenes.[61]

Similarly, a solution of **19c** (6.2×10^{-4} M) in deoxygenated hexane was photolysed, and time-resolved UV absorption spectra were recorded over the 190-450 ns, 3.8-6.0 μs, and 32-36 μs time intervals after the laser pulse. The spectra are shown in Figure 2.4.6 (a), 2.4.6 (b), and 2.4.6 (c), respectively. The first time window (190-450 ns, Figure 2.4.6 (a)) was recorded in an attempt to obtain an absorption spectrum free of the 450 nm transient species. This spectrum contains a broad absorption band with a maximum at λ_{max} = 325 nm and a prominent shoulder at 300 nm. The second time window (3.8-6.0 μs, Figure 2.4.6 (b)) clearly shows a new absorption at 450 nm, while the species at 325 nm has decreased. Finally, in the long time window (32-36 μs, Figure 2.4.6 (c)) the shorter lived transients are no longer present, revealing a broad absorption band with a maximum at 285 nm. A transient decay trace recorded at 280 nm shows predominantly a very long lived transient (Figure 2.4.5 (c)).

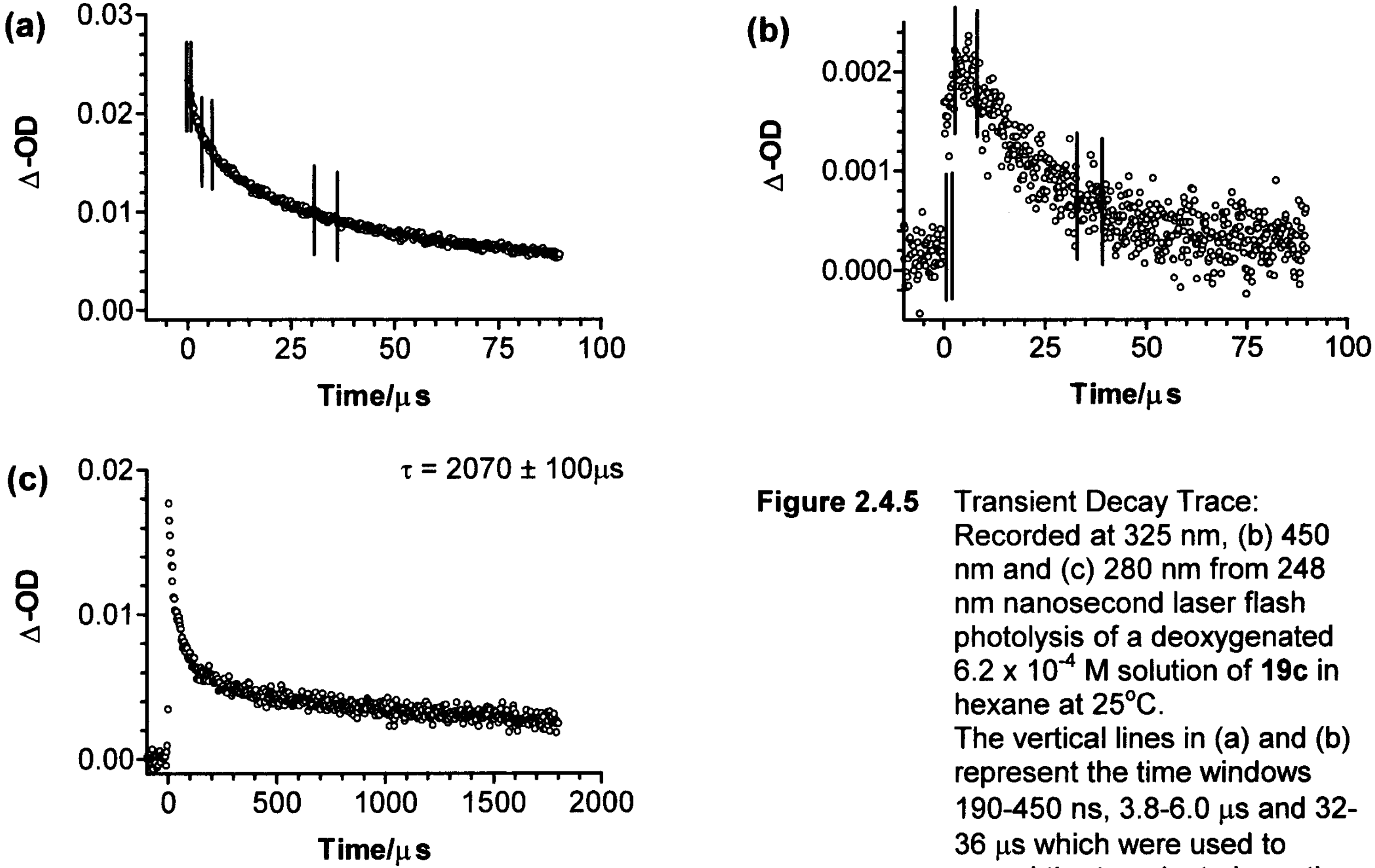

Figure 2.4.5 Transient Decay Trace: Recorded at 325 nm, (b) 450 nm and (c) 280 nm from 248 nm nanosecond laser flash photolysis of a deoxygenated 6.2 x 10^{-4} M solution of **19c** in hexane at 25°C. The vertical lines in (a) and (b) represent the time windows 190-450 ns, 3.8-6.0 μs and 32-36 μs which were used to record the transient absorption spectra in Figure 2.4.6 (a), (b) and (c), respectively.

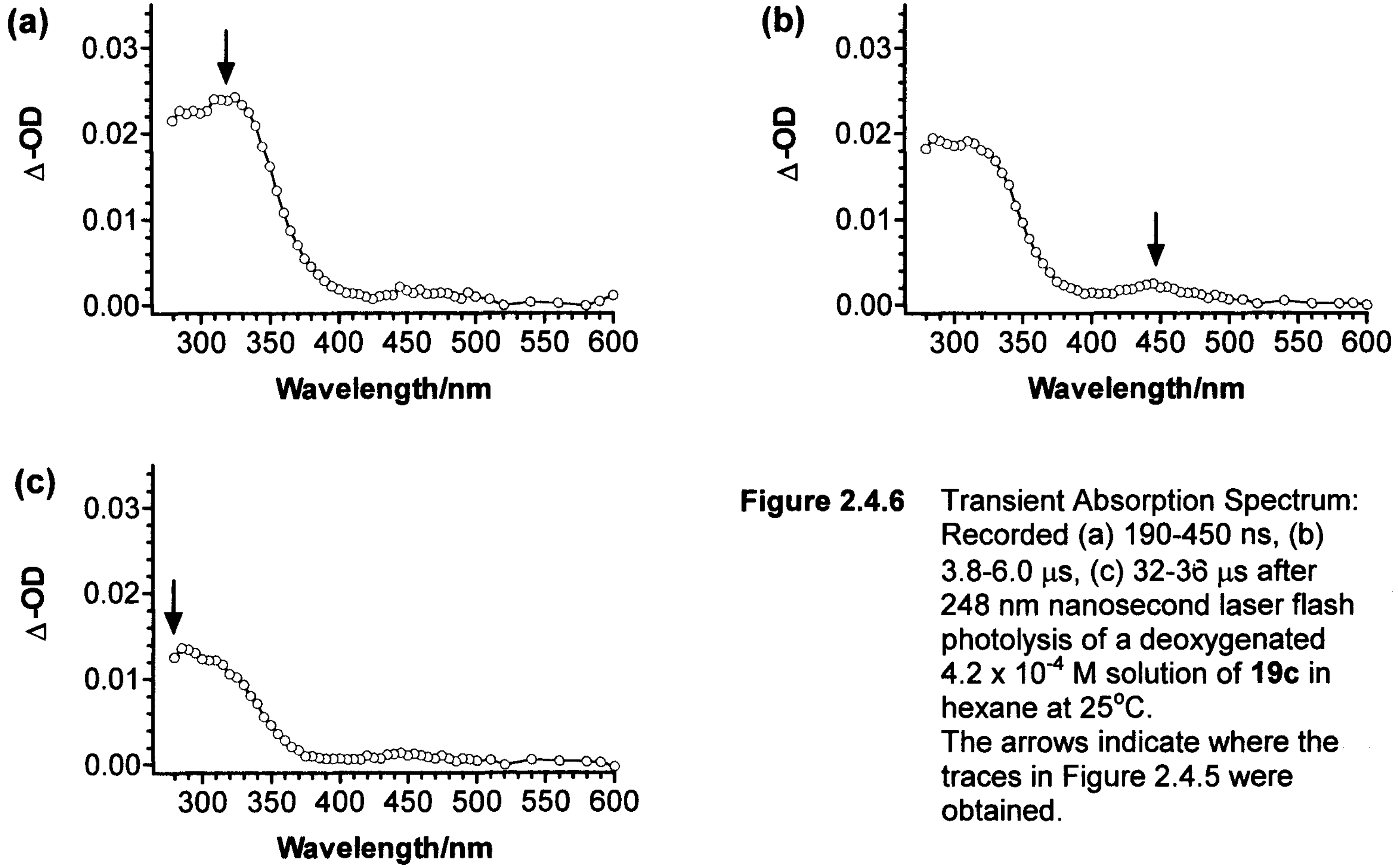

Figure 2.4.6 Transient Absorption Spectrum: Recorded (a) 190-450 ns, (b) 3.8-6.0 μs, (c) 32-36 μs after 248 nm nanosecond laser flash photolysis of a deoxygenated 4.2 x 10^{-4} M solution of **19c** in hexane at 25°C.
The arrows indicate where the traces in Figure 2.4.5 were obtained.

The transient absorption spectrum from the photolysis of **19c** is very similar to that of **19b** in that the spectrum shifts to shorter wavelengths with time. This indicates that more than one transient species is produced from the photolysis of **19c**, which decay with different rate constants. The subtraction of Figure 2.4.6 (c) from Figure 2.4.6 (a) allows for the isolation of the spectra of those species that are present immediately after the laser pulse, and which decay the fastest. The spectrum resulting from this manipulation is shown in Figure 2.4.7.

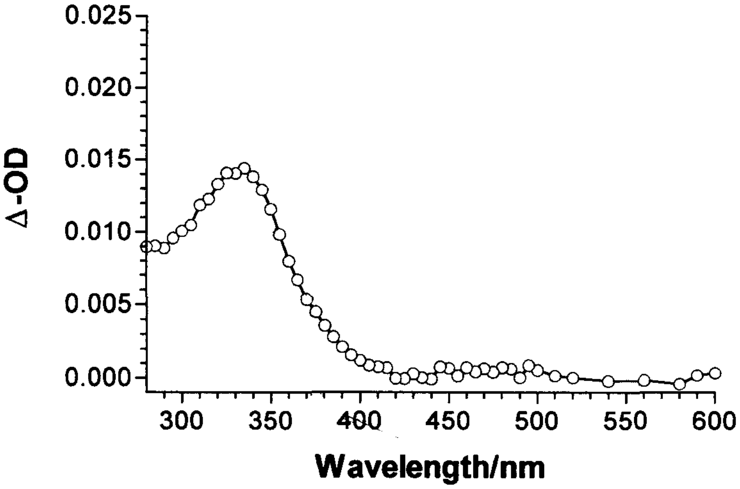

Figure 2.4.7 Transient Absorption Spectrum of **20c**: The subtraction of the long lived transient (Figure 2.4.6(c)) from the spectrum recorded immediately after the laser pulse (Figure 2.4.6(a)): laser flash photolysis of a deoxygenated 6.2 x 10^{-4} M solution of **19c** in hexane at 25 °C.

Comparison of Figure 2.4.6 (a) and Figure 2.4.6 (c) suggests that the transient in Figure 2.4.7 comprises ca. 50% of the initial transient absorption produced upon laser excitation. From the two-component analysis of the decay trace of Figure 2.4.5 (a), its lifetime is estimated to be 3.5 ± 0.3 μs in deoxygenated hexane solution at 25°C. The lifetime of the 285 nm transient is estimated to be 2100 ± 100 μs (errors reported are $\pm 2\sigma$ from least squares regression analysis). The error associated with the lifetime of the long lived transient is derived from the least squares analysis of the concentration-time data of Figure 2.4.5(c) and is underestimated considering the decay is monitored over only one half-life. A more reasonable estimate of the error would be ca. 30%.

The lifetime of the transient of Figure 2.4.7 is insensitive to the presence of oxygen, but is shortened upon addition of aliphatic alcohols or acetic acid to the solution (vide infra). The λ_{max} of the transient is 335 nm which is very close to λ_{max} of **20a** and **20b**. These observations allow for the transient to be assigned to 1,1-bis(bis-3,5-(trifluoromethyl)phenyl)germene **20c** (eq 2.11).

The kinetic behaviour of the transient absorbing at λ_{max} = 450 nm can only be described qualitatively because of its very low signal intensity. The species grows in over ca. 10 μs and then decays over tens of microseconds. It disappears entirely when small amounts of oxygen, aliphatic alcohols or acetic acid are added to the solution. On the basis of this behaviour and a comparison with **61a** and **61b**, this species is identified as tetrakis (bis-3,5-(trifluoromethyl)phenyl)digermenes **61c** formed by dimerization of bis (3,5-(trifluoromethyl)phenyl)germylene **59c**.

The long-lived transient with λ_{max} = 285 nm is comparable to the long lived transient observed from the photolysis of **19b**. The species has a lifetime of 2100 ± 100 μs and is sensitive to the presence oxygen. It is unknown whether this species forms immediately after the laser pulse or grows because its absorption band overlaps with the absorption band of germene **20c**. The structure of this transient could be speculated as a digermirane, the addition product of a germylene with a germene (eq 2.12). 1,1,2,2-tetrakis(2,6-diethylphenyl)digermirane has been previously prepared by Ando and coworkers[68, 69] and shown to have a λ_{max}=300 nm which is consistent with the absorption maximum of the long lived transient.

Time-resolved UV absorption spectra of a solution containing **19c** (5×10^{-4} M) in air saturated acetonitrile were recorded over the time intervals: 0.2-1.1 μs

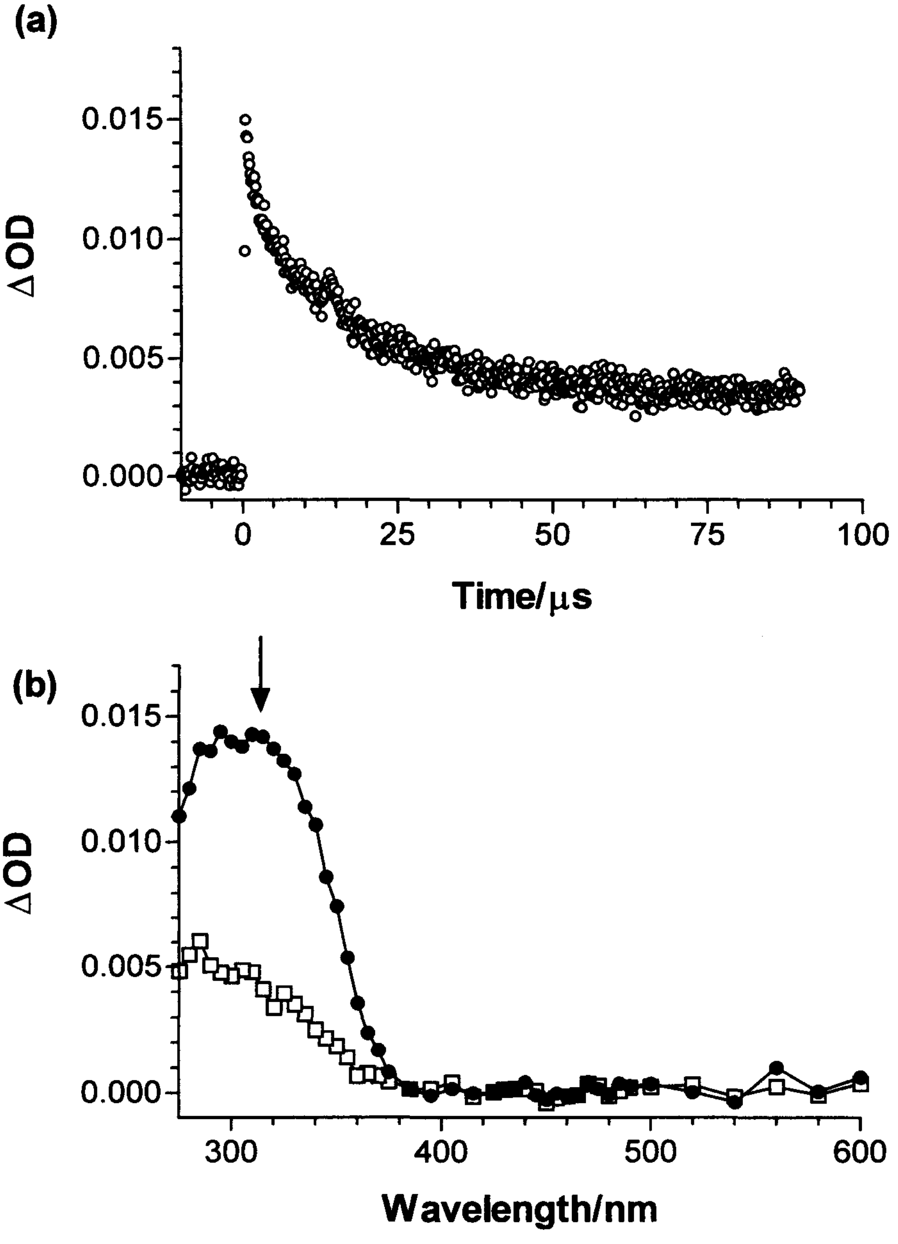

Figure 2.4.8 (a) Transient Decay Trace: Recorded at 325 nm from 248 nm nanosecond laser flash photolysis of a deoxygenated 5 x 10^{-4} M solution of **19c** in acetonitrile at 25 °C.
(b) Transient Absorption Spectra: Recorded 0.2-1.1 μs (●) and 60-89 μs (□) after 248 nm nanosecond laser flash photolysis of a deoxygenated 5 x 10^{-4} M solution of **19c** in acetonitrile at 25 °C.

and 60-89 μs after the laser pulse (Figure 2.4.8(b)). A transient decay trace at 325 nm exhibits complex kinetics, as shown in Figure 2.4.8(a). The transient absorption spectrum in the first time window (0.2-1.1 μs, Figure 2.4.8(b)) displays a broad band centred at 315 nm. In the second time window (60-89 μs, Figure 2.4.8(b)) shows an absorption band centered at >300 nm. The transient absorption spectrum from the photolysis of **19c** is very similar to that of **19b** in that the spectrum shifts to shorter wavelengths with time. This indicates that more than one transient species is produced from the photolysis of **19c**, which decay with different rate constants

Time-resolved UV absorption spectra of solutions containing **19b** (5.5×10^{-4} M) and **19c** (6.4×10^{-4} M) in dry, air-saturated hexane were recorded over the time intervals 1.2-1.9 μs and 1.3-3.8 μs, respectively, and are shown in Figure 2.4.9 (b) and Figure 2.4.10 (b). Under these conditions, there is no absorption observed at 450 nm indicating that the formation of the digermene **61b** and **61c** is suppressed in the presence of oxygen. Transient decay traces at 325 nm for the photolysis of both **19b** and **19c** exhibit transients that decay with complex kinetics; the decays can be fit to the sum of two first-order exponentials (Figure 2.4.9 (a) and Figure 2.4.10 (a)).

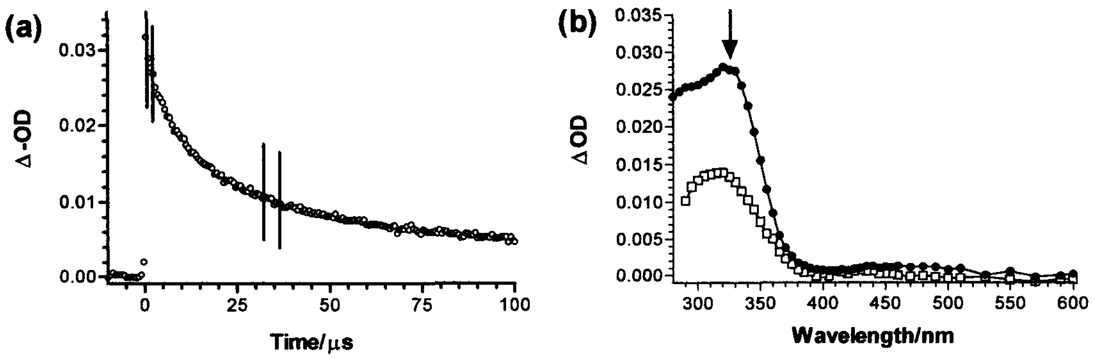

Figure 2.4.9 (a) Transient decay recorded at 325 nm from 248 nm nanosecond laser flash photolysis of an air-saturated 5.5 x 10^{-4} M solution of **19b** in hexane at 25°C.
The vertical lines represent the time windows 1.2-1.9 μs and 32-36 μs which were used to record the transient absorption spectra in Figure 2.4.9 (b).
(b) Transient absorption spectra recorded at 1.2-1.9 μs (●) and 32-36 μs (□), after 248 nm nanosecond laser flash photolysis of an air-saturated 5.5 x 10^{-4} M solution of **19b** in hexane at 25°C. The arrow indicates where the trace in Figure 2.4.9 (a) was obtained.

In order to accurately study the kinetics of germenes **20b** and **20c**, it is necessary to minimize the amount of germylene (**59b**, **59c**) present in solution. The most effective way of removing germylenes without affecting the yield or decay rate of the germene involves carrying out experiments in air-saturated solutions.[49, 70, 71] 1,1-Diphenylmetallaenes are relatively unreactive toward oxygen ($k_q \approx 5 \times 10^6$ $M^{-1}s^{-1}$),[49] whereas 1,1-diphenylgermylene has been show to be more reactive with oxygen ($k_q = 4 \times 10^7$ $M^{-1}s^{-1}$).[61] Therefore kinetic experiments performed in air-saturated conditions would significantly reduce the lifetime of the germylene allowing for accurate decay measurements of germenes **20b** and **20c**.

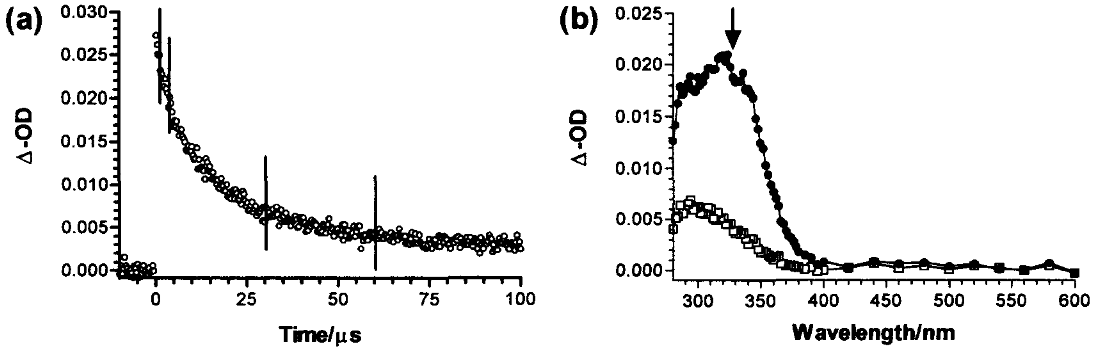

Figure 2.4.10 (a) Transient decay recorded at 325 nm from 248 nm nanosecond laser flash photolysis of an air-saturated 6.4 x 10^{-4} M solution of **19c** in hexane at 25°C.
The vertical lines represent the time windows 1.3-3.8 μs and 30-61 μs which were used to record the transient absorption spectra in Figure 2.4.10 (b).
(b) Transient absorption spectra recorded at 1.3-3.8 μs (●) and 30-61 μs (□) after 248 nm nanosecond laser flash photolysis of an air-saturated 6.4 x 10^{-4} M solution of **19c** in hexane at 25°C.
The arrow indicates where the trace in Figure 2.4.10 (a) was obtained.

2.4.3 Kinetic studies

Initial studies of **20b** were done in air-saturated hexane in order to eliminate interference from germylene **54b**. The addition of MeOH, MeOD or *t*-BuOH (0.005-0.02 M) cause the decay of germene **20b** to proceed with clean pseudo-first order kinetics as illustrated in Figure 2.4.11(a, b). At low concentrations of MeOH (<5x10^{-3} M) 2 neutral density filters were used to decrease the light intensity of the laser, thereby decreasing the amount of germene (**20b**) formed and suppressing the dimerization reaction.

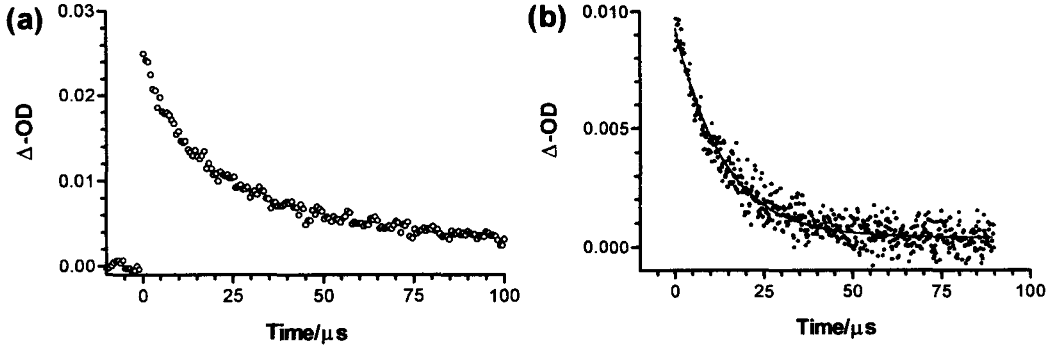

Figure 2.4.11 (a) Transient Decay Trace: Recorded at 325 nm from 248 nm nanosecond laser flash photolysis of an air-saturated 5 x 10^{-4} M solution of **19b** in hexane at 25°C.
(b)Transient Decay Trace: Same as (a), with [MeOH] = 1.07×10^{-3} M and 2 neutral density filters.

The lifetime of the transient varied in a quadratic fashion with alcohol concentration (Figure 2.4.12 and Figure 2.4.13). Least squares analysis using a quadratic fit of the data according to eq 2.14 gave fits with acceptable correlation coefficients ($R^2 > 0.98$). The bimolecular and termolecular rate constants determined from this expression are summarized in Table 2.1.

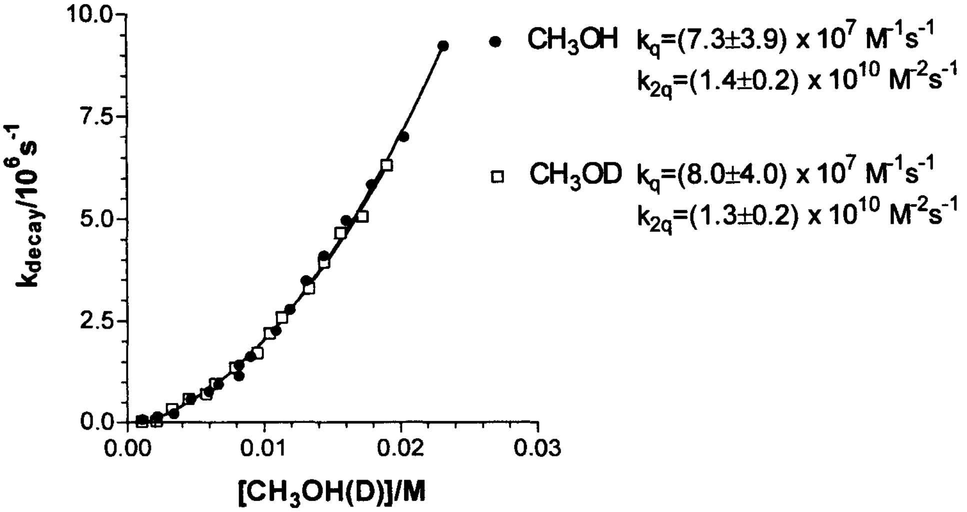

Figure 2.4.12 Quenching plots of k_{decay} of **20b** versus quencher concentration for: Methanol (●) (23.5°C) and Methanol-*d* (□) (25.5°C) in air-saturated hexane (Table 2.1).
Errors reported as ± 2σ from least squares regression analysis.

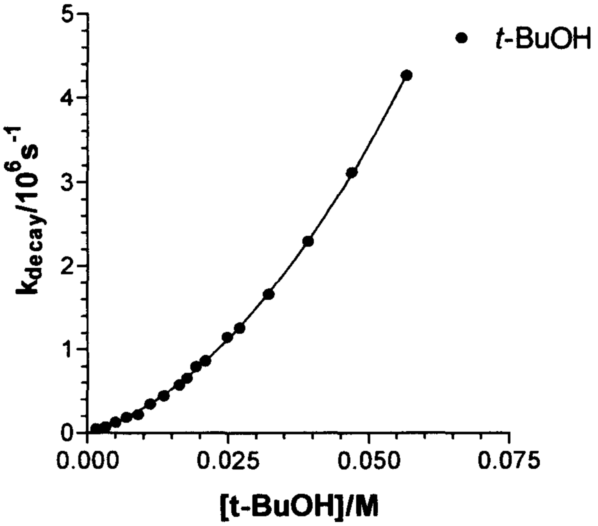

Figure 2.4.13 Quenching plots of k_{decay} of **20b** versus quencher concentration for: *t*-Butanol (●) (25.5°C) in air-saturated hexane (Table 2.1).
Errors reported as ± 2σ from least squares regression analysis.

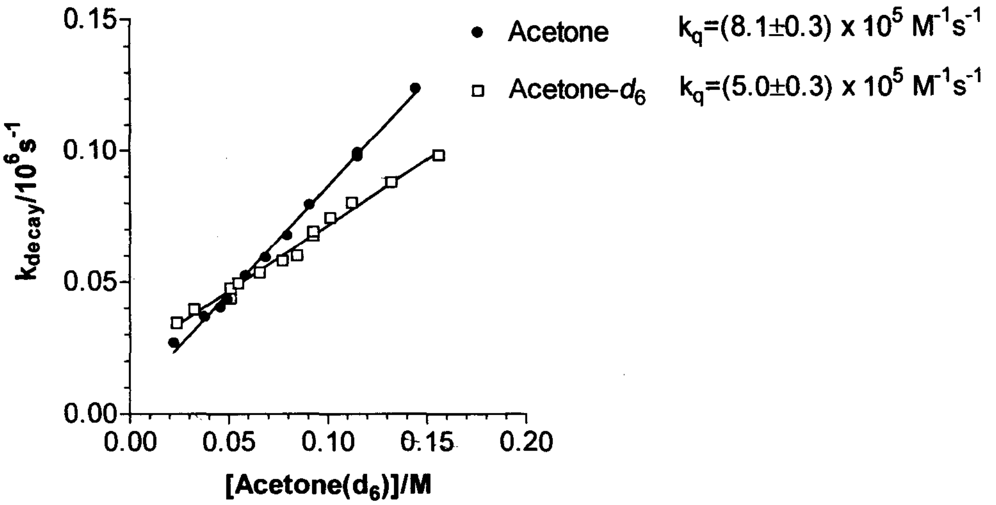

Figure 2.4.14 Quenching plots of k_{decay} of **20b** versus quencher concentration for: Acetone (●) (24.5°C) and Acetone-d_6 (□) (25.5°C) in air-saturated hexane (Table 2.1).

Errors reported as ± 2σ from linear least squares analysis.

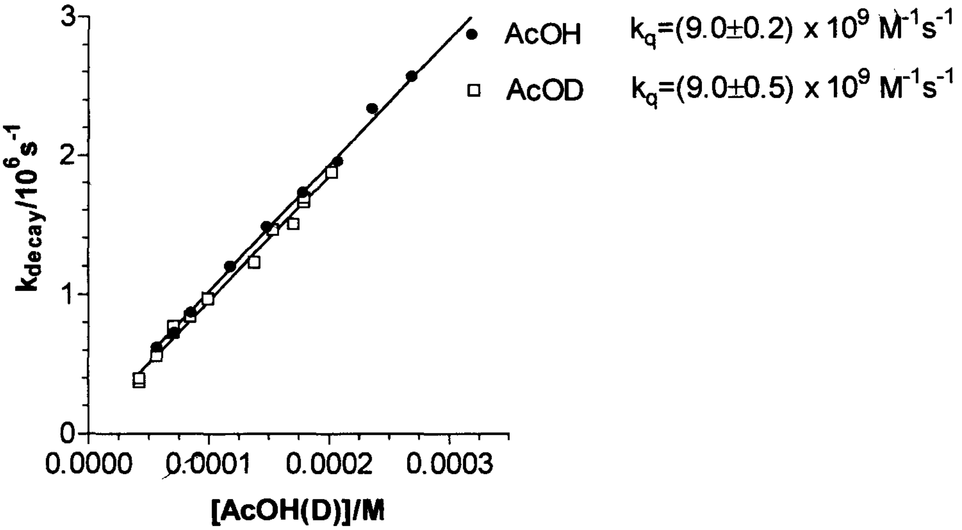

Figure 2.4.15 Quenching plots of k_{decay} of **20b** versus quencher concentration for: Acetic Acid (●) (25.5°C) and Acetic Acid-*d* (□) (25.0°C) in air-saturated hexane (Table 2.1).

Errors reported as ± 2σ from linear least squares analysis.

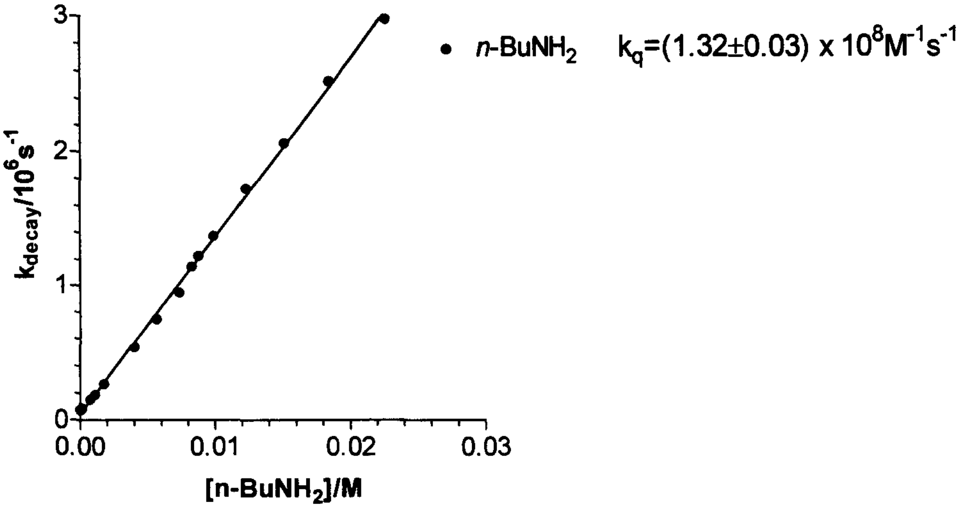

Figure 2.4.16 Quenching plots of k_{decay} of **20b** versus quencher concentration for: *n*-Butylamine (●) (25.0°C) in air-saturated hexane (Table 2.1).
Errors reported as ± 2σ from linear least squares analysis.

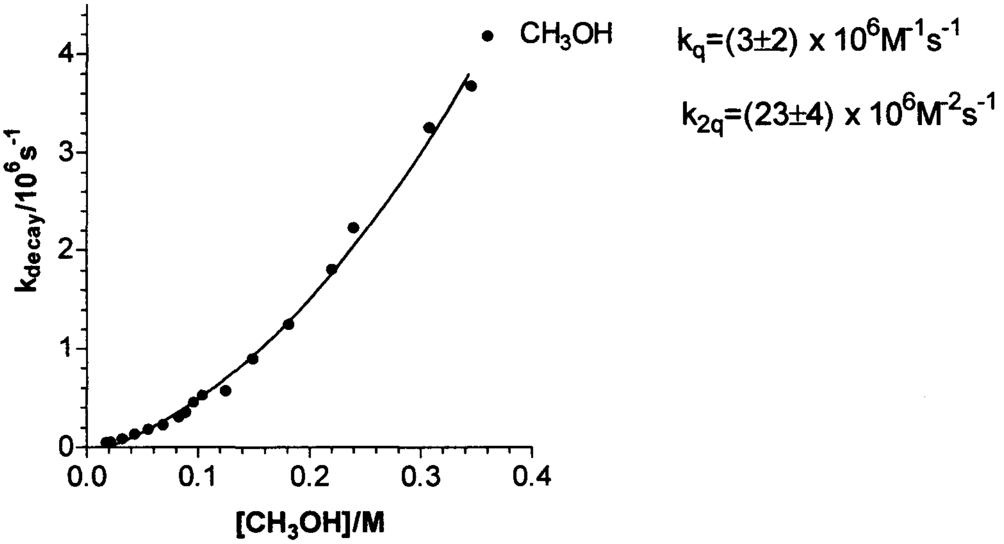

Figure 2.4.17 Quenching plot of k_{decay} of **20b** versus quencher concentration for: methanol (●) (25.0 °C) in deoxygenated acetonitrile.
Errors reported as ± 2σ from least squares regression analysis.

A plot of k_{decay} versus [Q] for methanol in acetonitrile is shown in Figure 2.4.17. This plot was fit to eq 2.14 to yield the following bi- and termolecular rate constants: (3 ± 2) x $10^6 M^{-1}s^{-1}$ and (23 ± 4) x $10^6 M^{-2}s^{-1}$. These rate constants are ca. 1 and 3 orders of magnitude, respectively, smaller than the corresponding rate constants measured in hexane (Table 2.1). 1,1-Diphenylsilene only shows a small reduction in its reactivity towards methanol in acetonitrile compared to hexane.[41]

Plots of k_{decay} versus [Q] for acetic acid, acetic acid-*d*, acetone, acetone-d_6 as well as *n*-butylamine are shown in Figure 2.4.14-Figure 2.4.16. The concentrations of acetic acid or acetic acid-*d* were corrected for oligomerization in hexane using the dimerization equilibrium constant for AcOH: K_{dimer} = 3200±500 dm^3/mol.[72] These plots gave excellent correlation coefficients when analysed by linear least-squares analysis according to eq 2.13. The bimolecular rate constants obtained in these experiments are shown in Table 2.1.

$$k_{decay} = k_d^o + k_q[Q] \qquad \textbf{2.13}$$

$$k_{decay} = k_d^o + k_q[Q] + k_{2q}[Q]^2 \qquad \textbf{2.14}$$

Kinetic studies of **20c** in nitrogen saturated hexane proved quite difficult because of the presence of the long lived transient which has a λ_{max} = 285 nm.

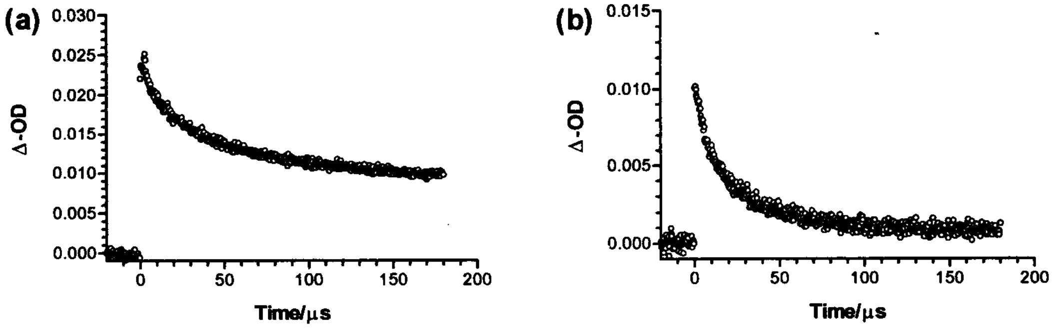

Figure 2.4.18 (a) Transient Decay Trace: Recorded at 325 nm from 248 nm nanosecond laser flash photolysis of a deoxygenated 6.2 x 10^{-4} M solution of **19c** in hexane at 25°C.
(b) Transient Decay Trace: Same as (a), with [Acetone] = 0.0218 M and 2 neutral density filters.

Transient decay traces at 325 nm exhibit a long lived residual absorption which complicates analysis of the decay (Figure 2.4.18(a)). However, upon addition of small amounts of quencher the Δ-OD of the residual absorption is greatly reduced and allows for determination of pseudo-first order decay rates (Figure 2.4.18(b)).

The addition of MeOH, MeOD, AcOH, AcOD and *n*-$BuNH_2$ (10^{-4} - 0.011 M) caused the decay of signal to proceed with mixed kinetics. The transient decays contained a short and long lived species that both decayed with first order kinetics in the presence of methanol. The longer lived transient was insensitive to the concentration of methanol. Therefore in order to determine rate constants of the germene **20c** from the decay traces, the data were analyzed using a two phase exponential decay analysis (eq 2.15).

$$y = A_{o1}e^{-(k1t)} + A_{o2}e^{-(k2t)} \qquad \textbf{2.15}$$

This analysis was used until the lifetime of germene was reduced to ≤ 1μs. Under these conditions, the long lived transient can be approximated as a non-decaying residual absorption, superimposed on a clean pseudo-first order decay of the germene.

It was found that the lifetime of germene **20c** varied in a quadratic fashion with alcohol concentration (Figure 2.4.19 and Figure 2.4.20). Least-squares analysis of the data according to eq 2.14 gave fits with acceptable correlation coefficients ($R^2 > 0.98$). The bi and termolecular rate constants are summarized in Table 2.2. Plots of k_{decay} vs. [Q] for acetic acid and acetic acid-*d*, and *n*-butylamine (Figure 2.4.22 and Figure 2.4.23) were analyzed using linear least-squares analysis (eq 2.12) and showed excellent correlations. Upon addition of acetone or acetone-d_6, germene **20c** decayed with clean pseudo-first order kinetics and plots of k_{decay} vs. [Q] displayed excellent linear correlations (Figure 2.4.21). The rate constants determined from these plots can be found in Table 2.2.

Since these experiments were carried out in nitrogen saturated hexane, a subsequent experiment was performed involving the reaction of methanol and **20c** in air-saturated hexane. This was done to determine whether the rate constants measured were affected by the presence of oxygen or not. The lifetime of **20c** varied in a quadratic fashion with methanol concentration and least-squares analysis with eq 2.14 gave an acceptable correlation coefficient ($R^2 > 0.996$). The bi- and termolecular rate constants were in good agreement with the corresponding rate constants found in nitrogen saturated solutions (Table 2.2). A plot of k_{decay} versus [Q] for methanol in acetonitrile is shown in Figure 2.4.24. This plot was fit to eq 2.13 to yield the bimolecular rate constant $(9.6 \pm 0.4) \times 10^6 M^{-1}s^{-1}$. In acetonitrile the transient being monitored only shows a first order dependence on methanol concentration with rate constants that are ca 1 order of magnitude smaller than the rate constant measured in hexane.

The kinetic isotope effects for the reaction of germene **20b** and **20c** with methanol, acetic acid and acetone are listed in Table 2.3. For comparison the equivalent kinetic isotope effects observed for 1,1-diphenylgermene **20a**[36] and 1,1-diphenylsilene **40**[35, 41] are included in Table 2.3.

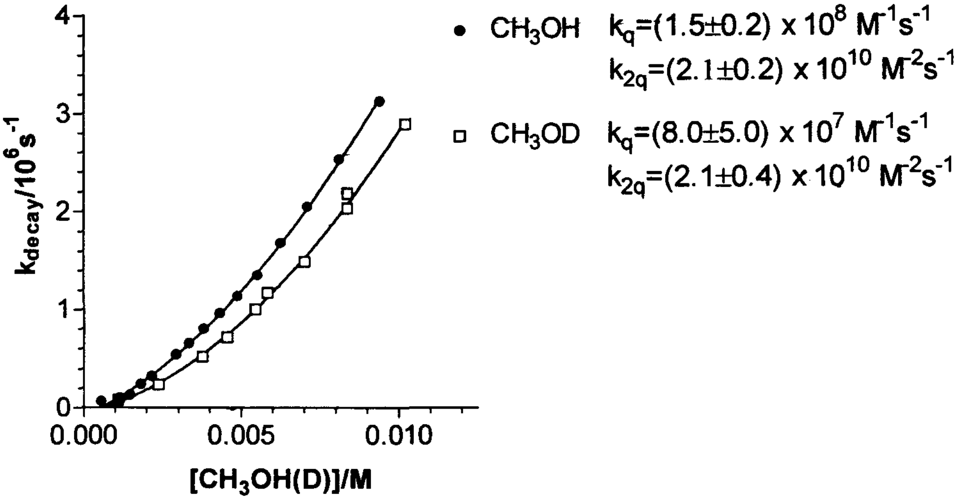

Figure 2.4.19 Quenching plots of k_{decay} of **20c** versus quencher concentration for: Methanol (●) (25.5°C) and Methanol-*d* (□) (24.5°C) in deoxygenated hexane (Table 2.2).
Errors reported as ± 2σ from least squares regression analysis.

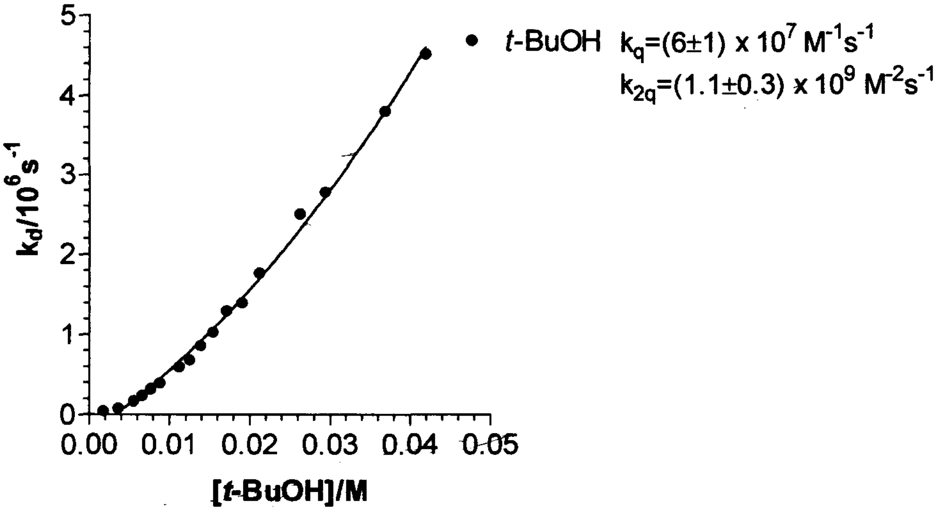

Figure 2.4.20 Quenching plots of k_{decay} of **20c** versus quencher concentration for: *t*-Butanol (●) (25.5°C) in deoxygenated hexane (Table 2.2).
Errors reported as ± 2σ from least squares regression analysis.

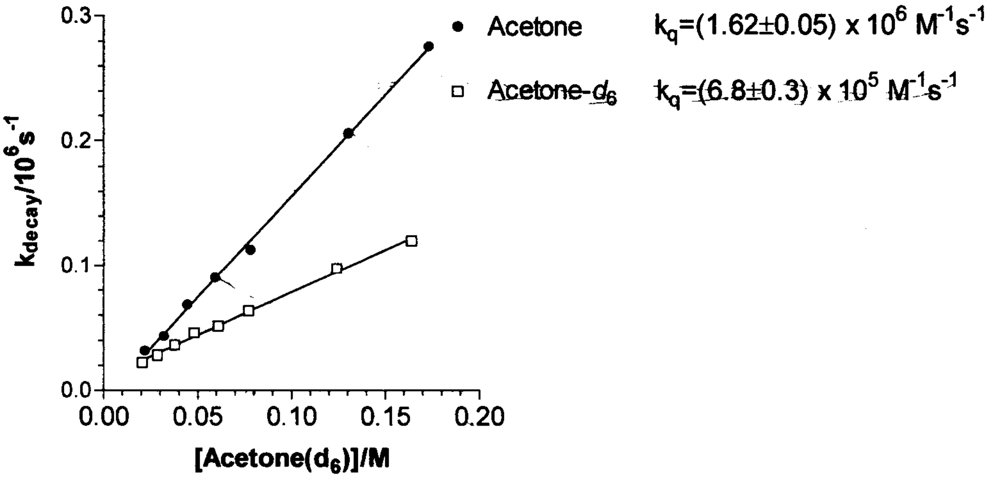

Figure 2.4.21 Quenching plots of k_{decay} of **20c** versus quencher concentration for: Acetone (●) (25.5°C) and Acetone-d_6 (□) (25.5°C) in deoxygenated hexane (Table 2.2).

Errors reported as ± 2σ from linear least squares analysis.

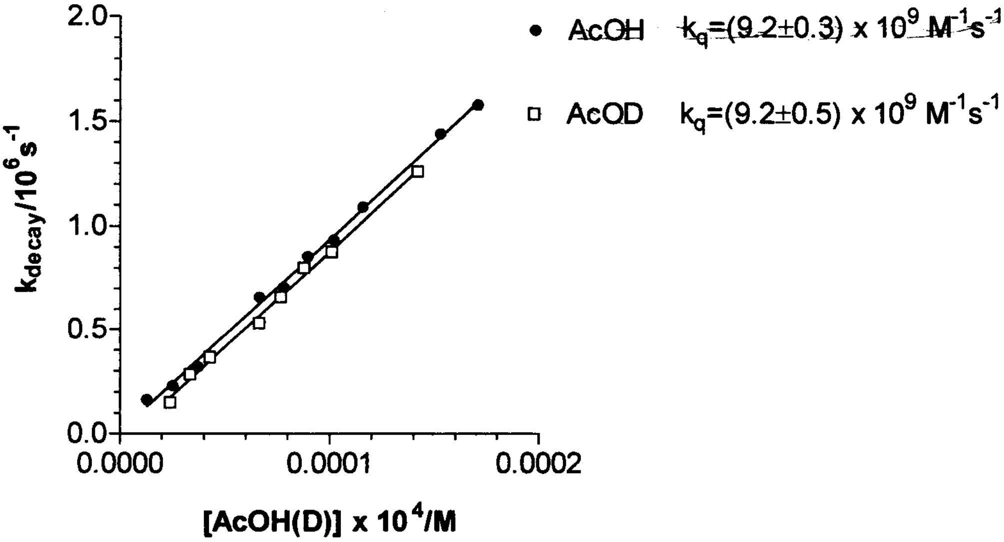

Figure 2.4.22 Quenching plots of k_{decay} of **20c** versus quencher concentration for: Acetic Acid (●) (25.5°C) and Acetic Acid-*d* (□) (25.5°C) in deoxygenated hexane (Table 2.2).

Errors reported as ± 2σ from linear least squares analysis.

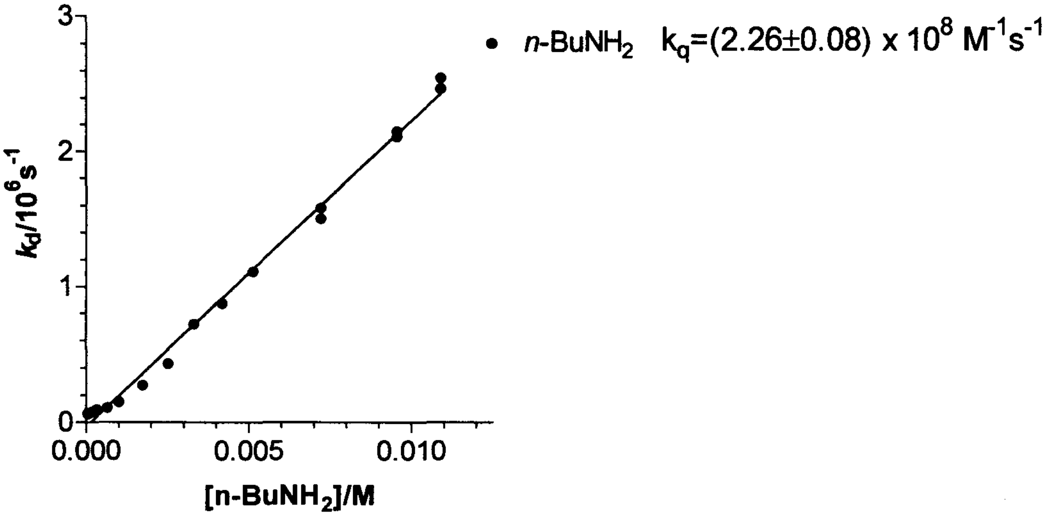

Figure 2.4.23 Quenching plots of k_{decay} of **20c** versus quencher concentration for: *n*-Butylamine (●) (25.5°C) in deoxygenated hexane (Table 2.2).
Errors reported as ± 2σ from linear least squares analysis.

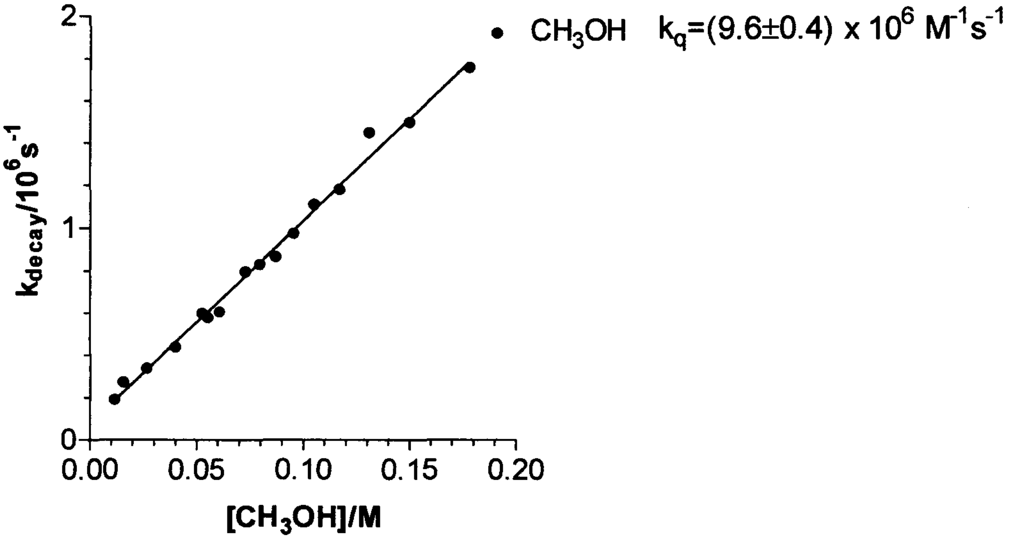

Figure 2.4.24 Quenching plots of k_{decay} of **20c** versus quencher concentration for: Methanol (●) (25.0°C) in deoxygenated acetonitrile.
Errors reported as ± 2σ from linear least squares analysis.

Table 2.1 Rate constants for Quenching of germene **20b** with Methanol (MeOH), Methanol-d (MeOH), *tert*-Butyl Alcohol (*t*-BuOH), Acetone, Acetone-d_6, Acetic Acid (AcOH), Acetic Acid-d (AcOD) and *n*-Butylamine (*n*-BuNH_2) in dried air-saturated Hexane Solutions at 23.5 - 25.5°C.[a]

Quencher	Temperature /(°C)	k_q/(x 10^7) $M^{-1}s^{-1}$	k_{2q}/(x 10^9) $M^{-2}s^{-1}$	R^2	# of Data Points
MeOH[b]	23.5	7.3 ± 3.9	14 ± 2	0.997	18
MeOD[b]	25.5	8.0 ± 4.0	13 ± 2	0.996	15
***t*-BuOH**[b]	25.5	2.2 ± 0.2	0.94 ± 0.04	1.000	17
Acetone[c]	24.5	0.081 ± 0.003	–	0.997	11
Acetone-*d*$_6$[c]	25.5	0.050 ± 0.003	–	0.989	13
AcOH[c]	25.5	900 ± 20	–	0.998	10
AcOD[c]	25.0	900 ± 50	–	0.997	13
***n*-BuNH_2**[c]	25.0	13.20 ± 0.03	–	0.999	16

a. Errors reported as ± 2σ from least squares analysis of k_{decay} – concentration data.
b. k_{decay} varies quadratically with [Q]; see eq 2.14.
c. k_{decay} varies linearly with [Q]; see eq 2.13.

Table 2.2 Rate constants for Quenching of germene **20c** with Methanol (MeOH), Methanol-d (MeOH), *tert*-Butyl Alcohol (*t*-BuOH), Acetone, Acetone-d_6, Acetic Acid (AcOH), Acetic Acid-d (AcOD) and *n*-Butylamine (*n*-$BuNH_2$) in dried nitrogen saturated Hexane Solutions at 23.5 - 25.5°C.[a]

Quencher	Temperature /(°C)	k_q/(x 10^7) $M^{-1}s^{-1}$	k_{2q}/(x 10^9) $M^{-2}s^{-1}$	R^2	# of Data Points
MeOH[b]	23.5	15 ± 2	21 ± 2	0.994	18
MeOH[b] **Air-saturated**	25.5	15 ± 4	16 ± 3	0.995	17
MeOD[b]	25.5	8.0 ± 5.0	21 ± 4	0.998	9
***t*-BuOH**[b]	25.5	6 ± 1	1.1 ± 0.3	0.996	17
Acetone[c]	25.5	0.162 ± 0.005	–	0.984	7
Acetone-*d*$_6$[c]	25.5	0.068 ± 0.003	–	0.986	8
AcOH[c]	25.5	920 ± 30	–	0.998	10
AcOD[c]	25.5	920 ± 50	–	0.996	8
***n*-BuNH$_2$**[c]	25.5	22.6 ± 0.8	–	0.995	17

a. Errors reported as ± 2σ from least squares analysis of k_{decay} – concentration data.
b. k_{decay} varies quadratically with [Q]; see eq 2.14.
c. k_{decay} varies linearly with [Q]; see eq 2.1.3.

Table 2.3 The bi- and termolecular kinetic isotope effects observed for the reaction of germenes **20a**, **20b**, **20c** and silene **40** with methanol, acetic acid and acetone.

	20a[36, 37]	**20b**		**20c**		**40**[35, 41]
Quencher	**Ter-**	**Bi-**	**Ter-**	**Bi-**	**Ter-**	**Bi-**
CH_3OH	1.3 ± 0.4[a]	0.9 ± 0.7[b]	1.1 ± 0.2[b]	1.9 ± 1.2[c]	1.0 ± 0.2[c]	1.5 ± 0.1[a]
AcOH	0.9 ± 0.2[a]	1.0 ± 0.1[b]	–	1.0 ± 0.1[c]	–	1.1 ± 0.1[a]
Acetone	–	1.6 ± 0.1[b]	–	2.4 ± 0.1[c]	–	1.5 ± 0.1[a]

a. Kinetic Isotope Effects reported in air-saturated acetonitrile
b. Kinetic Isotope Effects reported in air-saturated hexane
c. Kinetic Isotope Effects reported in deoxygenated hexane

CHAPTER 3: DISCUSSION

3.1 Synthesis of Diarylgermacyclobutanes 19b, 19c

The synthesis of **19b** and **19c** as shown in eq 2.1 resulted in final yields of 31.3% and 20.7% respectively. The main reason for the poor yields in these syntheses was the lack of selectivity in the first step of the preparation; addition of two equivalents of aryl Grignard reagent to germanium tetrachloride. Nucleophilic additions of Grignard reagents to halocarbons follow a S_N2 type mechanism, however in the case of heavier Group 14 centres such as silicon or germanium, this mechanism does not apply. For example, studies have shown that the general mechanism of nucleophilic substitution at silicon involves the formation of pentacoordinate intermediates.[73-75] This is because silicon and germanium have longer bond lengths and accessible *d* orbitals that can allow expansion of their coordination shells from four to five or even six.[76] The mechanism for addition of Grignard reagent to either $SiCl_4$ or $GeCl_4$ is shown in eq 3.1. One important thing to note is that it has been shown that pentacoordinate silanes are more reactive toward nucleophiles than the analogous tetracoordinate species($k_{Nu2}>k_{e1}$).[77]

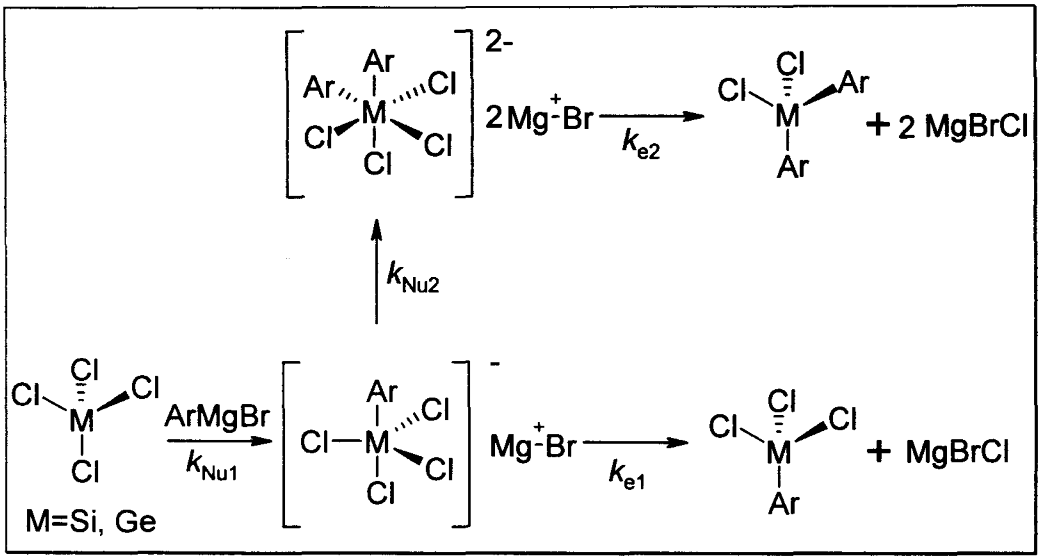

3.1

Consequently, multiple additions of aryl Grignard reagents to chlorogermanes lead to a mixture of mono-, di-, and tri-substitution products. An example of the difficulty in controlling nucleophilic additions to $SiCl_4$ is shown in eq 3.2. 2.25 molar equivalents of ethylmagnesium bromide were slowly added to $SiCl_4$ and the following substituted products and their mole ratios are shown below.[76]

$$2.25\ EtMgCl + SiCl_4 \longrightarrow EtSiCl_3 + Et_2SiCl_2 + Et_3SiCl + Et_4Si \qquad \textbf{3.2}$$

	$EtSiCl_3$	Et_2SiCl_2	Et_3SiCl	Et_4Si
Mole Ratios	1.9	0.4	1.0	0

Therefore in this work a very slow addition of 2 molar equivalents of Grignard reagent to $GeCl_4$ at low temperature with vigorous stirring is crucial in order to control the amount of substitution that occurs. Even under these conditions, GC analysis of the reaction mixtures showed a product distribution (mono : di : tri of 1:4:1 for **55b**:**56b**:**57b** and 1:6:1 for **55c**:**56c**:**57c**, respectively.

The desired disubstitution product was not separated from the reaction mixture prior to carrying out the subsequent ring closure step, as it proved difficult to separate from the mono- and trisubstituted products by distillation. Purification of the disubstituted product proved to be unnecessary, since the final germacyclobutanes **19b**, **19c** could be easily separated from the potential by-products of the reaction of **55b**, **55c** and **57b**, **57c** with the 1,3-diGrignard reagent by radial chromatography.

Compounds **19b** and **19c** were then recrystallized from methanol to give final overall yields of 31.3% and 20.7%, respectively. The two compounds were found to have purities of greater than 99.9% by GC analysis.

3.2 Steady-State Photolysis of 19b and 19c

3.2.1 In the presence of methanol

The photolysis of 1,1-bis(4-(trifluoromethyl)phenyl)germacyclobutane **19b** and 1,1-bis(3,5-bis(trifluoromethyl)phenyl)germacyclobutane **19c** in the presence of methanol leads to the formation of two germanium-containing photoproducts (<20% conversion) consistent with methanol addition to 1,1-diarylgermene **20b**, **20c** and 1,1-diarylgermylene **59b**, **59c** (eq 3.3). This is surprising since 1,1-

diphenylgermacyclobutane **19a** was always thought to be "clean" photochemical source of 1,1-diphenylgermene.[36] Although there are previously published results showing that germylene extrusion occurs thermally from germacyclobutanes,[32] this is the first example to indicate that the process also occurs photochemically.

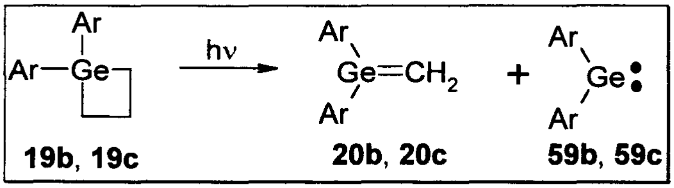

3.3

The ^{1}H NMR and mass spectra of the 1,1-diarylmethoxymethylgermanes **42b**, **42c**, are very similar to those of methoxymethyldiphenylgermane **42a**.[36] The high-frequency shifts of the singlets due to the methyl (0.1 ppm and 0.21 ppm) and methoxy (0.05 ppm and 0.009 ppm) groups in the NMR spectra of **42b** and **42c**, respectively, relative to those in the spectrum of the parent methoxymethyldiphenylgermane (**42a**) are consistent with the deshielding effect of the trifluoromethyl groups on the aromatic rings.[60] All three compounds show homologous fragmentation patterns in their mass spectra which is indicative of structurally similar compounds.

Authentic samples of the diarylmethoxymethylgermanes **42b**, **42c** could ultimately not be obtained because the synthetic approach (outlined in eq 2.3) to preparing the compounds proved to be very difficult and the yields therefrom were poor. It is worth noting that isolation of the diarylgermanes **60b** and **60c**, proved to be quite difficult. The crude reaction mixtures were viscous oils that were difficult to purify by vacuum distillation or sublimation. After several attempts to prepare and isolate the diarylgermanes, the yields of **60b**, **60c** were maximized at 22.4% and 24.3%, respectively.

Further steps along the synthetic route outlined in eq 2.6 were attempted.[61] After further complications involving difficult isolations the final products **42b** and **42c** were not obtained.

Germylenes are known to react with alcohols by insertion into the O-H bond.[61, 62, 71, 78] The corresponding diarylmethoxygermanes **58b**, **58c** show characteristic ^1H NMR signals at δ = 6.18 ppm and δ = 6.31 ppm respectively, due to the Ge-H protons. The methoxy protons in the two compounds display a slight high-frequency shift from the methoxy protons of **42b**, **42c**. Compounds **58b** and **58c** were further identified by GC co-injection with photolysates of a reaction between the germacyclopentenes **48b**, **48c** and methanol.

The chemical yields of diarylmethoxymethylgermane **42** and diarylmethoxygermane **58** were found to be 37.8 and 34.1%, respectively, for the photolysis of **19b** (after 17% conversion), and 30.4 and 51.7% for the photolysis of **19c** (after 13% conversion), respectively, after 20% conversion. The chemical yield of cyclopropane from both precursors should be identical to the yield of germylene-derived product, assuming there is quantitative reaction of germylene with methanol. Indeed, the chemical yields of cyclopropane in the photolysis of **19b** and **19c** were 25.0% and 50.6%, respectively. Presumably some of the cyclopropane evaporated from solution, considering it has a boiling point of –33°C.

The ratios of diarylmethoxymethylgermane **42** to diarylmethoxygermane **58** were 1.1:1 from the photolysis of **19b** and 0.6:1 from the photolysis of **19c**. This indicates that the presence of trifluoromethyl groups affects the photochemistry of 1,1-diarylgermacyclobutanes. It appears that the larger the number of trifluoromethyl substituents present on the aromatic rings, the greater the yield of germylene relative to germene formed upon photoexcitation.

Finally, the quantum yields for the formation of diarylmethoxymethylgermanes **42b**, **42c** were determined to be 0.11 ± 0.01 and 0.08 ± 0.01, respectively. This is a definite decrease in quantum yield compared to the parent compound methoxymethyl-1,1-diphenylgermane **42a** (Φ = 0.21 ±

0.03). These results are consistent with the formation of more germylene and less germene from the photolysis of the germacyclobutanes **19b** and **19c**.

3.2.2 In absence of quencher

The photolyses of **19b** and **19c** in the absence of quencher led to the formation of ethylene, cyclopropane, and a product that was tentatively identified as 1,1,3,3-tetraaryl-1,3-digermacyclobutane (**21b**, **21c**) on the basis of the ^{1}H NMR spectra of the crude reaction mixtures. The two dimers appear as singlets in the ^{1}H NMR spectra at δ = 1.71 ppm and δ = 1.87 ppm, respectively. A comparison of these values with the ^{1}H NMR singlet of 1,1,3,3-tetraphenyl-1,3-digermacyclobutane (**21a**), which appears at δ = 1.62 ppm, show high-frequency shifts of the singlets of **21b** and **21c** which is consistent with the deshielding effect of the trifluoromethyl groups[60].

The chemical yields of the two dimers **21b**, **21c** at <20% conversion of the starting materials represented only 7.1% and 3.4%, respectively, of the total amount of germacyclobutane consumed. The relative yields of the two digermacyclobutanes are consistent with less germene being produced from the photolysis of **19c** than **19b**. The low chemical yields of dimer may result from a competing reaction of germene with germylene to form polymeric material (eq 3.4) considering that germylenes are well known to react with polar bonds.[62] In addition, an intense, broad band was observed to form in the aromatic region during the photolysis of both precursors, which supports the formation of a substantial amount of polymeric material.

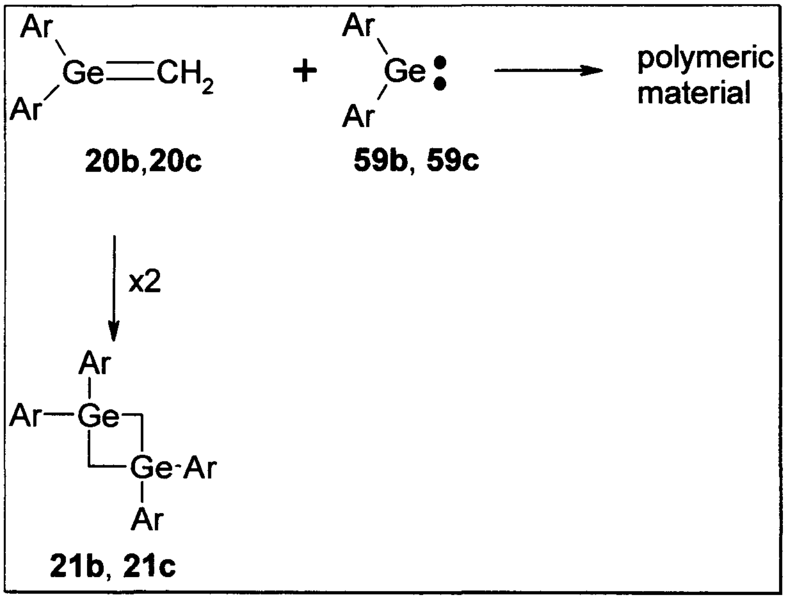

3.4

3.2.3 In the presence of 2,3-dimethyl-1,3-butadiene

In order to provide further evidence for the formation of diarylgermylene from the irradiation of germacyclobutanes, photolyses of **19b** and **19c** were conducted in the presence of 2,3-dimethyl-1,3-butadiene (DMB). DMB is known to be an efficient trapping agent for germylenes to produce the corresponding 3,4-dimethylgermacylopent-2-ene (eq 3.5).[62, 70, 71, 79] Upon photolysis of **19b** and **19c** in the presence of DMB, four major products were observed in each case: cyclopropane, ethylene, **21b** and **48b**, **48c**. Compounds **48b** and **48c** were rigorously identified by GC co-injection of the crude photolysates with authentic samples. The photolysis was kept <30% conversion of the starting materials and the chemical yields of **48b** and **48c** were 31.0% and 31.7% respectively. The product tentatively identified as **21b** was formed in a yield of 5.7%.

The parent compound, 1,1-diphenylgermacyclobutane (**19a**), was photolysed under similar conditions, and found to yield four products: cyclopropane, ethylene, **21a** and **48a**. **48a** was identified by GC co-injection of the crude photolysate with an authentic sample and was formed in a yield of 21%. The yield of **21a** was 18%.

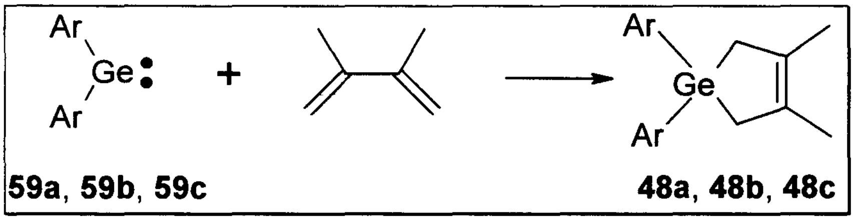

59a, **59b**, **59c** **48a**, **48b**, **48c**

3.5

The formation of **21b** as observed by ^{1}H NMR, indicates that the rate of dimerization of **20b** is greater than the rate of its reaction with DMB. On the other hand, **21c** could not be detected in the photolysis of **19c** in the presence of DMB. This might be due to a coincidence of the CH_2 proton resonance of **21c** at δ = 1.87 ppm with the CH_3 resonance of DMB at roughly the same position (δ = 1.86 ppm). Considering that **21b** was observed from the photolysis of **19b** with DMB, it is entirely plausible that **21c** would also form, although with a diminished yield. Another germanium containing product was observed in the reaction mixture, which might be the product of reaction between germene and DMB.

3.2.4 In the presence of acetone

The photolyses of **19b** and **19c** in the presence of acetone afforded a broad band in the aromatic region as well as a multitude of peaks in the aliphatic region of the ^{1}H NMR spectra. Moreover, GC analysis showed no major products at > 30% conversion of starting materials. These results are indicative of the formation of polymeric material, which is consistent with previously published results for the photolysis of 1,1-diphenylgermacyclobutane **19a**[36] under similar conditions.

The results in section 2.2 suggest that the lowest excited states of the diarylgermacyclobutanes **19a-c** react via two competing pathways to form reactive intermediates which can be trapped by added reagents: germene extrusion with the co-product ethylene (k_1) or germylene extrusion with the co-product cyclopropane (k_2) (eq 3.6). The reaction pathways leading to germylene and germene most likely involves the intermediacy of a 1,4-biradical, which forms from the excited singlet states of the precursors (eq 3.6). A similar 1,4-biradical intermediate has been suggested to be involved in the pyrolysis of 1,1-dimethylgermacyclobutane **44,**[32] as well as in the photolysis of 1,1,3,3-

tetraphenyl-1,3-digermene **21**.[39] The one general trend observed from the photolyses of the germacyclobutanes **19a-c** is that as more trifluoromethyl groups are substituted on the phenyl rings there is an increase in the rate of formation of germylene compared to germene from the biradical intermediate.

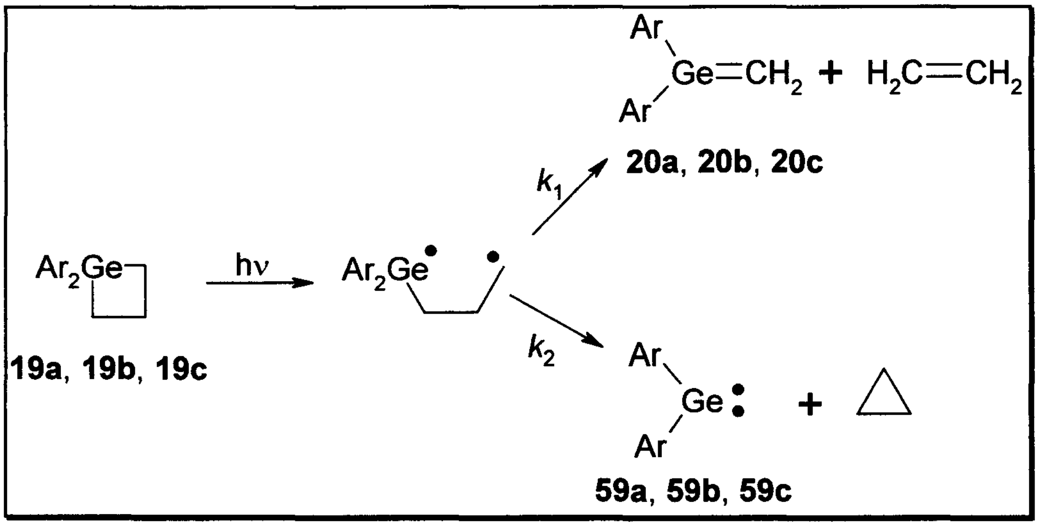

3.6

3.3 Nanosecond Laser Flash Photolysis

3.3.1 Transient Absorption Spectra

Nanosecond laser flash photolysis of **19b** in deoxygenated hexane allowed the detection of transients possessing absorption maxima centred at 330 nm, 450 nm and 310 nm, and lifetimes of 7.5 μs, 47 μs, and 2900 μs, respectively, as illustrated in Figures 2.4.1(a-c).

The transient species with λ_{max} = 330 nm (Figure 2.4.3) has been assigned to 1,1-diarylgermene **20b** based on the location of its ultraviolet absorption maximum, the insensitivity of its lifetime to oxygen, and its high reactivity with aliphatic alcohols.[36] Furthermore, under air or nitrogen saturated conditions the transient decays with predominant second order kinetics, suggesting that it undergoes dimerization.

The transient exhibiting an absorption maximum at 450 nm has been assigned to 1,1,3,3-tetraaryldigermene **61b**. This identification is based on its kinetic behaviour in the absence of quenchers as well as the location of its absorption maximum.[61] In air-saturated solutions this transient is completely absent (Figure 2.4.9(b)) which is also consistent with the behaviour of digermenes. One point that needs addressing is the absence of a transient absorption assignable to 1,1-diarylgermylene **59b**, which is expected to appear at ~500 nm.[61] The formation of digermene is the only transient spectroscopic evidence that germylene **59b** is formed. The fate of germylene **59b** under these conditions can only be speculated on. The presence of a third transient which has a λ_{max} = 310 nm may be the result of germylene **59b** inserting into the Ge=C bond of germene **20b** to form a digermirane. Germylenes are known to be very reactive to both unsaturated bonds and polar bonds,[62] so this type of reaction is certainly plausible. A similar digermirane has been shown to have a λ_{max}=300 nm consistent with this assignment.[68, 69]

Similarly, laser flash photolysis of **19c** in deoxygenated hexane solution afforded transients exhibiting absorption maxima centred at 330 nm, 450 nm and 285 nm and lifetimes of 3.9 μs, 21 μs, and 2100 μs, respectively, as illustrated in Figure 2.4.5 (a-c). The transient species with λ_{max}= 330 nm has been assigned to 1,1-diarylgermene **20c**, based on the same criteria described for germene **20b**. Similarly, the transient with an absorption maximum at 450 nm has been attributed to 1,1,3,3-tetraaryldigermene **61c**. As in the case of the photolysis of **19b**, no absorption was detected at ~ 500 nm, indicating the lack of direct evidence for 1,1-diarylgermylene **59c**.

Laser flash photolysis of **19b** and **19c** in acetonitrile yield transient absorption spectra that change (i.e. shift to shorter wavelengths) with time indicating that the photolysis of **19b** and **19c** yield more than one transient species, which decay with different rate constants. Since germylene-acetonitrile complexes have been shown to have a $\lambda_{max}\approx$320 nm,[61] and 1,1-diphenylgermene has a $\lambda_{max}\approx$320 nm in acetonitrile,[36] the absorption bands most likely consist of both the complex and the germene.

3.3.2 Kinetic Studies

The first issue that needs to be addressed here is the treatment of the transient decays in order to obtain accurate rate constants for reaction of **20b**, **20c** with various quenchers. In air-saturated hexane solutions of **19b**, the decay of germene **20b** proceeded with clean pseudo-first order kinetics upon addition of quencher. Absolute bi- and termolecular rate constants for reaction were obtained from fitting plots of [Q] vs. k_{decay} to either eq 2.13 or eq 2.14.

On the other hand, photolysis of solutions containing **19c** in the presence of acetic acid or methanol resulted in biexponential decays. This is due to the persistence of a long lived transient with an absorption band that overlaps with the absorption band of germene **20c**. A two phase exponential decay analysis, as outlined in section 2.4.2, was needed to obtain accurate rate constants at each concentration of quencher. In the presence of acetone, the decay of germene **20c** followed clean pseudo-first order kinetics indicating that the long lived transient is sensitive to acetone.

Alcohol oligomerization in hexane[80] allows for only a qualitative comparison of the reactivities of **20a-c** and **40** with methanol. Although the relative reactivity with methanol is as follows: **20a** < **20b** < **20c** < **40**. The lifetimes of germenes **20b,c** varied quadratically with the concentration of methanol and were hence fit to expression 2.14 yielding bi- and termolecular rate constants. These results indicate that increased electrophilicity of the Ge=C bond for germenes **20b,c** has altered the mechanism of addition of methanol. Recall that the parent 1,1-diphenylgermene **20a** reacts exclusively with methanol via a termolecular reaction pathway, involving 2 molecules of MeOH in the transition state for the rated determining step (see eq 1.22). In contrast, 1,1-diphenylsilene (**40**) reacts with methanol exclusively through an *intra*molecular proton transfer labelled as the top pathway in eq 1.19. The quadratic dependence on methanol concentration for germenes **20b,c** indicates that both reaction pathways are operative in these cases. Germenes **20b,c** react with methanol via both pathways labelled in eq 3.7.

The bi- and termolecular rate constants obtained from the reaction of **20b** with methanol in acetonitrile were ca. 20 and 500 times slower, respectively, than in hexane (Figure 2.4.17). In addition the reaction of **20c** with methanol in acetonitrile showed a linear dependence on methanol concentration with a rate constant ca 15 times smaller than the 2nd order rate constant in hexane (Figure 2.4.24). Considering that **19b** and **19c** produce two transients upon photolysis and that the observed kinetic behaviour at 325 nm is unusual, it is uncertain if the transients being monitored are the germenes **20b**, **20c**.

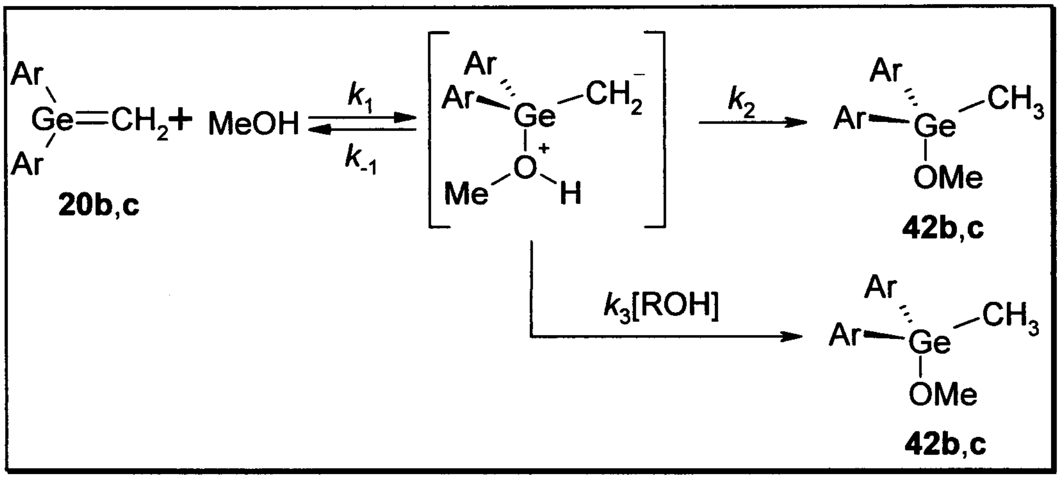

3.7

The difference in the reactivities of germenes **20b**,**c** compared to that of the parent 1,1-diphenylgermene **20a** is further exemplified by the reaction with acetone. 1,1-Diphenylgermene was reported to exhibit no detectable reactivity with acetone,[36] whereas germenes **20b**,**c** exhibit rate constants on the order of ~10^4-10^5 $M^{-1}s^{-1}$. Moreover, germenes **20b**,**c** show significant primary isotope effects with acetone indicating that the proton transfer is the rate-determining step. This is similar to reported kinetic isotope effects for silene **40.**[35] In spite of this, however, no products of the reaction could be detected in the steady state photolysis experiments.

Similarly germenes **20b**,**c** show increased reactivity toward *n*-butylamine and acetic acid in comparison with the parent germene **20a**. The kinetic isotope effects observed for reaction with acetic acid are near unity suggesting that proton transfer is not the rate determining step for reaction. These results are consistent with previously published results for 1,1-diphenylsilene **40**.[41] The rate constants measured for the reaction of germenes **20b,c** with various trapping reagents show a definite increase in comparison with the parent 1,1-diphenylgermene **20a**. This indicates that an increase in the electrophilicity of the Ge=C bond does indeed create a more reactive germene. However, the reactivity of the 'enhanced' germenes is still significantly less than the silicon analogue 1,1-diphenylsilene **40**.

CHAPTER 4: CONCLUSIONS

4.1 Contributions of the Study

This work is the first study to show that the photolyses of 1,1-diarylgermacyclobutanes (**19a-c**) yields two transient products: the corresponding diarylgermenes (**20a-c**) and diarylgermylenes (**59a-c**). Germenes (**20b,c**) were shown to be trapped by methanol as the corresponding diarylmethoxymethylgermanes (**42b,c**) in analogous fashion to previous results reported for 1,1-diphenylgermene.[36] Germylenes (**59b,c**) were trapped by methanol and 2,3-dimethylbutadiene (DMB) to produce the corresponding diarylmethoxygermanes (**58b,c**) and diarylgermacyclopentenes (**48b,c**). In addition, photolysis of 1,1-diphenylgermacyclobutane (**19a**) in the presence of methanol or DMB produced the germylene trapped products methoxydiphenylgermane (**58a**) and 1,1-diphenylgermacyclopentene (**48a**). These studies also show that the relative yields of the two products change significantly with the number of trifluoromethyl substituents on the phenyl rings. The greater the number of trifluoromethyl groups present in the precursor, the greater the yield of germylene relative to germene from the photolysis.

Laser flash photolysis of the diarylgermacyclobutanes (**19b,c**) led to three detectable transients in both cases. Two of these were identified as diarylgermene (**20b,c**) and tetraaryldigermene (**61b,c**), whereas the third remains unidentified. Kinetic studies of diarylgermenes (**20b,c**) show that there is a definite increase in reactivity toward alcohols in comparison to the parent 1,1-diphenylgermene. The kinetic behaviour is consistent with a mechanism involving the initial formation of a germene-methanol complex, similar to that proposed previously for 1,1-diphenylgermene and 1,1-diphenylsilene. In the case of 1,1-diphenylgermene the complex proceeds to product exclusively via an *inter*molecular process, whereas with 1,1-diphenylsilene the complex collapses via an *intra*molecular proton transfer. The present work shows that the methanol-germene complexes from germenes **20b,c** react via both proton transfer pathways competitively.

4.2 Future Work

Work is currently underway involving the photolysis of these precursors (**19b,c**) in hydrocarbon glasses at 77K. Using matrix isolation techniques, the transient absorption spectra of 1,1-diarylgermylenes (**59b,c**) and 1,1-diarylgermenes (**20b,c**) should be readily obtained.

It is worth mentioning that the usefulness of these precursors to study germenes is extremely limited. It has been shown that germylenes complex with polar aprotic solvents such as tetrahydrofuran or acetonitrile and that the resulting complex has an absorption maximum in the same region as the germenes.[61] Consequently an accurate study of germenes **20b**,**c** cannot be done in these solvents using the germacyclobutane precursors (**19b**,**c**). Therefore it is necessary to find a better precursor that will exclusively produce germenes in order to better study germene reactivity.

One particular precursor that has been reported to thermally generate germenes cleanly is the 2,5-norbornadiene derivative **4** first shown in section 1.1.[3] This type of precursor has also been shown to cleanly produce silenes.[27] It is reasonable to assume that these precursors will produce the corresponding metallaenes from photolysis considering many thermal reactions of reagents containing germanium have also been successful photochemically and vice versa.[32, 61, 81]

The synthetic preparation of **4** is outlined in eq 4.1. 1,1-Diethyl-2,3-dimethylgermacyclopent-3-ene (**62**) is reacted with dichlorocarbene to produce a cyclohexadiene **63**.[82] This cyclohexadiene **63** is then heated with perfluoro-2-butyne to provide quantitative conversion to the Diels-Alder adduct **4**. This synthetic scheme should also be adaptable to other germacyclopentenes such as **48a-c** in lieu of **62**. The corresponding 2,5-norbornadiene derivatives could then be photolysed to produce germene. The coproduct from this reaction is a benzene derivative which will not absorb in the same region as diarylgermenes.[60]

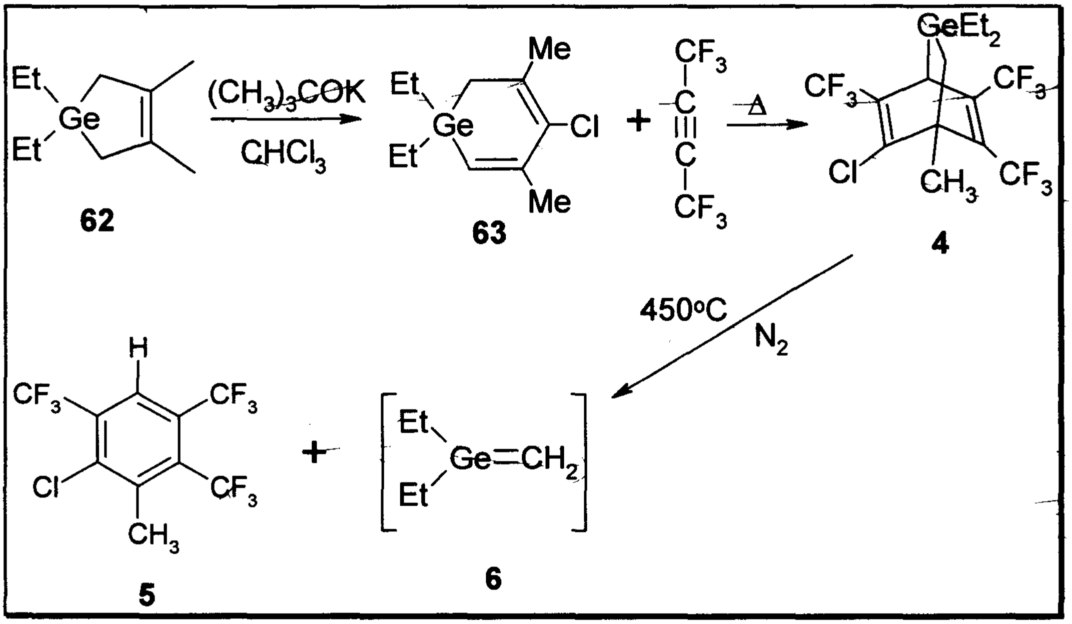

4.1

Chapter 5: Experimental

5.1 General

^{1}H NMR spectra were recorded on Bruker AV 200, DRX 500 or AV 600 NMR spectrometers in deuterated chloroform, benzene or cyclohexane-d_{12} solution and are reported in parts per million (δ) downfield from tetramethylsilane using the residual solvent-proton resonances as the internal standard. 125 MHz ^{13}C and 188 MHz ^{19}F NMR spectra were recorded on the DRX 500 and AV 200 spectrometers, respectively. Low and high resolution mass spectra were determined using a Micromass GCT Time-of-Flight (TOF) mass spectrometer with an EI source. Exact masses were determined for the molecular ion (M^+), employing a mass of 12.000000 for carbon-12. Ultraviolet absorption spectra were recorded on a Varian Cary 50 UV-Visible spectrophotometer. GC/MS analyses were carried out on a Hewlett-Packard 5890 gas chromatograph equipped with a HP-5971A mass selective detector and a DB-1 fused silica capillary column (DB-5; 30m x 0.25mm ID with 0.25 micron film; Chromatographic Specialties, Inc.). Infrared spectra were recorded on a BioRad FTS-40 FTIR spectrophotometer and are reported in wavenumbers (cm^{-1}). Guelph Chemical Laboratories performed the elemental analyses. Melting points were determined using a Mettler FP82 hot stage (controlled by a Mettler FP80 central processor) mounted on a microscope and are uncorrected. Analytical gas chromatographic analyses were carried out using a Hewlett-Packard 5890 gas chromatograph equipped with a flame ionization detector, conventional heated splitless injector (220 °C), a Hewlett-Packard 3396A recording integrator and one of the following fused silica capillary columns: (a) SPB-1 20m x 0.25mm ID with .25 micron film (b) DB-5 5m x 0.53mm ID with 1.5 micron film provided by J & W Scientific. The conditions under which all gas chromatographs were collected is as follows: 50°C initial temperature for 1 minute, 10°/minute ramp to a final temperature of 250°C which was maintained for 10 minutes, injection temperature 220°C, detector temperature 250°C and a flow rate of 4 mL/minute. Separations by radial chromatography employed a Chromatotron® (Harrison Research, Inc.), 4-mm silica gel 60 thick-layer plates, and hexane as eluant.

5.2 Commercial Reagents and Solvents

Hexane (BDH Omnisolv) and diethyl ether (Caledon Reagent) were dried using a Solv-Tek, Inc. solvent drying system, passing the solvents through pressurized stainless steel columns (65cm x 10cm) filled with neutral alumina (Labchem co.) that had been activated by heating at 330°C for ten hours under a stream of nitrogen. Acetonitrile (HPLC grade) was dried by passage through a column (1 x 6 inch) of neutral alumina (Labchem co.) that was activated by heating at 320°C for 24 hours under vacuum.

2,3-Dimethylbutadiene (Aldrich) and acetone (Aldrich) were distilled before use. Methanol, methanol-d, 1,3-dibromopropane, 4-trifluoromethylbromobenzene, 3,5-bis(trifluoromethyl)bromobenzene, 1-bromo-3-phenoxypropane, and acetic acid-d_1 were used as received from Aldrich Chemical Co. Chloroform-d_1, cyclohexane-d_{12} , benzene-d_6 and acetone-d_6 were used as received from Cambridge Isotope Labs. Germanium tetrachloride was used as received from Gelest, Inc.

5.3 Preparation and Characterization of Compounds

Glassware was flame-dried before use in all of the following syntheses.

1,1-Bis(4-(trifluoromethyl)phenyl)germacyclobutane (**19b**): Freshly ground magnesium turnings (2.43 g, 0.10 mol) and anhydrous ether (180 mL) were placed in a two-neck 250 mL round bottom flask fitted with an addition funnel, a condenser and kept under a nitrogen atmosphere. A solution of 4-trifluoromethylbromobenzene (10.49 g, 0.0466 mol) in anhydrous ether (50 mL) was added dropwise with vigorous stirring over a period of 3 hours and then left to stir for 12 hours at room temperature.

Germanium tetrachloride (5.00 g, 0.0233 mol) and anhydrous ether (100 mL) were added to a two-neck, 500 mL round bottom flask fitted with a 250 mL addition funnel under nitrogen and kept in a dry ice/isopropanol bath to maintain an internal temperature of –78 °C. The freshly made Grignard reagent was carefully decanted into the addition funnel and added dropwise with vigorous stirring over a period of 3 hours. The resulting solution was allowed to slowly warm to room temperature and was then left to stir for 12 hours. The reaction mixture was vacuum-filtered using a medium glass frit and the solvent was then removed on the rotary evaporator to yield an orange oil (mass = 12.27 g). Analysis of the oil by GC (using column b) showed three major products with the following retention times: 13.7 minutes, 15.8 minutes and 17.6 minutes. The ratio of these products was 1:6:1 respectively. The oil was used without further treatment in the next step.

The following procedure is a modification of the method of Bickelhaupt and co-workers.[59] Freshly ground magnesium turnings (28.34 g, 1.17 mol) and 250 mL of anhydrous ether were added to a two-neck, 500 mL round bottom flask fitted with an addition funnel, a condenser and kept under nitrogen atmosphere. A small crystal of iodine was added to the magnesium/ether mixture to activate the magnesium. A solution of 1,3-dibromopropane (11.83 mL, 0.116 moles) in anhydrous ether (60 mL) was added dropwise with vigorous stirring over a period of 2 hours and the reaction mixture was left to stir for a further 3 hours. The orange oil containing 1,1-bis(4-(trifluoromethyl)phenyl)germanium dichloride was then added rapidly and the mixture was left to stir at room temperature for 12 hours. The reaction mixture was decanted into a large flask and slowly quenched with distilled water (100 mL). The organic layer was separated and washed with water (25 mL), saturated aqueous ammonium chloride (50 mL), and water (25 mL), and then dried with anhydrous magnesium sulphate. The solvent was removed using a rotary evaporator to yield a golden oil (mass = 10.95 g). Subsequent purification was accomplished using radial chromatography and silica gel column chromatography with hexane as the eluting solvent, and recrystallization from methanol. The latter afforded the product as colourless needle (2.95 g, 7.30×10^{-3} mol , 31.3%)) with a >99% purity determined by GC analysis (column a). 1,1-bis(4-(trifluoromethyl)phenyl)germacyclobutane (**19b**) has a melting point of 46-47 °C and was identified on the basis of the following spectroscopic data:

^{1}H NMR ($CDCl_3$, 500 MHz): δ = 2.059 (t, ^3J = 8.2Hz, 4H), 2.450 (quin, ^3J = 8.2Hz, 2H), 7.666 (d, ^3J = 7.6Hz, 4H), 7.704 (d, ^3J = 7.6Hz, 4H).

^{13}C NMR (CDCl$_3$, 125 MHz): δ = 20.9, 21.6, 124.3 (q, ^{1}J (^{13}C-F) = 272Hz), 125.1, 131.7 (q, ^{2}J (^{13}C-F) = 32Hz), 134.4, 143.1.

^{19}F NMR (CDCl$_3$, 188 MHz): δ = -63.2 ppm (s).

IR (KBr Pellet, cm^{-1}): 2933 (m), 1929 (w), 1607 (m), 1395 (m), 1325 (s), 1165 (s), 1125 (s), 1101 (m), 1056 (s), 1017 (m), 826 (m), 689 (m), 597 (w), 565 (w), 494 (w), 446 (w).

Mass spectra: (EI, m/z (%)): 406 (20), 378 (50), 362 (45), 343 (8), 309 (10), 271 (85), 252 (85), 251 (50), 219 (95), 140 (100).

HRMS calculated for $C_{17}H_{14}F_6Ge$ ([M]$^+$), 406.0211 amu; observed 406.0210 amu.

Combustion analysis; calculated for $C_{17}H_{14}F_6Ge$: C, 50.43%, H, 3.49%. Found: C, 50.73%, H, 3.41%.

A sample suitable for structural determination by single-crystal X-ray diffraction (0.2 x 0.2 x 0.2 mm^3) was obtained by crystallization from methanol. Crystallographic data are presented in Appendix 1.

1,1-Bis(3,5-bis(trifluoromethyl)phenyl)germacyclobutane **19c** was prepared in an analogous manner to **19b**. Freshly ground magnesium turnings (2.46 g, 0.101 mol) and anhydrous ether (350 mL) were placed in a two-neck, 500 mL round bottom flask fitted with an addition funnel, a condenser and kept under nitrogen atmosphere. A solution of 3,5-bis(trifluoromethyl)bromobenzene (13.65 g, 0.0466 mol) in anhydrous ether (60 mL) was added dropwise with vigorous stirring over a period of 3 hours and then left to stir for 12 hours at room temperature.

Germanium tetrachloride (5.00 g, 0.0233 mol) and anhydrous ether (150 mL) were added to a two-neck, 500 mL round bottom flask fitted with an addition funnel under nitrogen and placed in a dry ice/isopropanol bath to maintain an internal temperature of –78 °C. The freshly made Grignard reagent was carefully decanted into the addition funnel and added dropwise with vigorous stirring over a period of 3 hours. The reaction mixture was allowed to warm slowly to room temperature and was left to stir for 12 hours. The resulting reaction mixture was vacuum-filtered using a coarse frit and the volatile solvent was removed using a rotary evaporator to yield a brown oil (mass = 13.1 g). Analysis of the oil by GC (column b) showed three major products with retention times of: 3.8 minutes, 5.8 minutes and 8.0 minutes in an intensity ratio of 1:4:1. The oil was used without further treatment in the next step.

Freshly-ground magnesium turnings (28.70 g, 1.18 mol) and 300 mL of anhydrous ether were put into a 2-neck round bottom flask fitted with a condenser, a 125 mL addition funnel and kept under nitrogen atmosphere. A small crystal of iodine was added to the magnesium/ether mixture to activate the magnesium. A solution of 1,3-dibromopropane (11.83 mL, 0.116 mol) in 60 mL of anhydrous ether was added dropwise with vigorous stirring over a period of 1½ hours. The reaction mixture was left to stir for an additional 3 hours. The brown oil containing 1,1-bis(3,5-bis(trifluoromethyl)phenyl)germanium dichloride was then quickly added and the resulting reaction mixture was left to stir for 12 hours at room temperature. The reaction mixture was then decanted into a large flask and slowly quenched with water (100 mL). The organic layer was extracted with distilled water (25 mL) and saturated ammonium chloride (50 mL). After separation of the organic layer, the solution was dried with anhydrous magnesium sulphate and filtered, followed by removal of the solvent to yield a yellow oil (13.03 g). The product was purified by radial chromatography and silica gel column chromatography, followed by recrystallizations from methanol to yield colourless needles (2.61 g, 4.83×10^{-3} mol, 20.7% yield) with a >99% purity determined by GC analysis (column a). 1,1-bis(3,5-bis(trifluoromethyl)phenyl)germacyclobutane (**19c**) has a melting point of 64-64.5°C and was identified from the following spectroscopic data:

^{1}H NMR ($CDCl_3$, 500 MHz): $\delta = 2.177$ (t, $^3J = 8.2$Hz, 2H), 2.502 (quin, $^3J = 8.2$Hz, 4H), 7.959 (s, 2H), 7.978 (s, 4H).

^{13}C NMR ($CDCl_3$, 125 MHz): δ = 21.5, 21.5, 123.5(q, ^{1}J (^{13}C – ^{19}F) = 273 Hz), 123.9, 131.9 (q, ^{2}J (^{13}C – ^{19}F) = 33 Hz), 133.8, 140.6.

^{19}F NMR ($CDCl_3$, 188 MHz): δ = -63.1 ppm(s)

IR (KBr pellet, cm^{-1}): 2911 (w), 1620 (w), 1359 (s), 1282 (s), 1174 (s), 1125 (s), 920 (w), 896 (m), 840 (m), 706 (m), 682 (s), 567 (w), 500 (w), 449 (w), 429 (w).

Mass spectra: (EI, m/z (%)) = 542 (15), 523 (25), 514(75), 500 (25), 388 (100), 387 (80), 287 (30), 208 (80), 194 (50), 175 (30), 155 (92)

HRMS calculated for $C_{19}H_{12}F_{12}Ge$ ($[M]^+$) = 541.9959 amu; observed, 542.0007 amu.

Combustion analysis calculated for $C_{19}H_{12}F_{12}Ge$: C, 42.19%, H, 1.89%. Found: C, 42.08%, H, 2.24%.

A sample suitable for structural determination by single-crystal X-ray diffraction (0.2 x 0.2 x 0.2 mm^3) was obtained by crystallization from methanol. Crystallographic data are presented in Appendix 1.

5.4 Steady-State Photolysis

5.4.1 General Methods

Steady-state photolysis experiments were carried out using a Rayonet Photochemical Reactor (Southern New England Ultraviolet Co.) equipped with 6 RPR-2537 lamps (254nm). Photolysis solutions were contained in 5 x 75 mm quartz NMR tubes sealed with rubber septa and degassed. Reactions were monitored by ^{1}H NMR spectroscopy, GC and GC/MS analyses. The concentrations of the products and starting materials at various times of photolysis were calculated using the following method. Initially all integrations were determined by use of an internal standard (either the solvent C_6D_{12} or tetramethylsilane (TMS)) and corrected for the number of protons that they represent. Subsequently, the ^{1}H integral of the starting materials at time = 0 seconds was set equal to their initial concentration. Using this ratio the rest of the product integrations were converted to absolute concentrations. The percent conversion was calculated by dividing the integration of starting material at different times by the initial integration of starting material. Photoproducts were identified by a combination of ^{1}H NMR spectroscopy, GC/MS and/or co-injection of authentic samples in the reaction mixture. The following section describes a typical experiment of this type.

5.4.2 Steady-State Photolysis Example

A 5 x 75 mm quartz NMR tube containing 0.75 mL of a solution containing **19b** (0.0189 M) in cyclohexane-d_{12} was sealed with a rubber septum. After degassing the sample for thirty minutes with a stream of Ar, methanol was added to a final concentration of 0.30 M. The sample was analyzed by ^{1}H NMR for initial integration values of the starting materials. Following this the sample was irradiated (2-6 lamps, 254 nm) for various lengths of time and monitored by ^{1}H NMR. The photolysis was continued until the conversion of the starting material **19b** was 56%. The chemical yields of the products were determined by converting the integrations of the products (^{1}H NMR) to absolute concentrations

5.4.3 Photoproduct Preparation and Identification

Cyclopropane was prepared following the method of Gragson and coworkers[83]. Freshly ground magnesium turnings (1.52 g, 0.0626 mol) and anhydrous ether (35 mL) were placed in a 100 mL, 2 neck round bottom flask equipped with a 60 mL addition funnel and septum, a stir bar and kept under nitrogen atmosphere. A cannula was used to connect the round bottom flask to a small vial sealed with a septum and kept under nitrogen atmosphere. The vial was kept in a dry ice/isopropanol bath to collect the cyclopropane produced from the reaction.

A solution of 1-bromo-3-phenoxypropane (9.96 g, 0.0463 mol) in anhydrous ether (20 mL) was slowly added dropwise to the round bottom flask. The reaction mixture began to bubble, turn white and cloudy, and warm up. The round bottom flask was then put in an ice bath to reduce the amount of ether that might be distilled into the vial from the reaction. During the addition the reaction mixture continued to bubble and a clear, colourless liquid began to collect in the bottom of the vial. Once the reaction appeared to slow down the cannula was removed and the vial was kept in dry ice/isopropanol. Identification of cyclopropane was confirmed by comparing the product's ^1H NMR spectrum with published results ($CDCl_3$, 200 MHz): $\delta = 0.20$ ppm[84].

The following is the characterization of the products from the photolysis of germacyclobutanes **19b** and **19c** in the presence of methanol.

Bis(4-(trifluoromethyl)phenyl)methoxymethylgermane **42b**:

^1H NMR (C_6D_{12}, 500 MHz): $\delta = 3.49$ ppm (singlet, OCH_3) and $\delta = 0.81$ ppm (singlet, CH_3).

GC/MS (m/z, (%)): 410 (5), 395 (100), 365 (78), 235 (36), 219 (52), 126 (90), 107 (85).

Bis(4-(trifluoromethyl)phenyl)methoxylgermane **58b**:

^{1}H NMR (C_6D_{12}, 500 MHz): δ = 6.18 ppm (singlet, Ge-H) and δ = 3.58 ppm (singlet, OCH_3).

GC/MS (m/z, (%)): 396 (2), 395 (12), 365 (33), 219 (38), 127 (100), 107 (50).

Bis(3,5-bis(trifluoromethyl)phenyl)methoxymethylgermane **42c**:

^{1}H NMR (C_6D_{12}, 500 MHz): δ = 3.53 ppm (singlet, OCH_3) and δ = 0.92 ppm (singlet, CH_3).

GC/MS (m/z, (%)): 546 (6), 531 (100), 501 (60), 303 (20), 287(50), 206 (55), 194(100), 174 (95), 144(60), 125 (70).

Bis(3,5-bis(trifluoromethyl)phenyl)methoxygermane **58c**:

^{1}H NMR (C_6D_{12}, 500 MHz): δ = 6.31 ppm (singlet, Ge-H) and δ = 3.63 ppm (singlet, OCH_3).

GC/MS (m/z, (%)): 534 (5), 533 (8), 501 (30), 287 (45), 195 (100), 175 (50), 144 (38), 125 (46).

1,1-Bis(4-(trifluoromethyl)phenyl)germane and 1,1-bis(3,5-bis(trifluoromethyl)phenyl)germane were synthesized following analogous procedures. For example, freshly ground magnesium turnings (1.51 g, 0.0621 mol) and anhydrous ether (60 mL) were put into a 100 mL, 2-neck round bottom fitted with a 60mL addition funnel, a condenser and kept under a nitrogen atmosphere. A solution of 4-trifluoromethylbromobenzene (8.28 g, 0.0368 mol) in anhydrous ether (30 mL) was added dropwise to the magnesium/ether mixture over a period of 2 hours. The reaction mixture was allowed to slowly warm and turned dark brown. After complete addition the reaction mixture was left to stir for three hours.

Germanium tetrachloride (3.95 g, 0.0184 mol) and anhydrous ether were placed in a 2-neck, 100 mL round bottom flasks equipped with a 60 mL addition funnel fitted with a septum, a stirrer and kept under a nitrogen atmosphere. The freshly made Grignard reagent was cannulated into the addition funnel. The round bottom flask was kept in a dry ice/isopropanol bath while the Grignard reagent was slowly added dropwise over a period of one hour, during which the solution turned orange. After the addition was complete the reaction mixture was left to slowly warm to room temperature and stir for 12 hours. The reaction mixture was left as is for the proceeding step.

Lithium aluminum hydride (0.70 g, 0.0185 mol) was carefully added to a flame-dried, 2-neck round bottom flask containing 50 mL of anhydrous THF and fitted with a 150 mL addition funnel, a stir bar and kept under nitrogen atmosphere. The reaction mixture from the previous step was carefully cannulated into the addition funnel and then slowly added dropwise to the $LiAlH_4$/THF solution. The reaction mixture turned yellow and contained a green precipitate. The resulting solution was carefully decanted and the solvent removed.

In the case of **60b**, vacuum distillation at 0.15mm Hg gave a clear, colourless oil (bp = 115°C); 1.50g (0.00411 mole, 22.4% yield) which was estimated to have a purity of 97.6% by GC analysis (column a). 1,1-Bis(4-(trifluoromethyl)

phenyl)germane was characterized by the following spectroscopic data:

^{1}H NMR (C_6D_6, 500 MHz): δ = 4.880 (s, 2H), 7.111 (d, 4H, ^3J = 7.7Hz), 7.294 (d, 4H, ^3J = 7.7Hz).

^{13}C NMR (C_6D_6, 125 MHz): δ = 124.7(q, ^1J ($^{13}C - {}^{19}F$) = 272 Hz), 125.1, 131.7 (q, ^2J ($^{13}C - {}^{19}F$) = 32 Hz),135.6, 138.2.

^{19}F NMR (C_6D_6, 188 MHz): δ = -62.3 ppm (s)

IR (Neat, cm^{-1}): 3416 (w), 3035 (w), 2074 (Ge-H) (m), 1607 (w), 1395 (m), 1326 (s), 1167 (s), 1130 (s), 1059 (s), 1019 (m), 863 (m), 829 (m), 754 (m), 720 (m), 690 (m), 423 (s).

Mass spectra: (EI, m/z (%)): 361/363/365 (5), 290 (5), 271 (7), 217(7), 146 (10), 127 (100), 107 (10), 77 (8).

HRMS calculated for $C_{14}H_9F_6Ge$ ($[M-H]^+$) = 364.982 amu; observed, 364.979 amu.

Compound **60c** was isolated by vacuum sublimation, in which the sample was heated to 75°C for three hours in a sublimator at 0.5 mm Hg. White hair-like crystals were recovered with an overall yield of 24.3%. The ^1H NMR spectrum was compared with previously published data[63] to confirm its identity.

^1H NMR (C_6D_6, 500 MHz): δ = 4.61 (s, 2H), 7.55 (s, 4H), 7.69 (s, 2H).

5.4.4 Quantum Yield Determination

Typical quantum yield experiments employ the use of 1,1-diphenylgermacyclobutane as a secondary actinometer (Φ = 0.21[36]). Cyclohexane-d_{12} solutions of **19b** (0.0189 M), **19c** (0.0204 M) and **19a** (0.0200 M) containing methanol (0.30 M) were placed in quartz NMR tubes, sealed with rubber septa and deoxygenated for thirty minutes by bubbling argon through the solutions. The tubes were placed in a merry-go-round apparatus inside a Rayonet Photochemical Reactor equipped with 6 RPR-2537 lamps (254 nm). The merry-go-round apparatus is essential as it ensures equal distribution of light to each of the samples. The disappearance of starting materials and the formation of diarylmethoxymethylgermane products **42b**, **42c** or **42a** were monitored by ^{1}H NMR spectroscopy using the CHD_{11} peak as an internal standard. A plot of product formation versus time yielded a straight line at <20% conversion of starting material, in each case, whose slope relative to that for 1,1-diphenylgermacyclobutane, corresponded to the quantum yield of the compound (Figures 2.3.2(b) and 2.3.4(b)).

5.5 Nanosecond Laser Flash Photolysis

Nanosecond laser flash photolysis experiments employed the pulses (248 nm; ca. ~20 ns; 70 – 120 mJ), from a Lambda-Physik complex 500 laser filled with F_2/Kr/He mixtures in conjunction with a Luzchem® LS-100 laser flash photolysis system. The system incorporates a brass sample holder whose temperature is controlled to within 0.1°C by a VWR 1166 constant temperature-circulating bath. Solutions of **19b** and **19c** were prepared at concentrations of 4.2×10^{-4} and 6.2×10^{-4} M, respectively, to ensure that the absorbance at the excitation wavelength (248 nm) was *ca.* 0.6-0.8. The photolysis solutions were continuously flowed from a 100 mL calibrated reservoir through a 7 x 7 mm Suprasil flow cell. The solutions were either deoxygenated continuously with a stream of dry nitrogen. Solution temperatures were monitored with a Teflon-coated copper/constantan thermocouple that was inserted directly into the flow cell. Quenchers were added directly to the reservoir by microlitre syringe as aliquots of standard solutions. Quenching rate constants were calculated by least squares analysis using a quadratic fit or linear least-squares analysis of decay rate (k_{decay}) versus quencher concentration data (6-25 points, depending on whether the plots were linear or curved) that spanned at least one order of magnitude in the transient decay rate using GraphPad Prism v.3.02. Errors are quoted as twice the standard deviation (±2σ) obtained from the least-squares analysis in each case.

5.6 X-Ray Crystallography

X-Ray crystallographic data were collected from single crystal samples, which were mounted on a glass fibre. A P4 Siemens diffractometer, equipped with a Siemens SMART 1K Charge-Coupled Device (CCD) Area Detector (using the program SMART) and a rotating anode using graphite-monochromated Mo-Kα radiation (λ = 0.71073 Å) was used for the single crystal diffraction experiments with **19b** and **19c**. The data collection was carried out in 512 x 512 pixel mode, utilizing 2 x 2 pixel binning and the crystal-to-detector distance was 3.991 cm. Determination of the initial unit cell parameters as carried out by a least-squares fit of the angular settings of the strong reflections, collected by a 4.5 degree scan in 15 frames over three different parts of reciprocal space (45 frames total). One complete hemisphere of data was collected, to better than 0.8 Å resolution. The program SAINT, which applies Lorentz and polarization corrections to three-dimensionally integrated diffraction spots, was used in processing the data. The program SADABS was utilized for the scaling of diffraction data, the application of a decay correction, and an empirical absorption correction based on redundant reflections. Both structures were solved by using the direct methods procedure in the Siemens SHELXTL program library. Refinement was carried out by using full-matrix least squares methods with anisotropic thermal parameters for all non-hydrogen atoms. Hydrogen atoms were added at calculated positions and refined using a riding model with isotropic displacement parameters equal to 1.2 times the equivalent isotropic displacement parameter of the attached carbon.[85-88]

In the case of **19b**, rotational disorder of the fluorine atoms F4, F5 and F6 on one of the aromatic rings was established by refinement of the population factors F4, F5, F6 and F4A, F5A, F6A, respectively, with a final occupancy ratio of 66:33. Rotational disorder for all of the fluorine atoms was observed in **19c** and established by refinement of the population factors in Table 5.1. The final occupancy ratios are also shown in Table 5.1.

Table 5.1 Population Factors and Occupancy Ratios for the fluorine atoms in the crystal structure of **19c.**

Population Factors	**Occupancy Ratio**
F1, F2, F3 and F1A, F2A, F3A	68:32
F4, F5, F6 and F4A, F5A, F6A	44:56
F7, F8, F9 and F7A, F8A, F9A	70:30
F10, F11, F12 and F10A, F11A, F12A	88:12

References

(1) Dasent, W. E. *Nonexistent Compounds*. Marcel Dekker: New York, **1965**.

(2) Gusel'nikov, L. E.; Flowers, M. C. *J. Chem. Soc., Chem. Commun.*, **1967**, 864-865.

(3) Barton, T. J.; Kline, E. A.; Garvey, P. M. *J. Am. Chem. Soc.*, **1973**. *95*, 3078.

(4) Escudie, J.; Couret, C.; Ranaivonjatovo, H.; Satge, J. *Coord. Chem. Rev.*, **1994**. *130*, 427-480.

(5) Satge, J. *Adv. Organomet. Chem*, **1982**. *21*, 241-287.

(6) Muller, T.; Ziche, W.; Auner, N. Silicon-carbon and silicon-nitrogen multiply bonded compounds, in *The chemistry of organic silicon compounds, Vol. 2*, Rappoport, Z. and Apeloig, Y., Editors. John Wiley & Sons: New York, **1998**; p. 857-1062.

(7) Brook, A. G.; Brook, M. A. *Adv. Organomet. Chem*, **1996**. *39*, 71-158.

(8) Raabe, G.; Michl, J. Multiple bonding to silicon, in *The chemistry of organic silicon compounds*, Patai, S. and Rappoport, Z., Editors. John Wiley & Sons: New York, **1989**; p. 1015-1142.

(9) Gusel'nikov, L. E.; Nametkin, N. S. *Chem. Rev.*, **1979**. *79*, 529-577.

(10) Barrau, J.; Escudie, J.; Satge, J. *Chem. Rev.*, **1990**. *90*, 283-319.

(11) Wiberg, N. *J. Organomet. Chem.*, **1984**. *273*, 141-177.

(12) Brown, W. H.; Foote, C. S. Alkenes II, in *Organic Chemistry*. Saunders College Publishing: Orlando, **1998**.

(13) Trinquier, G.; Barthelat, J. C.; Satge, J. *J. Am. Chem. Soc.*, **1982**. *104*, 5931-5936.

(14) Raabe, G.; Michl, J. *Chem. Rev.*, **1985**. *85*, 419-509.

(15) Trinquier, G.; Malrieu, J. P. *J. Am. Chem. Soc.*, **1981**. *103*, 6313-6319.

(16) Walsh, R. *J. Organomet. Chem.*, **1972**. *38*, 245-248.

(17) Dobbs, K. D.; Hehre, W. J. *Organometallics*, **1986**. *5*, 2057-2061.

(18) Kudin, K. N.; Margrave, J. L.; Khabashesku, V. J. *J. Phys. Chem. A*, **1998**. *102*, 744-753.

(19) Khabashesku, V. N.; Kudin, K. N.; Tamas, J.; Boganov, S. E.; Margrave, J. L.; Nefedov, O. M. *J. Am. Chem. Soc.*, **1998**. *120*, 5005-5016.

(20) *Handbook of Chemistry and Physics 83rd edition*, ed. Lide, D.R. CRC Press: New York, **2002**. 9-76.

(21) Brook, A. G.; Nyburg, S. C.; Abdesaken, F.; Gutekunst, B.; Gutekunst, G.; Kallury, R. K. M. R.; Poon, Y. C.; Chang, Y-M.; Wong-Ng, W. *J. Am. Chem. Soc.*, **1982**. *104*, 5667-5672.

(22) Apeloig, Y.; Karni, M. *J. Am. Chem. Soc.*, **1984**. *106*, 6676-6682.

(23) Couret, C.; Escudie, J.; Satge, J.; Lazraq, M. *J. Am. Chem. Soc.*, **1987**. *109*, 4411-4412.

(24) Lazraq, M.; Escudie, J.; Couret, C.; Satge, J. *Angew. Chem., Int. Ed. Engl.*, **1988**. *27*, 828-829.

(25) Baines, K. M.; Stibbs, W. G. *Adv. Organomet. Chem*, **1996**. *39*, 275-324.

(26) Wiberg, N.; Kim, C. K. *Chem. Ber.*, **1986**. *119*, 2966-2979.

(27) Barton, T. J. *Pure & Appl. Chem.*, **1980**. *52*, 615-624.

(28) Brook, A. G. The photochemistry of organosilicon compounds, in *The chemistry of organic silicon compounds*, Rappoport, Z., Editor. John Wiley & Sons: New York, **1989**; p. 965-1005.

(29) Barton, T. J.; Hoekman, S. K. *J. Am. Chem. Soc.*, **1980**. *102*, 1584-1591.

(30) Jones, P. R.; Lee, M. E. *J. Am. Chem. Soc.*, **1983**. *103*, 6725-6726.

(31) Bertrand, G.; Mazerolles, P.; Ancelle, J. *Tetrahedron*, **1981**. *37*, 2459.

(32) Conlin, R. T.; Namavari, M. *Organometallics*, **1992**. *11*, 3307.

(33) Gusel'nikov, L. E.; Nametkin, N. S.; Vdovin, V. M. *Acc. Chem. Res.*, **1975**. *8*, 18-25.

(34) Auner, N.; Grobe, J. *J. Organomet. Chem.*, **1980**. *188*, 25-52.

(35) Bradaric, C. J.; Leigh, W. J. *Can. J. Chem.*, **1997**. *75*, 1393-1402.

(36) Toltl, N. P.; Leigh, W. J. *J. Am. Chem. Soc.*, **1998**. *120*, 1172-1178.

(37) Leigh, W. J. *Pure & Appl. Chem.*, **1999**. *71*, 453-462.

(38) Becerra, R.; Walsh, R. Thermochemistry, in *The Chemistry of Organic Silicon Compounds*, Apeloig, Y., Editor. John Wiley & Sons: New York, **1998**; p. 153-180.

(39) Toltl, N. P.; Morkin, T. L.; Stradiotto, M.; Leigh, W. J. *Organometallics*, **1999**. *18*, 5643-5652.

(40) Toltl, N. P.; Leigh, W. J. *Organometallics*, **1996**. *15*, 2554-2561.

(41) Leigh, W. J.; Bradaric, C. J.; Kerst, C.; Banisch, J. H. *Organometallics*, **1996**. *15*, 2246-2253.

(42) Leigh, W. J.; Sluggett, G. W. *J. Am. Chem. Soc.*, **1994**. *116*, 10468-10476.

(43) Kira, M.; Maruyama, T.; Sakurai, H. *J. Am. Chem. Soc.*, **1991**. *113*, 3986-3987.

(44) Wade, Jr., L. G. *Organic Chemistry, 3rd edition*. Prentice Hall: New Jersey, **1995**.

(45) Sluggett, G. W.; Leigh, W. J. *Organometallics*, **1994**. *13*, 269-281.

(46) Sluggett, G. W.; Leigh, W. J. *J. Am. Chem. Soc.*, **1992**. *114*, 1195-1201.

(47) Ishikawa, M.; Fuchikami, T.; Kumada, M. *J. Organomet. Chem.*, **1976**. *118*, 139-153.

(48) Ishikawa, M.; Fuchikami, T.; Kumada, M. *J. Organomet. Chem.*, **1977**. *127*, 261-272.

(49) Bradaric, C. J.; Sluggett, G. W.; Leigh, W. J. *J. Am. Chem. Soc.*, **1993**. *115*, 5332-5333.

(50) Morkin, T. L.; Owens, T. R.; Leigh, W. J. Kinetic studies of the reactions of Si=C and Si=Si double bonds, in *The chemistry of organosilicon compounds*, 3, Apeloig, Y., Editor. John Wiley & Sons: New York, **2001**; p. 949-1026.

(51) Bradaric, C. J.; Leigh, W. J. *Organometallics*, **1998**. *17*, 645-651.

(52) Leigh, W. J.; Owens, T. R.; Harrington, C. R.; Pace, T. C. S. *Organometallics*, **2003**. *in press*.

(53) Li, X.; Leigh, W. J. *J. Phys. Chem. A*, **2003**. *107*, 1517-1524.

(54) Potter, G. D. *BSc. Thesis*. McMaster University, **2001**.

(55) Sluggett, G. W.; Leigh, W. J. *J. Am. Chem. Soc.*, **1993**. *115*, 7531.

(56) Leigh, W. J.; Toltl, N. P.; Apodaca, P.; Castuita, M.; Pannell, K. H. *Organometallics*, **2000**. *19*, 3232-3241.

(57) Chatgilialoglu, C.; Ingold, K. U.; Lusztyk, J.; Nazran, A. S.; Scaiano, J. C. *Organometallics*, **1983**. *2*, 1332.

(58) Chatgilialoglu, C. in *CRC handbook of photochemistry, Vol II*, Scaiano, J.C., Editor. CRC press: Boca Raton, Fl, **1989**; p. 3-11.

(59) Bickelhaupt, F.; Seetz, J. W. F. L.; Heisteeg, B J. J. Van de; Schat, G.; Akkerman, O. S. *J. Organ. Chem.*, **1984**. *277*, 319-322.

(60) Silverstein, R. M.; Bassler, G. C.; Morrill, T. C. *Spectrometric Identification of Organic Compounds*. 5th edition ed. John Wiley & Sons, Inc.: New York, **1991**.

(61) Harrington, C. R.; Leigh, W. J. *unpublished results*.

(62) Neumann, W. P. *Chem. Rev.*, **1991**. *91*, 311-334.

(63) Bender IV, J. E.; Litz, K. E.; Giarikos, D.; Wells, N. J.; Holl, M. M. Banaszak; Kampf, J. W. *Chem. Eur. J.*, **1997**. *3*, 1793-1796.

(64) Satge, J.; Castel, A.; Riviere, P.; Ko, H. Y. *Organometallics*, **1990**. *9*, 205-210.

(65) Scaiano, J. C. in *CRC Handbook of Organic Photochemistry*, Vol. II, Scaiano, J.C., Editor. CRC Press: Boca Raton, Fl., **1989**; p. 343-346.

(66) Hadel, L. M. in *CRC Handbook of Organic Photochemistry*, Vol. I, Scaiano, J.C., Editor. CRC Press: Boca Raton, Fl., **1989**; p. 279-292.

(67) Bonneau, R.; Wirz, J.; Zuberbuhler, A. D. Methods for the Analysis of Transient Absorbance Data, in *Pure & Appl. Chem.*, 69; p. 1-16.

(68) Tsumuraya, T.; Sato, S.; Ando, W.. *Organometallics*, **1990**. *9*, 2061-2067.

(69) Ando, W.; Tsumuraya, T. *Organometallics*, **1988**. *7*, 1882-1883.

(70) Becerra, R.; Boganov, S. E.; Egorov, M. P.; Lee, V. Y.; Nefedov, O. M.; Walsh, R. *Chem. Phys Lett.*, **1996**. *250*, 111-119.

(71) Bobbitt, K. L.; Maloney, V. M.; Gaspar, P. P. *Organometallics*, **1991**.

(72) Fujii, Y.; Yamada, H.; Mizuta, M. *J. Phys. Chem. A*, **1988**. *92*, 6768-6772.

(73) Bassindale, A. R.; Borbaruah, M. *J. Chem. Soc., Chem. Commun.*, **1991**, 1499.

(74) Voronkov, M. G.; Frolov, Y. L.; D'Yakov, V. M.; Chipanina, N. N.; Gubanova, G. I.; Favrilova, G. A.; Klyba, L. V.; Aksametova, T. N. *J. Organomet. Chem.*, **1980**. *201*, 165.

(75) Yoder, C. H.; Ryan, C. M.; Martin, G. F.; Ho, P. S. *J. Organomet. Chem.*, **1980**. *190*, 1.

(76) Brook, M. A. *Silicon in Organic, Organometallic, and Polymer Chemistry.* John Wiley & Sons, Inc.: Toronto, **2000**.

(77) Boudin, A.; Cerveau, G.; Chiut, C.; Corriu, R. J. P.; Reye, C. *Angew. Chem., Int. Ed. Engl.*, **1986**. *25*, 473.

(78) Mochida, K.; Yoneda, I.; Wakasa, M. *J. Organomet. Chem.*, **1990**. *399*, 53-62.

(79) Mochida, K.; Tokura, S. *Bull. Chem. Soc. Jpn.*, **1992**. *65*, 1642-1647.

(80) Landeck, H.; Wolff, H.; Gotz, R. *J. Phys. Chem*, **1977**. *81*, 718-722.

(81) Ando, W.; Itoh, H.; Tsumuraya, T. *Organometallics*, **1989**. *8*, 2759-2766.

(82) Seyferth, D.; Jula, T. F.; Mueller, D. C.; Mazerolles, P.; Manuel, G.; Thoumas, F. *J. Am. Chem. Soc.*, **1970**. *92*, 657-666.

(83) Gragson, J. T.; Greenlee, K. W.; Derfer, J. M.; Boord, C. E. *J. Org. Chem.*, **1955**. *20*, 275-282.

(84) Crecely, K. M.; Watts, V. S.; Goldstein, J. H. *J. Mol. Spectroscopy*, **1969**. *30*, 184-191.

(85) SAINT (2000), Version 6.02a; Siemens Energy And Automation Inc., Madison, WI 53719.

(86) SMART (1997), Version 5.611; Siemens Energy And Automation Inc., Madison, WI 53719.

(87) Sheldrick, G. M. SADABS (Siemens Area Detector Absorption Corrections) (1997); Siemens Crystallographic Research Systems, Madison, WI 53719.

(88) Sheldrick, G. M. Siemens SHELXTL (1997), Version 5.1; Siemens Crystallographic Research Systems, Madison, WI 53719.

APPENDIX 1: X-RAY CRYSTALLOGRAPHIC DATA

Refinement Data and Metrical Parameters

Table A1. Crystal Data and Structure Refinement Parameter for **19b** and **19c**

	19b	**19c**
Empirical formula	$C_{17}H_{14}F_6Ge$	$C_{19}H_{12}F_{12}Ge$
Molecular Weight	406.02	542.00
Description	colourless needle	colourless needle
Temperature, K	173	173
Crystal System	monoclinic	monoclinic
Space Group	$P2_1/n$	$P2_1/n$
a, Å	13.596(6)	10.429(4)
b, Å	6.412(3)	8.075(3)
c, Å	20.243(9)	24.930(9)
α, deg.	90	90
β, deg.	107.081	100.969
γ, deg.	90	90
Volume, Å^3	1686.8	2061.19
Z	4	4
Calcd Density, g/cm^3	1.594	1.743
Scan Mode	ϕ and ω scans	ϕ and ω scans
θ – range, deg.	1.61 to 27.54	1.66 to 27.53
Index ranges	$-17 \le h \le 17$	$-13 \le h \le 13$
	$-8 \le k \le 8$	$-10 \le k \le 10$
	$-26 \le l \le 25$	$-30 \le l \le 32$
No. Refl. Collected	14478	18346
No. Indep. Refl.	3867	4731
Data / rest. / param.	3867 / 0 / 246	4731 / 6 / 402
Goodness-of-fit on F^2	0.993	1.026
Final R indices ($I>2\sigma(I)$)*	R1 = 0.0369	R1 = 0.0308
	wR2 = 0.0735	wR2 = 0.0747
R indices (all data)*	R1 = 0.0869	R1 = 0.0563
	wR2 = 0.0899	wR2 = 0.0857
Mean shift/error	<0.001	<0.01
Max. shift/error	<0.001	<0.01
Trans. (max., min.)	0.783647	0.787088
Largest diff. Peak, e/ Å^3	0.530	0.446
Largest diff. Hole, e/ Å^3	-0.411	-0.496

*$R1 = \Sigma\ (Fo - Fc)/\ \Sigma Fo$; $wR2 = [\Sigma\ [w(Fo^2 - Fc^2)^2]/\ \Sigma\ [w(Fo^2)^2]]^{0.5}$; $P = (Fo^2 + 2Fc^2)/\ 3)$

Table A2. Complete Listing of Bond Lengths [Å] for **19b**

Ge(1)-C(1)	1.944(3)
Ge(1)-C(8)	1.945(3)
Ge(1)-C(17)	1.958(3)
Ge(1)-C(15)	1.965(4)
C(1)-C(6)	1.381(4)
C(1)-C(2)	1.387(4)
C(2)-C(3)	1.383(4)
C(3)-C(4)	1.371(5)
C(4)-C(5)	1.383(4)
C(4)-C(7)	1.481(5)
C(5)-C(6)	1.383(4)
C(7)-F(1)	1.306(4)
C(7)-F(2)	1.313(4)
C(7)-F(3)	1.328(4)
C(8)-C(13)	1.386(4)
C(8)-C(9)	1.387(4)
C(9)-C(10)	1.380(5)
C(10)-C(11)	1.383(5)
C(11)-C(12)	1.377(5)
C(11)-C(14)	1.495(5)
C(12)-C(13)	1.377(5)
C(14)-F(4)	1.216(2)
C(14)-F(5)	1.350(2)
C(14)-F(6)	1.252(2)
C(14)-F(4A)	1.216(2)
C(14)-F(6A)	1.252(2)
C(14)-F(5A)	1.350(2)
C(15)-C(16)	1.517(6)
C(16)-C(17)	1.512(6)

Table A3. Complete Listing of Bond Angles [deg] for **19b**

C(1)-Ge(1)-C(8)	108.63(13)
C(1)-Ge(1)-C(17)	117.49(14)
C(8)-Ge(1)-C(17)	118.16(15)
C(1)-Ge(1)-C(15)	118.66(15)
C(8)-Ge(1)-C(15)	114.91(15)
C(17)-Ge(1)-C(15)	76.28(17)
C(6)-C(1)-C(2)	117.8(3)
C(6)-C(1)-Ge(1)	121.3(2)
C(2)-C(1)-Ge(1)	120.8(2)
C(3)-C(2)-C(1)	121.1(3)
C(4)-C(3)-C(2)	120.3(3)
C(3)-C(4)-C(5)	119.5(3)
C(3)-C(4)-C(7)	119.5(3)
C(5)-C(4)-C(7)	121.0(3)
C(6)-C(5)-C(4)	119.8(3)
C(1)-C(6)-C(5)	121.4(3)
C(13)-C(8)-C(9)	118.0(3)
C(13)-C(8)-Ge(1)	119.9(2)
C(9)-C(8)-Ge(1)	122.1(2)
C(10)-C(9)-C(8)	121.0(3)
C(9)-C(10)-C(11)	120.0(3)
C(12)-C(11)-C(10)	119.7(3)
C(12)-C(11)-C(14)	120.3(3)
C(10)-C(11)-C(14)	120.0(3)
C(13)-C(12)-C(11)	119.9(3)
C(12)-C(13)-C(8)	121.4(3)
C(16)-C(15)-Ge(1)	88.3(2)
C(17)-C(16)-C(15)	106.2(3)
C(16)-C(17)-Ge(1)	88.7(3)
F(1)-C(7)-F(2)	107.8(4)
F(1)-C(7)-F(3)	105.1(3)
F(2)-C(7)-F(3)	103.8(3)
F(1)-C(7)-C(4)	112.7(3)
F(2)-C(7)-C(4)	114.4(3)
F(3)-C(7)-C(4)	112.3(3)
F(4)-C(14)-F(6)	110.7(14)
F(4)-C(14)-F(5)	104.3(18)
F(6)-C(14)-F(5)	103.8(14)

Table A3 cont. Complete Listing of Bond Angles [deg] for **19b**

F(4)-C(14)-C(11)	115.4(8)
F(6)-C(14)-C(11)	111.1(8)
F(5)-C(14)-C(11)	110.7(10)
F(4A)-C(14)-F(6A)	110.7(14)
F(4A)-C(14)-F(5A)	104.3(18)
F(6A)-C(14)-F(5A)	103.8(14)
F(4A)-C(14)-C(11)	115.4(8)
F(6A)-C(14)-C(11)	111.1(8)
F(5A)-C(14)-C(11)	110.7(10)

Table A4. Complete Listing of Bond Lengths [Å] for **19c**

Ge(1)-C(1)	1.946(2)
Ge(1)-C(9)	1.950(2)
Ge(1)-C(19)	1.959(2)
Ge(1)-C(17)	1.960(2)
C(1)-C(2)	1.393(3)
C(1)-C(6)	1.397(3)
C(2)-C(3)	1.386(3)
C(3)-C(4)	1.381(3)
C(3)-C(7)	1.499(4)
C(4)-C(5)	1.383(3)
C(5)-C(6)	1.390(3)
C(5)-C(8)	1.498(3)
C(7)-F(1)	1.287(10)
C(7)-F(2)	1.333(6)
C(7)-F(3)	1.294(5)
C(7)-F(1A)	1.252(16)
C(7)-F(2A)	1.186(15)
C(7)-F(3A)	1.338(14)
C(8)-F(4)	1.238(12)
C(8)-F(5)	1.297(17)
C(8)-F(6)	1.413(16)
C(8)-F(4A)	1.368(10)
C(8)-F(5A)	1.292(13)
C(8)-F(6A)	1.255(14)
C(9)-C(14)	1.390(3)
C(9)-C(10)	1.392(3)
C(10)-C(11)	1.388(3)
C(11)-C(12)	1.391(3)
C(11)-C(15)	1.498(4)
C(12)-C(13)	1.381(3)
C(13)-C(14)	1.388(3)
C(13)-C(16)	1.500(3)
C(15)-F(7)	1.334(9)
C(15)-F(8)	1.340(7)
C(15)-F(9)	1.333(5)
C(15)-F(7A)	1.235(18)
C(15)-F(8A)	1.23(2)
C(15)-F(9A)	1.315(13)

Table A4 cont. Complete Listing of Bond Lengths [Å] for **19c**

C(16)-F(10)	1.327(4)
C(16)-F(11)	1.321(4)
C(16)-F(12)	1.317(4)
C(16)-F(10A)	1.26(3)
C(16)-F(11A)	1.28(3)
C(16)-F(12A)	1.39(3)
C(17)-C(18)	1.499(4)
C(18)-C(19)	1.532(5)

Table A5. Complete Listing of Bond Angles [deg] for **19c**

C(1)-Ge(1)-C(9)	108.15(9)
C(1)-Ge(1)-C(19)	118.60(10)
C(9)-Ge(1)-C(19)	116.56(11)
C(1)-Ge(1)-C(17)	116.04(10)
C(9)-Ge(1)-C(17)	118.89(11)
C(19)-Ge(1)-C(17)	76.11(12)
C(2)-C(1)-C(6)	117.6(2)
C(2)-C(1)-Ge(1)	120.61(17)
C(6)-C(1)-Ge(1)	121.73(16)
C(3)-C(2)-C(1)	121.0(2)
C(4)-C(3)-C(2)	121.0(2)
C(4)-C(3)-C(7)	119.3(2)
C(2)-C(3)-C(7)	119.7(2)
C(3)-C(4)-C(5)	118.8(2)
C(4)-C(5)-C(6)	120.6(2)
C(4)-C(5)-C(8)	120.1(2)
C(6)-C(5)-C(8)	119.3(2)
C(5)-C(6)-C(1)	121.0(2)
C(14)-C(9)-C(10)	118.1(2)
C(14)-C(9)-Ge(1)	121.14(17)
C(10)-C(9)-Ge(1)	120.77(17)
C(11)-C(10)-C(9)	120.8(2)
C(10)-C(11)-C(12)	120.5(2)
C(10)-C(11)-C(15)	119.8(2)
C(12)-C(11)-C(15)	119.6(2)
C(13)-C(12)-C(11)	118.9(2)
C(12)-C(13)-C(14)	120.5(2)
C(12)-C(13)-C(16)	120.5(2)
C(14)-C(13)-C(16)	119.0(2)
C(13)-C(14)-C(9)	121.2(2)
C(18)-C(17)-Ge(1)	89.3(2)
C(17)-C(18)-C(19)	105.7(3)
C(18)-C(19)-Ge(1)	88.41(18)
F(1)-C(7)-F(3)	109.9(6)
F(1)-C(7)-F(2)	106.1(6)
F(3)-C(7)-F(2)	102.2(4)
F(1)-C(7)-C(3)	113.0(5)
F(3)-C(7)-C(3)	114.4(3)
F(2)-C(7)-C(3)	110.4(4)

Table A5 cont. Complete Listing of Bond Angles [deg] for **19c**

F(4)-C(8)-F(5)	111.0(12)
F(4)-C(8)-F(6)	106.1(9)
F(5)-C(8)-F(6)	101.5(13)
F(4)-C(8)-C(5)	115.9(7)
F(5)-C(8)-C(5)	113.6(10)
F(6)-C(8)-C(5)	107.4(7)
F(9)-C(15)-F(7)	112.0(6)
F(9)-C(15)-F(8)	102.6(5)
F(7)-C(15)-F(8)	105.3(6)
F(9)-C(15)-C(11)	112.8(3)
F(7)-C(15)-C(11)	110.0(5)
F(8)-C(15)-C(11)	113.8(3)
F(11)-C(16)-F(12)	106.0(3)
F(11)-C(16)-F(10)	105.1(3)
F(12)-C(16)-F(10)	107.6(3)
F(11)-C(16)-C(13)	111.8(3)
F(12)-C(16)-C(13)	112.8(3)
F(10)-C(16)-C(13)	113.0(3)
F(2A)-C(7)-F(1A)	105.6(16)
F(2A)-C(7)-F(3A)	111.1(15)
F(1A)-C(7)-F(3A)	100.0(12)
F(2A)-C(7)-C(3)	116.5(9)
F(1A)-C(7)-C(3)	115.7(9)
F(3A)-C(7)-C(3)	106.7(7)
F(6A)-C(8)-F(5A)	109.9(11)
F(6A)-C(8)-F(4A)	103.9(7)
F(5A)-C(8)-F(4A)	102.4(10)
F(6A)-C(8)-C(5)	115.1(6)
F(5A)-C(8)-C(5)	113.5(9)
F(4A)-C(8)-C(5)	110.9(6)
F(8A)-C(15)-F(7A)	105.4(14)
F(8A)-C(15)-F(9A)	116.7(15)
F(7A)-C(15)-F(9A)	93.9(13)
F(8A)-C(15)-C(11)	111.7(10)
F(7A)-C(15)-C(11)	116.1(10)
F(9A)-C(15)-C(11)	111.9(8)
F(10A)-C(16)-F(11A)	114(3)
F(10A)-C(16)-F(12A)	96(3)
F(11A)-C(16)-F(12A)	108(3)

Table A5 cont. Complete Listing of Bond Angles [deg] for **19c**

F(10A)-C(16)-C(13)	111.1(18)
F(11A)-C(16)-C(13)	117.9(11)
F(12A)-C(16)-C(13)	107.1(11)

Table A6. Atomic Coordinates (x 10^4) and Equivalent Isotropic Displacement Parameters ($Å^2$ x 10^3) for **19b**. U(eq) is defined as one third of the trace of the orthogonalized Uij tensor.

	x	y	z	U(eq)
Ge(1)	8872(1)	2012(1)	1902(1)	36(1)
C(1)	9675(2)	710(4)	2757(2)	34(1)
C(2)	10112(3)	-1243(5)	2753(2)	44(1)
C(3)	10671(3)	-2193(5)	3361(2)	48(1)
C(4)	10799(2)	-1216(5)	3983(2)	41(1)
C(5)	10369(3)	733(5)	3998(2)	47(1)
C(6)	9811(3)	1671(5)	3388(2)	45(1)
C(7)	11395(3)	-2262(6)	4628(2)	57(1)
C(8)	9768(2)	3845(5)	1573(2)	38(1)
C(9)	10821(3)	3929(5)	1890(2)	47(1)
C(10)	11434(3)	5318(5)	1669(2)	51(1)
C(11)	11000(3)	6661(5)	1127(2)	45(1)
C(12)	9956(3)	6587(5)	806(2)	51(1)
C(13)	9352(3)	5182(5)	1024(2)	47(1)
C(14)	11657(3)	8218(7)	905(3)	60(1)
C(15)	7522(3)	3199(6)	1858(2)	58(1)
C(16)	7040(3)	1664(7)	1284(3)	107(2)
C(17)	7901(3)	249(6)	1226(2)	54(1)
F(1)	11077(3)	-4159(5)	4681(2)	132(1)
F(2)	11409(2)	-1254(4)	5196(1)	94(1)
F(3)	12384(2)	-2458(4)	4669(1)	86(1)
F(4)	11720(40)	7990(60)	321(11)	158(14)
F(5)	12640(14)	8100(50)	1310(17)	119(10)
F(6)	11390(30)	10040(20)	990(30)	143(13)
F(4A)	11720(40)	7990(60)	321(11)	158(14)
F(5A)	12640(14)	8100(50)	1310(17)	119(10)
F(6A)	11390(30)	10040(20)	990(30)	143(13)

Table A6. Atomic Coordinates (x 10^4) and Equivalent Isotropic Displacement Parameters (Å^2 x 10^3) for **19c**. U(eq) is defined as one third of the trace of the orthogonalized Uij tensor.

	x	y	z	U(eq)
Ge(1)	7691(1)	4969(1)	501(1)	29(1)
C(1)	9169(2)	3764(3)	916(1)	28(1)
C(2)	9378(2)	2108(3)	801(1)	31(1)
C(3)	10463(2)	1264(3)	1077(1)	33(1)
C(4)	11365(2)	2037(3)	1476(1)	34(1)
C(5)	11164(2)	3675(3)	1600(1)	31(1)
C(6)	10077(2)	4529(3)	1326(1)	32(1)
C(7)	10668(4)	-511(4)	940(1)	53(1)
C(8)	12100(3)	4533(3)	2043(1)	46(1)
C(9)	6900(2)	6266(3)	1012(1)	29(1)
C(10)	6831(2)	5646(3)	1527(1)	33(1)
C(11)	6244(2)	6554(3)	1886(1)	35(1)
C(12)	5701(2)	8099(3)	1737(1)	38(1)
C(13)	5779(2)	8728(3)	1229(1)	34(1)
C(14)	6376(2)	7824(3)	872(1)	33(1)
C(15)	6248(3)	5903(4)	2449(1)	49(1)
C(16)	5243(3)	10411(3)	1060(1)	47(1)
C(17)	6552(3)	3714(3)	-74(1)	42(1)
C(18)	6852(6)	4931(5)	-488(1)	108(2)
C(19)	7903(3)	6080(3)	-175(1)	45(1)
F(1)	9613(10)	-1376(11)	875(7)	129(5)
F(2)	11095(12)	-616(8)	469(2)	105(4)
F(3)	11587(9)	-1251(7)	1276(3)	87(2)
F(4)	12930(20)	3642(16)	2323(7)	107(6)
F(5)	12630(20)	5840(20)	1877(9)	67(4)
F(6)	11362(17)	5220(30)	2407(9)	102(5)
F(7)	7354(10)	6332(14)	2783(4)	103(3)
F(8)	6200(8)	4247(8)	2477(3)	66(2)
F(9)	5197(6)	6362(10)	2644(3)	64(2)
F(10)	4630(5)	11102(4)	1423(2)	81(1)
F(11)	6177(3)	11467(3)	1005(2)	67(1)
F(12)	4427(4)	10399(4)	586(2)	88(2)

Table A6 cont. Atomic Coordinates (x 10^4) and Equivalent Isotropic Displacement Parameters ($Å^2$ x 10^3) for **19c**. U(eq) is defined as one third of the trace of the orthogonalized Uij tensor.

	x	y	z	U(eq)
F(1A)	9740(20)	-1190(20)	624(9)	99(10)
F(2A)	11610(20)	-800(30)	760(20)	213(15)
F(3A)	10660(50)	-1388(11)	1394(5)	151(10)
F(4A)	13265(13)	3706(15)	2158(8)	112(4)
F(5A)	12449(19)	5982(18)	1903(8)	72(4)
F(6A)	11743(19)	4620(20)	2495(4)	91(4)
F(7A)	7332(16)	5730(50)	2745(10)	97(7)
F(8A)	5720(40)	4540(40)	2437(9)	126(8)
F(9A)	5870(50)	7030(40)	2767(6)	113(13)
F(10A)	5130(50)	11280(40)	1469(16)	130(20)
F(11A)	5730(80)	11190(70)	700(30)	200(30)
F(12A)	3920(30)	10230(30)	860(30)	160(20)